Ruthenium Piano-Stool

Complexes Incorporating Novel

Bis(pyrrolidinyl)alkylphosphines

by

Michael T. Beach

RUTHENIUM PIANO-STOOL COMPLEXES INCORPORATING NOVEL BIS(PYRROLIDINYL)ALKYLPHOSPHINES

by

Michael T. Beach

Submitted to

The Department of Chemistry, Lakehead University, in Partial Fulfilment of the Requirements for the Degree of Master of Science

Supervisor: Dr. G. J. Spivak

Department of Chemistry, Lakehead University,

Thunder Bay, Ontario, Canada, P7B 5E1

December, 2011

<u>SIGNED OFFICIAL THESIS ACCEPTANCE FORM GOES HERE</u>

To the people I love so much, my family, Timothy, Armyline, Nick, Melissa, Frankie, Monkey, Moosey and Sheena. Thank you for your unwavering support and encouragement throughout this project.

Abstract

Conventional phosphine ligands (*i.e.*, those typically bearing alkyl and/or aryl substituents) have played a crucial role in the development of transition metal coordination chemistry. Many structural and electronic variants have been explored, including the class of bis(*N*-pyrrolidinyl)alkylphosphines. These phosphines generally possess moderate steric properties, yet exhibit exceptional electron-donating properties. The greater Lewis basicity of bis(*N*-pyrrolidinyl)alkylphosphines likely can be attributed to the additional electron density provided by the lone pair of the planar nitrogen atoms through a dative interaction with the phosphorus donor atom. A series of ruthenium piano-stool complexes incorporating either monodentate bis(*N*-pyrrolidinyl)alkylphosphines, $R(pyr)_2P$ (R = Me or ^{t}Bu; pyr = pyrrolidinyl), or a new bidentate analogue, 1,2-bis(dipyrrolidin-1-ylphosphino)ethane (abbreviated dpyrpe), were synthesized to provide insight into the role of these ligands in ruthenium chemistry. These complexes include [Cp*Ru(PP)Cl], (PP = $[Me(pyr)_2P]_2$, **1**; dpyrpe, **2**), [CpRuCl(dpyrpe)], **3**, and [(*p*-cymene)Ru(R(pyr)$_2$P)Cl$_2$] (R = Me, **8**; ^{t}Bu, **9**). Further examination of the substitution chemistry of these species afforded the complexes [Cp*Ru(L)(PP)][BAr$^f_4$] (PP = $[Me(pyr)_2P]_2$: L = MeCN, **5a**; CO, **5b**; N_2, **5c**; PP = dpyrpe: L = MeCN, **6a**; CO, **6b**; N_2, **6c**; H_2, **6d**; Ar^f = 3,5-bis(trifluoromethyl)phenyl), [(*p*-cymene)Ru(R(pyr)$_2$P)(MeCN)$_2$][BAr$^f_4$]$_2$ (R = Me, **10**; ^{t}Bu, **11**), and [(*p*-cymene)Ru(R(pyr)$_2$P)(CO)Cl][BAr$^f_4$] (R = Me, **12**; R= ^{t}Bu, **13**). In addition, the complexes, [Cp*Ru(CO)(MePPh$_2$)$_2$][BAr$^f_4$], **7a**, and [Cp*Ru(CO)(dppe)][BAr$^f_4$], **7b**, were synthesized in order to allow comparisons between conventional phosphines and bis(*N*-pyrrolidinyl)alkylphosphines using IR spectroscopy. The identities of all new ruthenium species were determined primarily through NMR spectroscopic analysis. The X-ray crystal structures of **1**, **3**, **6a** and **11** were also obtained, and revealed interesting structural features of the pyrrolidinyl groups as part of these complexes.

Acknowledgements

First and foremost, I would like to express my profound gratitude to my supervisor, Dr. Greg Spivak for his encouragement, guidance, and patience throughout my time in his laboratory. His passionate view of chemistry and infectious enthusiasm for the pursuit of knowledge has been a constant inspiration. I will greatly miss our culinary discussions.

I would also wish to thank my fellow lab mates Jesse Walker and Tim Larocque for their helpful insights, assistance, and light hearted banter. Countless songs will never be the same without your improvised accompaniment. The members of the Lakehead University Chemistry Department have also contributed immensely to my personal and professional growth. Various research groups have been a source of friendship, collaboration, and sound advice.

Lastly, I would like to thank the most tenacious person I know, my brother, Nick. He is the reason I pursued chemistry and without him I would have not been able to accomplish what I have.

Contents

List of Figures

List of Tables

List of Schemes

Abbreviations

θ	cone angle (°)
δ	chemical shift (ppm)
Ar^f	3,5-bis(trifluoromethyl)phenyl
Bz	benzyl ($C_6H_5CH_2$)
br	broad
^{t}Bu	*tert*-butyl
ν(CO)	carbonyl stretch (cm^{-1})
COD	cyclooctadiene
Cp	cyclopentadienyl
Cp*	1,2,3,4,5-pentamethylcyclopentadienyl
Cy	cyclohexyl
$^{13}C\{^1H\}$	proton decoupled carbon-13 NMR spectrum
d	doublet
DCM	dichloromethane
dippe	1,2-bis(diisopropylphosphino)ethane
dppe	1,2-bis(diphenylphosphino)ethane
dpyrpe	1,2-bis(dipyrrolidin-1-ylphosphino)ethane
Et	ethyl
g	grams
GC	gas chromatography
^1H	proton NMR spectrum
Hz	Hertz
HPLC	high performance liquid chromatography
IR	infrared
J	coupling constant (Hz)
L	general ligand
M	moles per litre
m	multiplet

Me	methyl
MHz	megahertz
min	minutes
μmol	micromoles
mmol	millimoles
mol	moles
mor	morpholinyl
NMR	nuclear magnetic resonance
p	para
ppm	parts per million
Ph	phenyl
ppy	2-phenylpyridinyl
pip	piperidinyl
^{i}Pr	isopropyl
$^{31}P\{^{1}H\}$	proton decoupled phosphorus-31 NMR spectrum
pyr	pyrrolidinyl
R	alkyl or aryl group
s	singlet
sept	septet
THF	tetrahydrofuran
THT	tetrahydrothiophene
tpy	2-(2'-thienyl)pyridine
UV	ultraviolet
xs	excess

1. Introduction

The search for effective phosphorus-containing ligands has been of great interest in organometallic chemistry for the last few decades. Conventional alkyl- and aryl-substituted phosphines have played a vital role in the development of countless organometallic complexes, mechanistic studies, and perhaps most importantly in catalysis.[2] Their ability to control effectively the stability and reactivity of metal complexes in a wide range of catalytic applications through their electronic and steric contributions continues to make the exploration of these ligands a strong focus in organometallic chemistry.[3] Perhaps as a prominent, more recent example, the incorporation of tricyclohexylphosphine into the first and second generation Grubbs' metathesis catalysts has produced some of the most active catalysts; this research contributed to a (shared) award of the Nobel Prize in Chemistry in 2005.[4] Thus, by varying the phosphine substituents, the electronic and steric properties can be tailored. Some of the strongest Lewis basic phosphines contain alkyl substituents which also makes them rather large (**Figure 1.1**). For example, $^{t}Bu_3P$ is one of the strongest donor phosphines known, but it is also quite bulky (cone angle,θ, of 182°).[5]

Figure 1.1: Measuring the steric contribution or cone angle (θ) of a phosphine

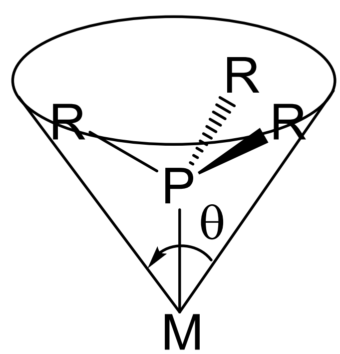

Strongly donating phosphines possessing larger substituents often also sterically crowd the metal center, which may lead to adverse conditions for catalytic activity.[6] Alterations of the substituents have been examined in an attempt to remedy this correlation between strong Lewis basicity and large cone angle. One such modification that has shown promise is the utilization of specific nitrogen containing substituents, where the substituents are linked to the phosphorus atom through a P-N bond (*i.e.*, P-NR_2).[1] In general, donation of the lone pair on the nitrogen atom into a suitable orbital on the phosphorus atom might lead to an overall increase in the donor properties of the phosphine. Indeed, members of this class of phosphine have been observed to possess enhanced donor properties. More importantly, the substituents are often comparatively smaller, and thus yield a relatively strongly Lewis basic phosphine with smaller bulk. Several studies suggest the lone pair on the nitrogen atom can interact with the phosphorus atom to which it is directly attached. For example, variable temperature NMR spectroscopic studies on phosphines containing P-N bonds generally show a higher barrier of rotation about the P-N bond, compared to analogous hydrazine and ethane derivatives.[7,8] This was attributed to a large degree of nitrogen lone pair delocalization into the P-N bond.[9] Infrared spectroscopic studies of free amine-substituted phosphines[8] and metal-carbonyl complexes containing amine-substituted phosphine ligands[10] suggest $p\pi$-$d\pi$ electron delocalization and conjugative resonance of the nitrogen lone pair with the *d*-orbitals of the phosphorus atoms. Thus, it appears the additional interaction between the nitrogen and phosphorus atoms likely could enhance the Lewis basicity of these phosphines compared to their conventional alkyl or aryl counterparts.

1.1 Phosphines Bearing Nitrogen-Containing Substituents (P-N Phosphine Ligands)

Numerous examples of P-N bond containing phosphines can be found in the literature, both in bidentate and monodentate forms. The synthesis of these unique phosphines is generally done under milder conditions compared to their conventional phosphine counterparts, which require the use of highly reactive, pyrophoric, alkyl- or aryllithium reagents.[11] The number of possible amine-phosphine combinations has given rise to a large group of phosphines containing P-N bonds; only a few of the more relevant examples will be covered here. The synthesis and properties of these example ligands are presented in the sections that follow.

1.1.1 Bidentate P-N Phosphine Ligands

Bidentate phosphines are four electron-donating ligands that coordinate via the two linked phosphorus atoms in a chelating fashion. The link or backbone connecting the phosphorus atoms can be varied to affect the bite angle of the ligand or even the donating properties. Modifications of the steric demands and electronic properties can also be achieved through the alteration of the other phosphine substituents not participating in the phosphorus bridge. In this way, nitrogen-containing substituents also serve as the linkers between the two phosphorus atoms in addition to serving as donor substituents.

1.1.1.1 Bidentate P-N Phosphines Incorporating Nitrogen-Containing Backbones

Research by Rodriguez i Zubiri *et al.* reported on the synthesis of a series of bidentate phosphines utilizing piperazine and homopiperazine for the backbone.[12] The synthesis of these ligands, $R_2PN(C_2H_4)_2NPR_2$ and $R_2PN(C_5H_{10})NPR_2$ (R = Ph, ^{i}Pr) involved reactions of either piperazine or homopiperazine with two equivalents of the corresponding chlorodialkyl- or chlorodiarylphosphine. An equivalent of triethylamine was also added to the reaction mixture to remove the HCl (as $[Et_3NH]Cl$) generated during the reaction (**Scheme 1.1**).[12]

Scheme 1.1: Synthetic route to the ligands $R_2PN(C_2H_4)_2NPR_2$ and $R_2PN(C_5H_{10})NPR_2$[12]

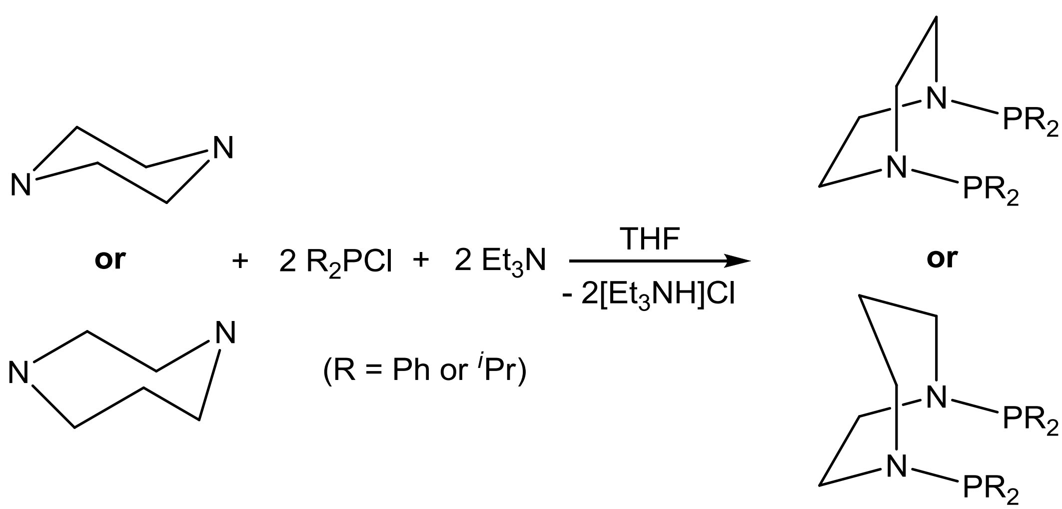

Palladium and platinum complexes, incorporating these ligands were prepared through the addition of the corresponding ligand $R_2PN(C_2H_4)_2NPR_2$ or $R_2PN(C_5H_{10})NPR_2$ (R = Ph, ^{i}Pr) to dichloromethane solutions of *cis*-$[(COD)MCl_2]$ (M = Pd, Pt; COD = cyclooctadiene) in a 1:1 ratio yielding the complexes, *cis*-$[(R_2PN(C_2H_4)_2NPR_2)MCl_2]$ and *cis*-$[(R_2PN(C_5H_{10})NPR_2)MCl_2]$ (M = Pd, Pt; R = Ph, ^{i}Pr), respectively (**Scheme 1.2**).[12]

Scheme 1.2: Synthetic route to the complexes *cis*-[($R_2PN(C_2H_4)_2NPR_2$)MCl_2] and *cis*-[($R_2PN(C_5H_{10})NPR_2$)MCl_2][12]

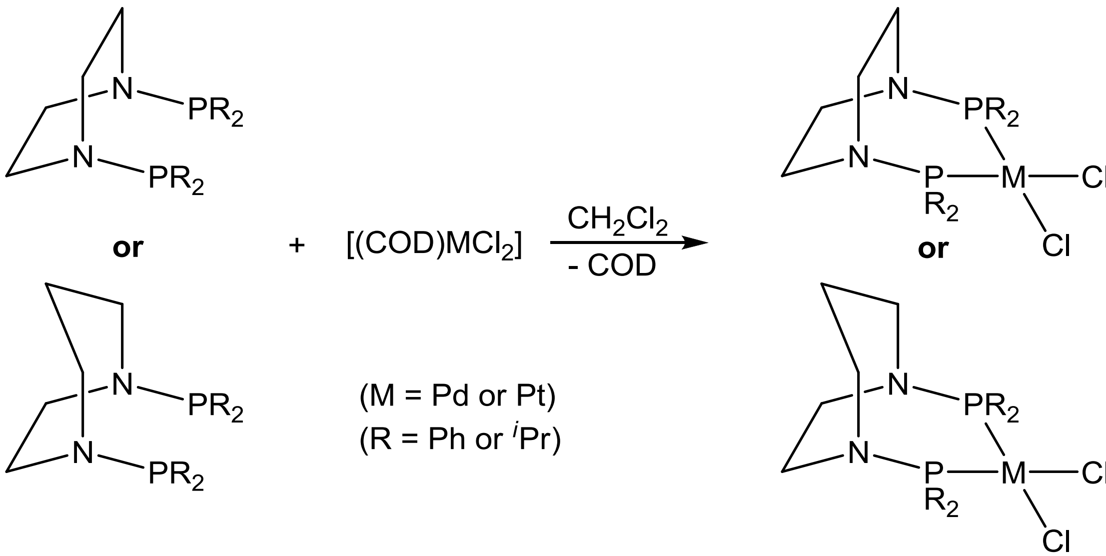

The identity of the majority of these species was confirmed through ^{1}H, $^{31}P\{^{1}H\}$, and ^{195}Pt NMR spectroscopic analysis. Single crystals were obtained for both *cis*-[($Ph_2PN(C_2H_4)_2NPPh_2$)$PdCl_2$] and *cis*-[($Ph_2PN(C_5H_{10})NPPh_2$)$PtCl_2$], which allowed for X-ray crystallographic studies; the general structures are illustrated in **Figure 1.2** and **Figure 1.3**, respectively, and key bond lengths and angles are listed in **Table 1.1** and **Table 1.2**, respectively.[12]

Figure 1.2: Structure of *cis*-[($Ph_2PN(C_2H_4)_2NPPh_2$)$PdCl_2$][12]

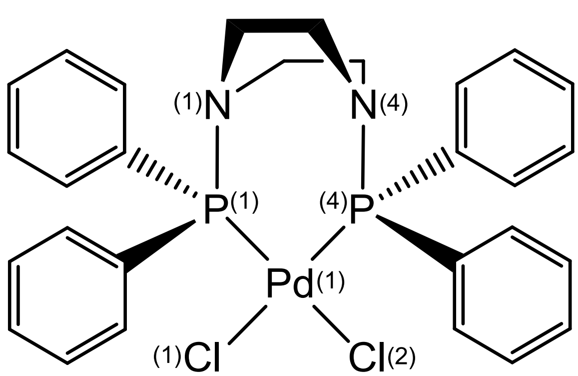

Table 1.1: Selected bond lengths and angles for *cis*-[($Ph_2PN(C_2H_4)_2NPPh_2$)$PdCl_2$][12]

Selected Bond Lengths (Å)		Selected Bond Angles (°)	
Pd(1)–P(1)	2.246(5)	P(1)–Pt(1)–P(4)	93.9(2)
Pd(1)–P(4)	2.256(5)	Cl(1)–Pt(1)–Cl(2)	92.1(2)
Pd(1)–Cl(1)	2.391(4)	Pt(1)–P(1)–N(1)	120.1(5)
Pd(1)–Cl(2)	2.381(5)	Pt(1)–P(4)–N(4)	123.3(5)
P(1)–N(1)	1.697(13)	sum of angles for N(1)	349.2
P(1)–N(4)	1.666(13)	sum of angles for N(4)	347.7

Figure 1.3: Structure of *cis*-[($Ph_2PN(C_5H_{10})NPPh_2$)$PtCl_2$][12]

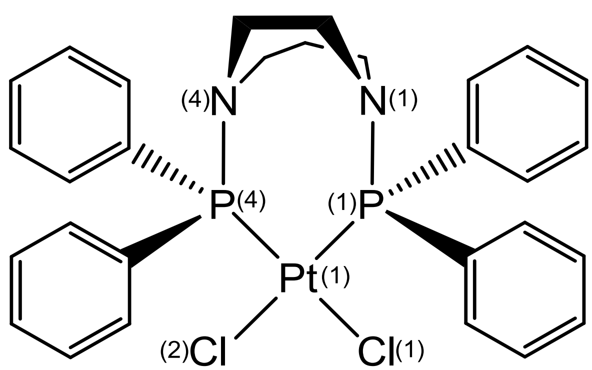

Table 1.2: Selected bond lengths and angles for *cis*-[($Ph_2PN(C_5H_{10})NPPh_2$)$PtCl_2$][12]

Selected Bond Lengths (Å)		Selected Bond Angles (°)	
Pt(1)–P(1)	2.255(6)	P(1)–Pt(1)–P(4)	97.3(1)
Pt(1)–P(4)	2.215(6)	Cl(1)–Pt(1)–Cl(2)	89.1(1)
Pt(1)–Cl(1)	2.358(7)	Pt(1)–P(1)–N(1)	119.0(8)
Pt(1)–Cl(2)	2.388(5)	Pt(1)–P(4)–N(4)	125.0(8)
P(1)–N(1)	1.70(2)	sum of angles for N(1)	359.1
P(1)–N(4)	1.64(2)	sum of angles for N(4)	345.8

The X-ray structure of *cis*-[($Ph_2PN(C_2H_4)_2NPPh_2$)$PdCl_2$] possesses the expected square-planar geometry about the Pd centre, although it is somewhat distorted, with the bite angle of the phosphine being larger than the ideal 90°, at 93.9°, and Cl-Pd-Cl bond angle of 92.1°. The piperazine backbone of the ligand adopts a boat conformation and forms an "umbrella-like" structure around the Pd centre. The nitrogen atoms of the piperazine backbone display a tetrahedral geometry, affording a less strained bite angle, which is necessary to allow for the chelation of the phosphine. Similarly, the X-ray structure of *cis*-[($Ph_2PN(C_5H_{10})NPPh_2$)$PtCl_2$] displays a distorted square planar geometry, with a larger phosphine bite angle of 97.3°. The homopiperazine backbone also forms a pseudo-boat conformation, which again shrouds the Pt centre. Interestingly, one of the nitrogen atoms of the homopiperazine bridge displays a near planar geometry, with a bond angle totalling 359.1°, while the other displays a tetrahedral geometry, unlike the tetrahedral nature of both of the piperazine nitrogens. This planar nature along with the larger bite angle was explained by the greater size of the homopiperazine backbone, yielding a greater separation between the coordinating phosphine units.[12] The bidentate phosphines possessing a nitrogen-containing linker display relatively short Pd-P and Pt-P bond lengths at 2.246(5) and 2.256(5), and 2.255(6) and 2.215(6) Å, respectively, indicating a stronger interaction between the metal centre and the phosphine ligands.[13] This suggests the presence of nitrogen-containing substituents likely result in a more electron donating bidentate phosphine, allowing for a more electron rich metal centre.

The same research group went on to introduce the application of these phosphines as bridging ligands in gold and ruthenium chemistry.[12] The synthesis of the bridged gold complex began with the addition of one-half equivalent of either $Ph_2PN(C_2H_4)_2NPPh_2$ or $Ph_2PN(C_5H_{10})NPPh_2$ to solutions of [AuCl(THT)] (THT = tetrahydrothiophene) and yielded the products [$(AuCl)_2$(μ-$Ph_2PN(C_2H_4)_2NPPh_2$)] and [$(AuCl)_2$(μ-$Ph_2PN(C_5H_{10})NPPh_2$)] (**Scheme 1.3**).[12]

Scheme 1.3: Synthetic route to the complexes [(AuCl)$_2$(μ-Ph$_2$PN(C$_2$H$_4$)$_2$NPPh$_2$)] and [(AuCl)$_2$(μ-Ph$_2$PN(C$_5$H$_{10}$)NPPh$_2$)][12]

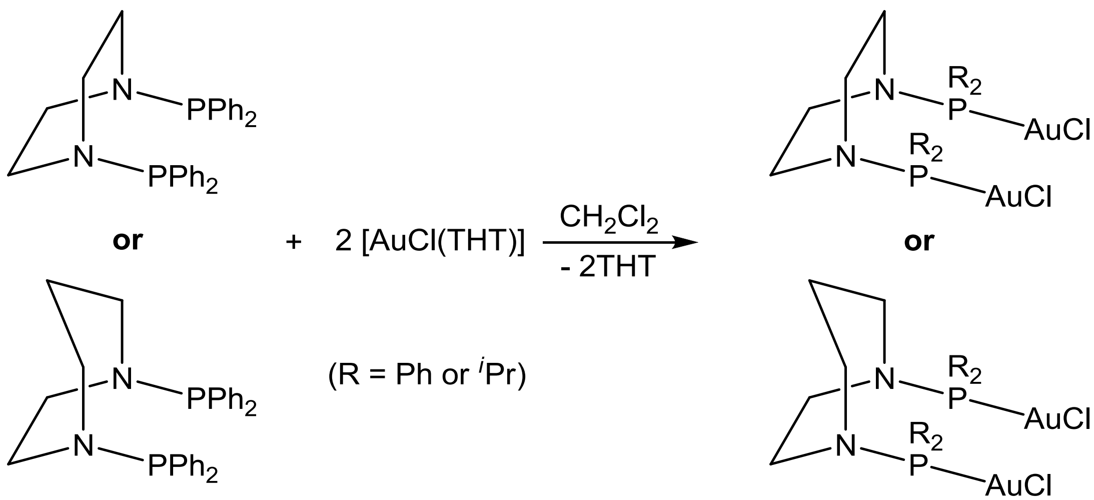

Similarly, the synthesis of the bridged ruthenium complex began with the addition of an equivalent of Ph$_2$PN(C$_2$H$_4$)$_2$NPPh$_2$ to a THF solution of [(*p*-cymene)RuCl$_2$]$_2$, and gave the product [((*p*-cymene)RuCl$_2$)$_2$(μ-Ph$_2$PN(C$_2$H$_4$)$_2$NPPh$_2$)] (**Scheme 1.4**).[12] Attempts to utilize the bidentate phosphine, R$_2$PN(C$_5$H$_{10}$)NPR$_2$, in the bridging of ruthenium complexes were not reported. The preference for bridging over chelation is interesting in these particular cases, and contrasts what was observed for the platinum and palladium complexes. Similar results were

Scheme 1.4: Synthetic route to the complex [((*p*-cymene)RuCl$_2$)$_2$(μ-Ph$_2$PN(C$_2$H$_4$)$_2$NPPh$_2$)][12]

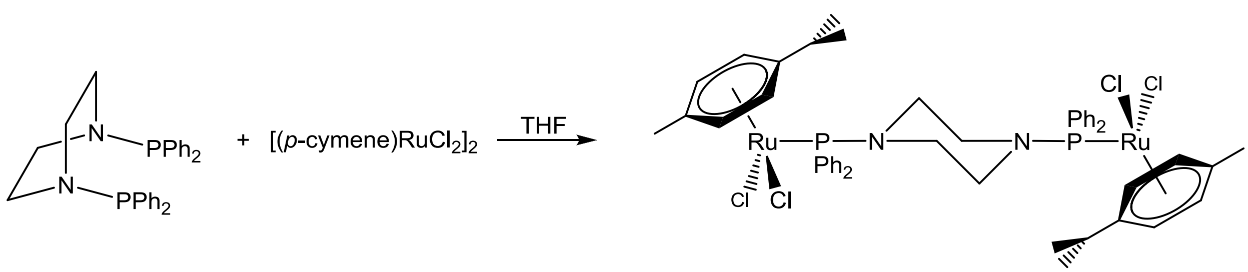

observed in our own investigations involving similar ligands in ruthenium-Cp* coordination chemistry (Cp* = 1,2,3,4,5-pentamethylcyclopentadiene). For example, a structurally similar ruthenium bridged species was synthesized in our laboratory using the isopropyl analogue ${}^{i}Pr_2PN(C_2H_4)_2NP^{i}Pr_2$ to bridge two {Cp*RuCl} fragments.[14] This was accomplished through the addition of two equivalents of ${}^{i}Pr_2PN(C_2H_4)_2NP^{i}Pr_2$ to $[Cp^*RuCl]_4$, resulting in a blue solution. Upon workup, a spectroscopically and microanalytically pure blue solid, with the identity $[(Cp^*RuCl_2)_2(\mu\text{-}{}^{i}Pr_2PN(C_2H_4)_2NP^{i}Pr_2)]$, was obtained (**Scheme 1.5**). Unfortunately, an attempt at an X-ray crystallographic study revealed the crystals were of rather poor quality, and thus reliable structural data was not obtained. Nonetheless, the connectivity of this species was at least confirmed.[14]

Scheme 1.5: Synthetic route to the complex $[(Cp^*RuCl_2)_2(\mu\text{-}{}^{i}Pr_2PN(C_2H_4)_2NP^{i}Pr_2)]$[14]

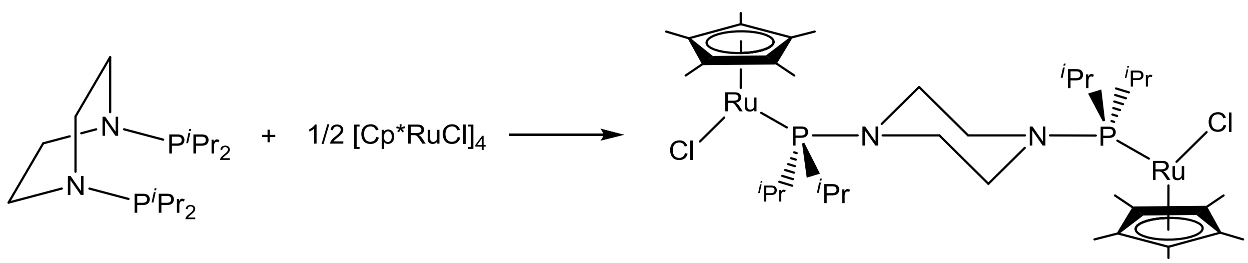

Further exploration of these bidentate phosphine ligands in molybdenum chemistry led to the synthesis of a series of molybdenum-carbonyl complexes (**Scheme 1.6**).[1e,12]. Thus, the introduction of an equivalent of either $Ph_2PN(C_2H_4)_2NPPh_2$ or $R_2PN(C_5H_{10})NPR_2$) to $[Mo(CO)_4(pip)_2]$ yielded the products *cis*-$[Mo(CO)_4(\eta^2\text{-}Ph_2PN(C_2H_4)_2NPPh_2)]$ or *cis*-$[Mo(CO)_4(0^2\text{-}R_2PN(C_5H_{10})NPR_2)]$ (R = Ph, ^{i}Pr). The carbonyl stretching frequencies, ν(CO), of these complexes were also measured. These data can be used to assess the electronic nature of the metal, and ultimately provide an indirect assessment of the relative donating properties of the ligands used.

Scheme 1.6: Synthetic route to the complexes *cis*-[Mo(CO)$_4$(η^2-R$_2$PN(C$_2$H$_4$)$_2$NPR$_2$] and *cis*-[Mo(CO)$_4$(η^2-R$_2$PN(C$_5$H$_{10}$)NPR$_2$] (R = Ph, ^{i}Pr)[12]

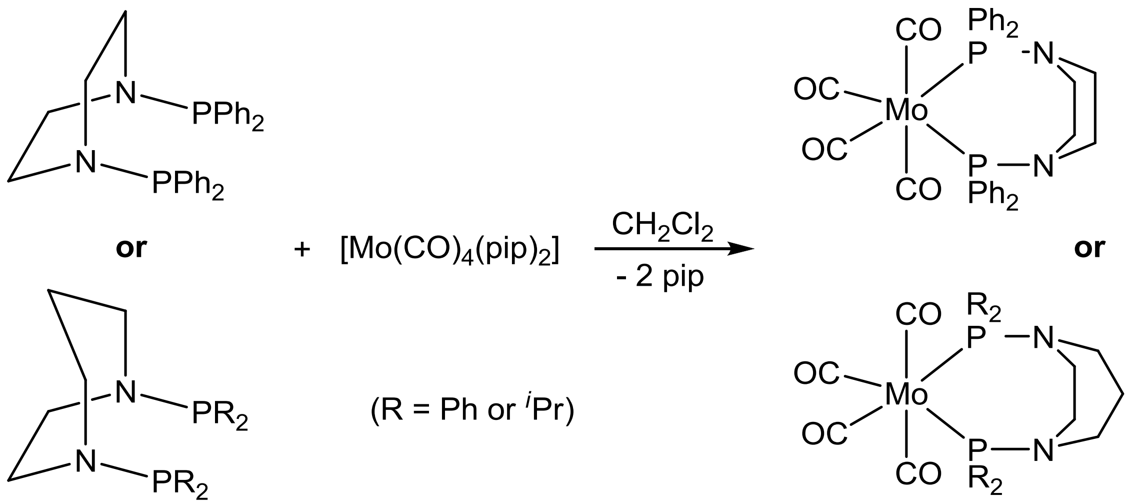

The IR spectroscopic analysis of *cis*-[Mo(CO)$_4$(η^2-R$_2$PN(C$_5$H$_{10}$)NPR$_2$)] (R = Ph, ^{i}Pr) was compared to those obtained for similar complexes containing more conventional bidentate phosphines.[1e] These results are listed in **Table 1.3**.

Table 1.3: ν(CO) of analogous *cis*-[Mo(CO)$_4$(P-P)][1e]

(P-P)	ν(CO) cm^{-1}
^{i}Pr$_2$PN(C$_5$H$_{10}$)NP^{i}Pr$_2$	2004
Et$_2$PCH$_2$CH$_2$PEt$_2$	2012
Ph$_2$PN(C$_5$H$_{10}$)NPPh$_2$	2014
Cy$_2$PCH$_2$CH$_2$PCy$_2$	2016
Ph$_2$PCH$_2$CH$_2$PPh$_2$	2021
(pyrrole)$_2$PCH$_2$CH$_2$P(pyrrole)$_2$	2043

The conventional bidentate analogues show near typical results, with Ph$_2$PCH$_2$CH$_2$PPh$_2$ displaying the weakest donor properties, and Et$_2$PCH$_2$CH$_2$PEt$_2$ the strongest. As expected, the ν(CO) values for the new ligands R$_2$PN(C$_5$H$_{10}$)NPR$_2$ (R = Ph, ^{i}Pr) suggest they possess electron donating character that is equal to or greater than the strongest of the conventional bidentate phosphine analogues presented in this study, with ν(CO) values 8 cm^{-1} lower than the strongest typical phosphine. Another nitrogen-substituted bidentate phosphine, $(pyrrole)_2PCH_2CH_2P(pyrrole)_2$, was employed in this study. It is interesting to note, the pyrrolyl substituents appear to mitigate the basicity of the phosphine to the point where it compares more closely with analogous bidentate phosphites and some fluorinated chelating phosphines.[1e] Moloy *et al.* proposed the origin of the poor σ-donor properties of the pyrrole-substituted phosphine through a series of resonance forms (**Figure 1.4**).[15]

Figure 1.4: Proposed resonance forms of pyrrole when attached to $–PR_2$[15]

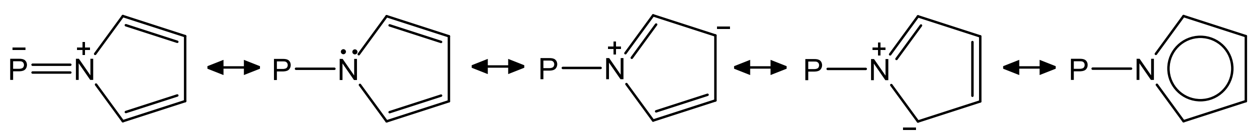

A **B** **C** **D** **E**

Qualitatively, aromatic delocalization of the nitrogen lone pair into the ring may eliminate any N-P π-donation (**A**), and generates a partial positive charge on the nitrogen adjacent to phosphorus (**C** and **D**). In order to circumvent the delocalization of the nitrogen lone pair into a ring substituent, it was suggested that perhaps the saturated counterpart, pyrrolidine, would better serve as a substituent. Thus, the nitrogen lone pair would be free to contribute to the phosphorus.[15]

1.1.2 Monodentate P-N Phosphine Ligands

Monodentate P-N containing phosphine ligands possess some similarities to their bidentate counterparts, and bear a nitrogen-containing substituent which allows for enhanced electronic properties compared to more traditional alkyl- and arylphosphines. A variety of monodentate P-N phosphine analogues having unique structural and electronic properties have been prepared, and their coordination chemistry studied.[1,16,17,18]

1.1.2.1 Monodentate P-N Phosphines Incorporating Dibenzylamine Substituents

In 1977, Verstuyft *et al.* reported on the use of dibenzylamine substituted phosphines in the synthesis of the complexes $[(Ph_n(Bz_2N)_{3-n})_2PdX_2]$ (Bz = $PhCH_2$; X = Cl, N_3; n = 1-3).[16] These complexes represent the first examples of the synthesis and coordination of tertiary aminoalkylphosphine or aminoarylphosphine ligands. The synthesis of $(Bz_2N)_3P$ was accomplished through the addition of dibenzylamine to a solution of PCl_3 (excess amine is used, and serves not only as a source of the phosphine substituent, but also to remove HCl as it is generated). Similarly, the phosphines $Ph(Bz_2N)_2P$ and $Ph_2(Bz_2N)P$ were synthesized starting with $PhPCl_2$ and Ph_2PCl, respectively (**Scheme 1.7**).[16]

Scheme 1.7: Synthetic route to the ligands, $Ph_n(Bz_2N)_{3-n}P$[16]

$$\underset{(n = 1 - 3)}{Ph_nPCl_{3-n} \quad + \quad 2n\ Bz_2NH} \xrightarrow[-\ Bz_2NHCl]{\text{diethyl ether}} Ph_n(Bz_2N)_{3-n}P$$

Interestingly, ^{1}H and $^{13}C\{^{1}H\}$ NMR and IR spectral analysis of the products containing the ligands $(Bz_2N)_3P$ and $Ph(Bz_2N)_2P$ revealed a *trans* geometry, while those with $Ph_2(Bz_2N)P$ adopted *cis* configurations. It was proposed that the *trans* geometry was the result of the greater steric demand for the phosphine ligands $(Bz_2N)_3P$ and $Ph(Bz_2N)_2P$ compared to $Ph_2(Bz_2N)P$.

1.1.2.2 Monodentate P-N Phosphines Incorporating Morpholine Substituents

The incorporation of a morpholinyl substituent into a tertiary phosphine framework was reported by Stangeland *et al.* in 1973, with the synthesis of the monodentate phosphine ligand tris(morpholinyl)phosphine, $(mor)_3P$.[17] Shortly thereafter, Thorstenson *et al.* reported on the relative reactivities of a series of tertiary morpholinyl-phosphine ligands, including $(mor)_3P$, $Ph(mor)_2P$, $Ph_2(mor)P$, and Ph_3P.[18] The reactivity of each of these phosphines towards MeI (yielding the corresponding phosphonium salts, $[R_3PMe]I$) was studied. All of the reactions were nearly quantitative, and yielded high purity products. The reactions were monitored by UV spectroscopy. From the UV data, the relative reactivities of the phosphines were determined to be $(mor)_3P$ > $Ph(mor)_2P$ > $Ph_2(mor)P$ > Ph_3P, suggesting a greater number of morpholine substituents produces a stronger Lewis base.

In 1996, Balashev *et al*. reported on the crystal structures of two $(mor)_3P$-containing platinum complexes, [Pt(ppy)($(mor)_3P$)Cl] and [Pt(tpy)($(mor)_3P$)Cl] (ppy = 2-phenylpyridinyl, tpy = 2-(2'-thienyl)pyridine).[19] The focus of the report was to test the luminescent properties of these complexes. The crystal structures of these complexes revealed interesting results regarding the geometry of the $(mor)_3P$ nitrogen atoms (key bond lengths and angles for each complex are listed in **Table 1.4** and **Table 1.5**).[19] The general structure of these complexes are illustrated in **Figure1.5** and **Figure 1.6**, respectively.

Figure 1.5: Structure of [Pt(ppy)($(mor)_3P$)Cl][19]

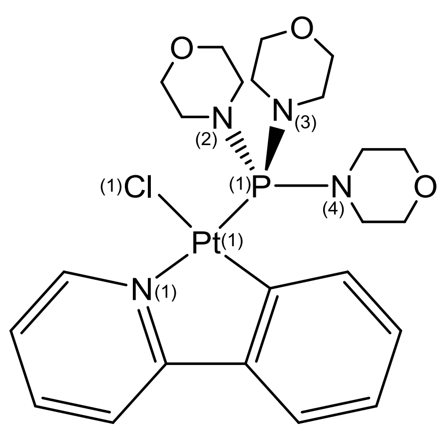

Table 1.4: Selected bond lengths and angles for [Pt(ppy)($(mor)_3P$)Cl][19]

Selected Bond Lengths (Å)		Selected Bond Angles (°)	
Pt(1)–P(1)	2.233(2)	Cl(1)–Pt(1)–P(1)	90.04(6)
Pt(1)–Cl(1)	2.388(2)	Cl(1)–Pt(1)–N(1)	90.7(2)
P(1)–N(2)	1.670(5)	Cl(1)–Pt(1)–C(11)	169.5(2)
P(1)–N(3)	1.663(5)	P(1)–Pt(1)–N(1)	174.6(2)
P(1)–N(4)	1.674(5)	sum of angles for N(2)	356(1)
		sum of angles for N(3)	360(1)
		sum of angles for N(4)	352(1)

Figure 1.6: Structure of [Pt(tpy)((mor)$_3$P)Cl][19]

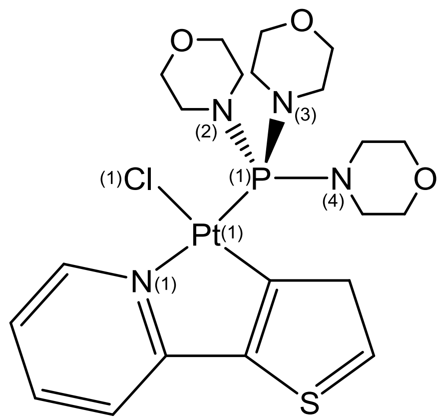

Table 1.5: Selected bond lengths and angles for [Pt(tpy)((mor)$_3$P)Cl][19]

Selected Bond Lengths (Å)		Selected Bond Angles (°)	
Pt(1)–P(1)	2.221(1)	Cl(1)–Pt(1)–P(1)	94.72(4)
Pt(1)–Cl(1)	2.327(1)	Cl(1)–Pt(1)–N(1)	91.4(1)
P(1)–N(2)	1.674(3)	Cl(1)–Pt(1)–C(11)	171.3(1)
P(1)–N(3)	1.678(3)	P(1)–Pt(1)–N(1)	173.9(1)
P(1)–N(4)	1.680(3)	sum of angles for N(2)	356(1)
		sum of angles for N(3)	351(1)
		sum of angles for N(4)	356(1)

The platinum centre in both complexes adopts the expected square planar geometry, with little deviation from idealized ligand orientation. The P-N bond lengths and geometries about the nitrogen atoms for both complexes show a correlation, with shorter P-N bonds observed for those nitrogen atoms with an increasingly higher degree of planarity. This suggests a greater extent of nitrogen lone pair donation to the phosphorus atom, thus decreasing the tetrahedral nature of the nitrogen atom while increasing the P-N bond strength. Interestingly, one of the nitrogen atoms of the phosphine ligand, in both of the complexes, displays an increased tetrahedral distortion, likely due to the inability of the phosphorus atom to accept the electron density effectively.[19]

Further evidence of the ability of the morpholinyl substituent to interact with the phosphorus atom was provided in the series of molybdenum-carbonyl complexes [$Mo(CO)_5(Ph(mor)_2P)$], [$Mo(CO)_5((pip)_3P)$] (pip = piperidine) and [$Mo(CO)_5(Ph(mor)(^{i}Pr_2N)P)$] (**Figure 1.7**, **Figure 1.8**, and **Figure 1.9**, respectively).[20]

Figure 1.7: Structure of [$Mo(CO)_5(Ph(mor)_2P)$][20]

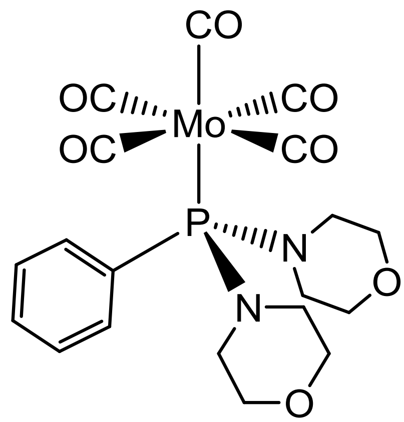

Figure 1.8: Structure of [$Mo(CO)_5((pip)_3P)$][20]

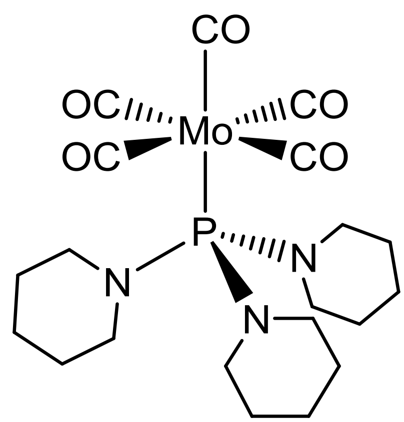

Figure 1.9: Structure of $[Mo(CO)_5(Ph(mor)(^iPr_2N)P)]$[20]

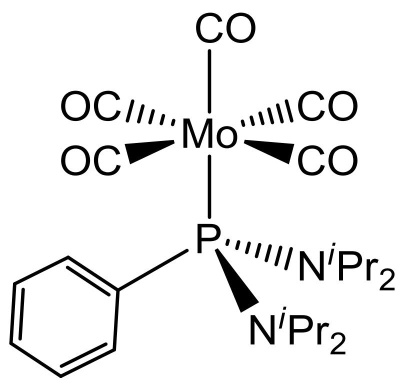

Analysis of the Mo-P bond lengths for these structures (2.547 Å, 2.569 Å, and 2.604 Å, respectively) suggested a relative donor strength order of $Ph(mor)_2P$ > $(pip)_3P$ > $Ph(mor)(N^iPr_2)P$. Comparing these results to the Mo-P bond lengths observed in the complexes $[Mo(CO)_5(Ph_3P)]$ (2.560 Å)[21] and $[Mo(CO)_5(Me_3P)]$ (2.508 Å)[22], the electron donating capabilities of the phosphine ligand $Ph(mor)_2P$ can be expected to be between those of the conventional phosphines, Ph_3P and Me_3P.

1.1.2.3 Monodentate P-N Phosphines Incorporating Pyrrolidine Substituents

Moloy *et al.* described the synthesis of the aminophosphine tris(pyrrolidinyl)phosphine (pyr = pyrrolidinyl) and its utilization in molybdenum- and rhodium-carbonyl complexes.[15] Infrared spectroscopic analysis of the ν(CO) values for these species indicated that the ligand possessed stronger donating properties compared to the similar phosphine initially employed, tris(pyrrolyl)phosphine (see Section **1.1.1.1**).[15] Synthesis of tris(pyrrolidinyl)phosphine was accomplished through the addition of excess pyrrolidine, which serves as a source of the pyrrolidinyl substituent and also to remove the HCl (as pyrrolidinium chloride), to a solution of PCl_3 (**Scheme 1.8A**).[15]

Scheme 1.8A: Synthetic route to the ligand $(pyr)_3P$[15]

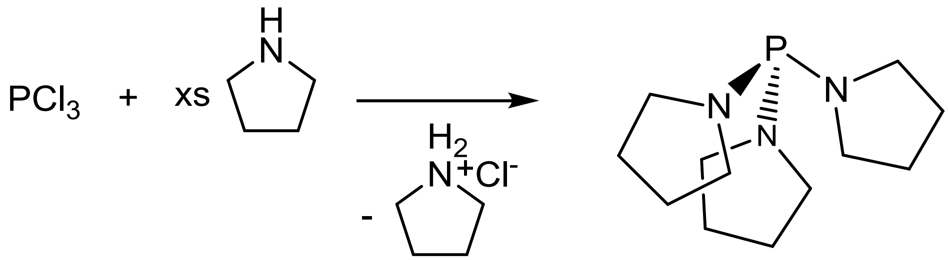

Woollins *et al*. studied the relative Lewis basicity of mono-, bis-, and tris(pyrrolidinyl)phosphines. Through a modification of Moloy's synthesis (**Scheme 1.8A**)[15] a chloroalkyl- or chloroarylphosphine, $R_{3-n}Cl_nP$ (n = 1 or 2), was used allowing for the corresponding mono- or bis(pyrrolidinyl)alkylphosphine or -arylphosphine, $R_{3-n}(pyr)_nP$, to be prepared (**Scheme 1.8B**).[1c]

Scheme 1.8B: Synthetic route to the ligand $R_{3-n}(pyr)_nP$[1c]

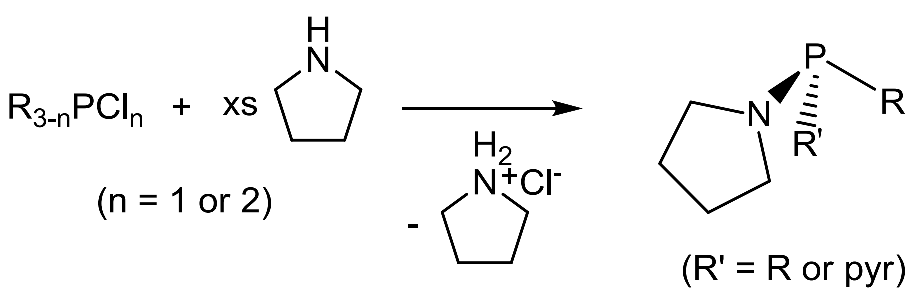

One of the approaches used to assess the donating potential of these phosphines was to examine their structural features in the solid state as part of metal complexes. As was observed previously in similar systems, planar nitrogen atoms, and M-P and P-N bond lengths should give some indication of the extent of nitrogen lone pair delocalization. The first examples involved X-ray crystallographic studies on the complexes $[((pyr)_3P)_2PtCl_2]$ and $[(Me(pyr)_2P)_2PtCl_2]$. The general structures are presented in **Figure 1.10**, **Figure 1.11** and **Figure 1.12**, with important bond lengths and angles of the crystal structures listed in **Table 1.6** and **Table 1.7**, respectively.[1b,c]

Figure 1.10: Structure for $[((pyr)_3P)_2PtCl_2]$[1b]

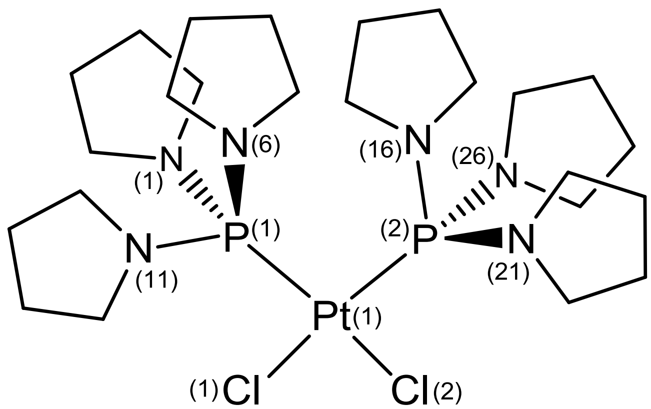

Table 1.6: Selected bond lengths and angles for $[((pyr)_3P)_2PtCl_2]$[1c]

Selected Bond Lengths (Å)		Selected Bond Angles (°)	
Pt(1)–P(1)	2.270(3)	P(1)–Pt(1)–Cl(1)	86.3(1)
Pt(1)–P(2)	2.246(3)	P(2)–Pt(1)–Cl(2)	90.4(1)
Pt(1)–Cl(1)	2.398(3)	Cl(2)–Pt(1)–Cl(1)	85.1(1)
Pt(1)–Cl(2)	2.371(3)	P(1)–Pt(1)–P(2)	98.2(1)
P(1)–N(1)	1.63(1)	sum of angles for N(1)	358.9
P(1)–N(6)	1.72(1)	sum of angles for N(6)	358.2
P(2)–N(11)	1.64(1)	sum of angles for N(11)	357.4
P(2)–N(16)	1.66(1)	sum of angles for N(16)	356.9
P(2)–N(21)	1.68(1)	sum of angles for N(21)	355.0
P(2)–N(26)	1.678(9)	sum of angles for N(26)	357.7

Figure 1.11: Structure of [(Me(pyr)$_2$P)$_2$PtCl$_2$][1b]

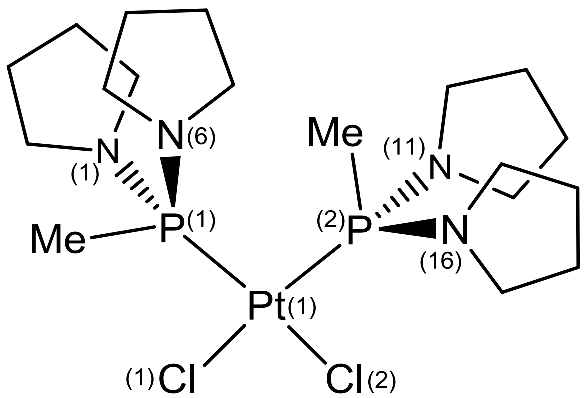

Table 1.7: Selected bond lengths and angles for [(Me(pyr)$_2$P)$_2$PtCl$_2$][1c]

Selected Bond Lengths (Å)		Selected Bond Angles (°)	
Pt(1)–P(1)	2.226(2)	P(1)–Pt(1)–Cl(1)	91.32(8)8
Pt(1)–P(2)	2.255(2)	P(2)–Pt(1)–Cl(2)	89.32(8)
Pt(1)–Cl(1)	2.372(2)	Cl(2)–Pt(1)–Cl(1)	86.14(8)
Pt(1)–Cl(2)	2.391(2)	P(1)–Pt(1)–P(2)	93.37(7)
P(1)–N(1)	1.652(7)	sum of angles for N(1)	356.6
P(1)–N(6)	1.675(7)	sum of angles for N(6)	353.3
P(2)–N(11)	1.643(6)	sum of angles for N(11)	359.5
P(2)–N(16)	1.676(6)	sum of angles for N(16)	353.5

The crystal structure of [(Me(pyr)$_2$P)$_2$PtCl$_2$] shows a similar square planar coordination environment to [((pyr)$_3$P)$_2$PtCl$_2$], with both displaying *cis*-chloride ligands. Looking at the Pt-P bond lengths, however, it is evident that [(Me(pyr)$_2$P)$_2$PtCl$_2$] displays slightly shorter bond lengths (2.226(2) and 2.255(2) Å), compared to [((pyr)$_3$P)$_2$PtCl$_2$] (2.270(3) and 2.246(3) Å) suggesting a greater extent of bonding between the phosphine ligand and the platinum metal in [(Me(pyr)$_2$P)$_2$PtCl$_2$]. The angle between the phosphines is notably larger in [((pyr)$_3$P)$_2$PtCl$_2$] (98.2(1)°) and the angle between the chlorides is consequently smaller, compared to [(Me(pyr)$_2$P)$_2$PtCl$_2$] (91.32(8)8°), suggesting that Me(pyr)$_2$P is less sterically demanding than (pyr)$_3$P. A correlation between the P-N bond lengths (1.643(6) Å, 1.652(7) Å, 1.675(7) Å, and

1.676(6) Å) and the extent of planarity about the nitrogen atoms (359.5°, 356.6°, 353.3°, and 353.5°, respectively), where the shorter bond length corresponds to the greater planarity, is also present for [(Me(pyr)$_2$P)$_2$PtCl$_2$], again illustrating the greater donation of the nitrogen lone pair. In contrast, [((pyr)$_3$P)$_2$PtCl$_2$] does not show as strong of a correlation.[1b,c]

The Woollins research group also reported on the synthesis and X-ray crystallographic studies of the complexes *trans*-[(^{t}Bu$_2$(pyr)P)$_2$RhCl(CO)] and *trans*-[(Cy$_3$P)$_2$RhCl(CO)], allowing for the solid state comparison of the two phosphines, since they both contain sterically demanding ligands, ^{t}Bu$_2$(pyr)P and Cy$_3$P, with strong donating properties.[1c] The general structure of these complexes are illustrated in **Figure 1.12** and **Figure 1.13**. Attempts to synthesize the analogous complex, *trans*-[(^{t}Bu$_3$P)$_2$RhCl(CO)], yielded the formation of a tetrahedral complex as a result of the great steric demand of the ^{t}Bu$_3$P ligands, thus an accurate comparison could not be made.

Figure 1.12: Structure of *trans*-[(^{t}Bu$_2$(pyr)P)$_2$RhCl(CO)][1c]

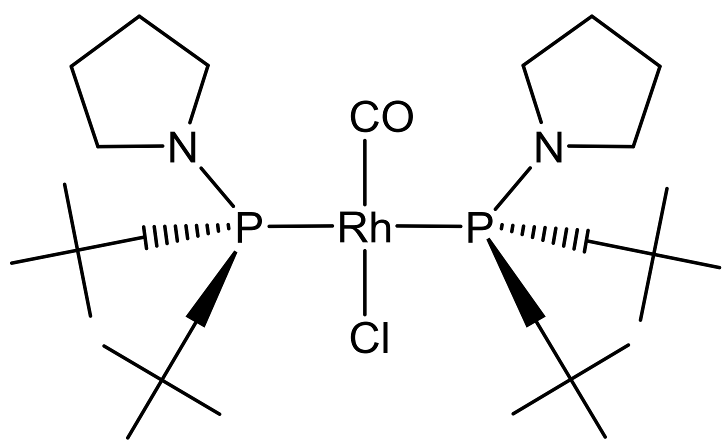

Figure 1.13: Structure of *trans*-[$(Cy_3P)_2RhCl(CO)$][1c]

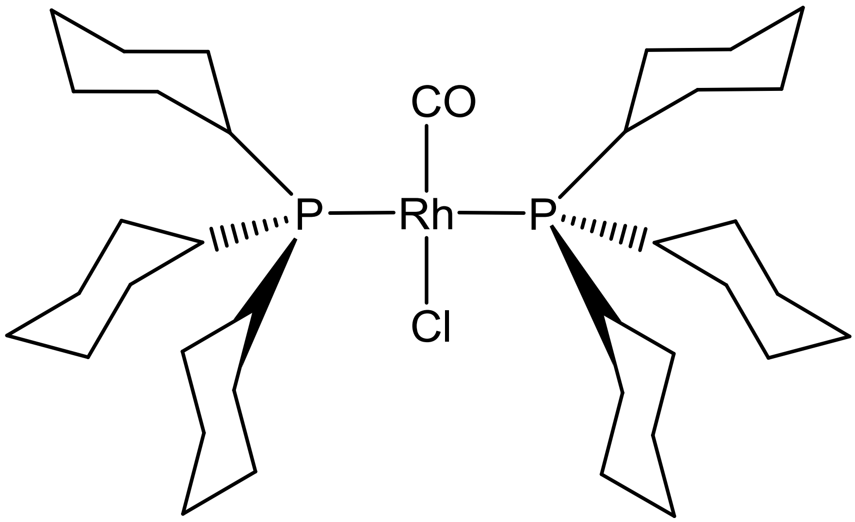

The rhodium centre in both complexes is square planar with little deviation from idealised geometry. The complex *trans*-[$(^{t}Bu_2(pyr)P)_2Rh(CO)Cl$] displays longer Rh-P bond lengths (2.370(1) Å and 2.375(1) Å), and shorter Rh-Cl and Rh-CO bond lengths (2.378(1) and 1.793(5) Å, respectively), compared to *trans*-[$(Cy_3P)_2Rh(CO)Cl$] (Rh-P bond lengths of 2.352(3) Å and 2.358(3) Å; and Rh-Cl and Rh-CO bond lengths of 2.422(4) Å and 1.93(1) Å, respectively), suggesting Cy_3P may be a stronger donating ligand. Interestingly, a steric interaction between the tertiary butyl substituent of $^{t}Bu_2(pyr)P$ and the carbon on the pyrrolidinyl substituent was observed, resulting in distortion of the pyrrolidine ring. It was tentatively suggested that the inability of the nitrogen atom to adopt a more symmetrical geometry may lead to a weaker N-P donor interaction, therefore, reducing the donor strength of the ligand.[1c]

Carbonyl stretching frequencies of metal-carbonyl-phosphine complexes perhaps provide more useful insight into phosphine donor properties. Using the complex *trans*-[$(R_3P)_2Rh(CO)Cl$] as a model complex, ν(CO) has been measured for a series of phosphines, including those bearing pyrrolidinyl substituents (**Table 1.8**).[1c,15]

Table 1.8: ν(CO) of analogous *trans*-[$(R_3P)_2Rh(CO)Cl$][1c,15]

(R_3P)	ν(CO) cm^{-1}	Cone Angle
Me_3P	1960	118
Et_3P	1956	132
Ph_3P	1965	145
Cy_3P	1943	170
$(pyr)_3P$	1952	145
$Me(pyr)_2P$	1947	136
$Ph(pyr)_2P$	1949	145
$^tBu(pyr)_2P$	1942	157
$^tBu_2(pyr)P$	1955	154
$^iPr_2(pyr)P$	1954	155

As can be seen from **Table 1.8**, for the more conventional phosphines, the position of ν(CO) follows the expected trend, with Ph_3P – the weakest donor in the series – showing the highest energy, and Cy_3P – the strongest donor – the lowest. Interestingly, the data for the bis(pyrrolidinyl)alkylphosphine and bis(pyrrolidinyl)arylphosphines, $R(pyr)_2P$ (R = Me, ^{t}Bu, of Ph), suggest they possess greater donating abilities compared to the conventional phosphines, with $^tBu(pyr)_2P$ displaying nearly the same results as Cy_3P. The steric nature of $Me(pyr)_2P$ and Et_3P is determined to be similar, with cone angles of 136° and 132°, respectively, yet $Me(pyr)_2P$ displays a significantly greater donating ability. These data suggest the specific combination of alkyl and pyrrolidinyl substituents in the bis(pyrrolidinyl)alkylphosphine ligands maximize their donor properties. For example, the ν(CO) values of the other pyrrolidinyl-substituted phosphines, $(pyr)_3P$ and $R_2(pyr)P$ (R = ^{t}Bu and ^{i}Pr), suggest they are comparatively poorer donors compared to the bis(pyrrolidinyl)alkylphosphine and bis(pyrrolidinyl)arylphosphines. The weaker nature of the $R_2(pyr)P$ phosphines may be attributed to the steric bulk of the R groups which prevent the nitrogen substituents from adopting an orientation that is conducive to a strong interaction with the phosphorus atom. In the case of the $(pyr)_3P$ phosphine, the third pyrrolidinyl substituent is likely unable to donate charge properly to the phosphorus atom, and thus merely serves as an electron-withdrawing substituent (**Figure 1.14**).[1b-d]

Figure 1.14: Proposed electronic properties of pyrrolidinyl-substituted phosphines[1b-d]

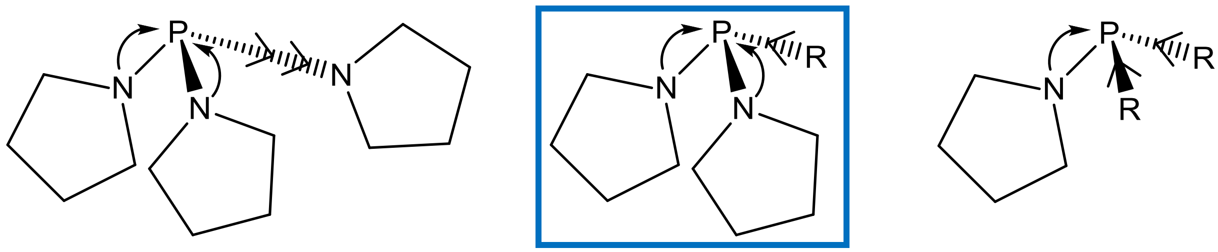

1.1.3 Summary of P-N Phosphine Ligands

Through a series of solid state and spectroscopic studies, phosphine ligands bearing a specific combination of saturated amino substituents, and alkyl or aryl substituents have been shown to exhibit enhanced donor properties. In addition, the general ease of synthesis of these aminoalkylphosphine ligands compared to the preparations required for more traditional phosphines, make this an attractive class of ligands for exploration. Applications of these aminoalkylphosphine ligands in the synthesis of a variety of metal-carbonyl complexes afforded a greater understanding of their coordination properties, and more importantly, their electronic properties. As well, spectroscopic and structural analyses of these complexes indicate these unique ligands likely possess an enhanced electron-donating ability compared to their conventional alkyl- and arylphosphine counterparts. Thus, these aminoalkylphosphine ligands possess considerable potential as highly Lewis basic ligands in metal-catalyzed homogeneous applications.

2. Research Intentions

The development and exploration of unique phosphorus-based ligands continues to play a prominent role in coordination and organometallic chemistry. This attention is attributed to the vast potential for structural and electronic modifications through the alteration of the ligand's substituents. As presented in the Introduction, one promising substituent variant is the pyrrolidinyl group, more specifically the combination of pyrrolidinyl and alkyl groups which yield bis(*N*-pyrrolidinyl)alkylphosphines. The moderate size of the pyrrolidinyl group and additional dative donation of the nitrogen lone pair to the phosphorus, together with the inductive donor properties of the alkyl group, leads to an overall enhancement of the donating properties of this phosphine ligand.[1b-d] While these ligands display promising electronic and structural properties, only a few examples of their coordination to transition metal complexes exist, none of which involve ruthenium. Ruthenium continues to receive an enormous amount of attention due to the high catalytic reactivity and versatility its complexes have displayed over the past decades.[23] Although ruthenium is known to coordinate a wide variety of ligands, facially bound ligands, such as cyclopentadienyl and arene ligands, represent a large portion of the ligands that have been explored in ruthenium chemistry. Ruthenium-Cp* complexes are some of the most effective catalysts utilized in a myriad of organic reactions[24] and have proven exceptionally useful in the activation of numerous bonds, with C-H, H-H, Si-H and B-H representing some of the primary examples.[25] Similarly, ruthenium-arene chemistry has been motivated by their catalytic activity in a vast array of synthetic applications, including: hydrogenation, hydrosilylation, dehydrohalogenation, borylation and cycloaddition, to name just a few.[26] For these reasons, this research focuses on two specific ruthenium piano-stool frameworks for the application of these ligands, specifically ruthenium-Cp* and ruthenium-*p*-cymene, both of which have proven fruitful due to the ease of the synthesis of precursor complexes, and the large body of applicable information that exists in the literature. Thus, the goals of the research are: (i) to design a synthetic route to the preparation and isolation of ruthenium piano-stool complexes incorporating these novel bis(pyrrolidinyl)alkylphosphines; (ii) examine the substitution chemistry of these new complexes; (iii) investigate the structural and electronic features of these complexes and, where possible, draw comparisons to traditional phosphine analogues; and (iv) assess the catalytic potential of these species using model reactions.

3. Experimental

3.1 General Considerations

The following experiments were performed under an inert atmosphere of prepurified N_2 using standard Schlenk line techniques unless otherwise indicated. The dry and N_2-purged solvents used (DCM, hexanes and benzene) were collected in N_2-purged, Teflon tapped Strauss flasks using a customized solvent delivery system utilizing aluminum oxide-dried, HPLC grade solvents. To ensure optimally dry and degassed solvents, each Strauss flask contained activated (heated to ~300 °C under vacuum for 24 hours) 4A molecular sieves, and the solvents were purged with N_2 for an additional 15-30 min after dispensing from the solvent delivery system. Other solvents were dried using conventional procedures and stored in Teflon tapped Strauss flasks: THF and diethyl ether, sodium metal; DCE and acetonitrile, 4A molecular sieves. Solvents were dispensed from the flasks with the use of syringes. All non-room temperature reaction mixtures were either cooled using isopropanol/N_2(*l*) cold baths or heated using oil baths as required. The drying and degassing of NMR solvents involved stirring the bottled solvent with appropriate drying agents ($CDCl_3$, $CaCl_2$; CD_2Cl_2, CaH_2; C_6D_6, sodium metal; CD_3CN, 4A molecular sieves) followed by vacuum distillation and a threefold freeze-pump-thaw degassing process, at which point the solvents were stored under N_2, in a Teflon tap sealed flask. All NMR data (^1H and ^{31}P) were acquired through the use of a Varian Unity INOVA 500MHz spectrometer, with sample chemical shifts in ppm referenced to residual protio solvent peaks (^1H) and external 85% H_3PO_4 (^{31}P). Elemental analyses were either acquired in-house by the Lakehead University Instrumentation Laboratory (LUIL) using a CEC 240XA analyser, or from Guelph Chemical Laboratories. The starting materials $[Cp^*RuCl]_4$,[27] $[Cp^*RuCl_2]_2$,[28] $[CpRuCl(PPh_3)_2]$,[29] and $[(p\text{-cymene})RuCl_2]_2$,[30] as well as the ligand $R(pyr)_2P$ (R = Me or ^{t}Bu)[1c] were prepared according to the literature procedures and were stored as solids under dynamic vacuum. Solid $RuCl_3{\bullet}xH_2O$ was purchased from Pressure Chemicals. All other reagents were purchased from Aldrich or Strem, used without further purification, and stored either under vacuum or nitrogen.

3.2 Synthesis of 1,2-bis(dipyrrolidin-1-ylphosphino)ethane (dpyrpe)

The ligand dpyrpe was prepared using a modified literature procedure.[1c] $Cl_2PCH_2CH_2PCl_2$ (2.00 g, 8.64 mmol) was added to a flame-dried Schlenk tube/dropping funnel assembly, followed by dry diethyl ether (40 mL). The solution was then cooled in an ice-water bath. Next, pyrrolidine (7.1 mL, 86.4 mmol) in dry diethyl ether (20 mL) was added dropwise to the cooled solution over *ca.* 5 minutes with vigorous stirring yielding copious amounts of white solid. The bath was removed and the mixture was allowed to stir for 4 hours. The mixture was then filtered through Celite into a flame-dried flask. Removal of the volatiles under reduced pressure yielded a free-flowing, extremely air-sensitive white solid. Yield: 2.72 g (85%). ^1H NMR (499.9 MHz, C_6D_6, 22°C): 3.15 (m, 16H, -CH_2NCH_2-), 2.06 (m, 4H, -PCH_2CH_2P-), 1.52 (m, 16H, -NCH$_2$CH_2CH_2CH$_2$-). $^{31}P\{^1H\}$ NMR (202.3 MHz, C_6D_6, 22°C): 72.8 (s, -*P*CH$_2$CH$_2$*P*-).

3.3 Synthesis of [Cp*Ru(Me(pyr)$_2$P)$_2$Cl], 1

3.3.1 Method A

To a hexane (10 mL) suspension of [Cp*RuCl]$_4$ (0.040 g, 0.037mmol) was added a 0.5M diethyl ether solution of Me(pyr)$_2$P (0.588 mL, 0.294 mmol). The mixture was allowed to stir for 1 hour, at which time the volatiles were removed *in vacuo* yielding a bright orange oily solid. The solid was redissolved in diethyl ether (4 mL) and placed into a cold bath (~ -60°C) to facilitate precipitation. After standing for several minutes, a microcrystalline bright orange solid had deposited. The supernatant was cannulated off, and the product was dried under reduced pressure. Yield: 0.072 g (76%). Anal. Calcd. For $C_{28}H_{53}N_4P_2ClRu$: C, 52.20; H, 8.29; N, 8.70. Found: C, 52.20; H, 8.40; N, 8.45. ^1H NMR (499.9 MHz; C_6D_6, 22°C): 3.20, 3.07, 2.90 (3 × m, 16H, -CH_2NCH_2-), 1.67 (s, 15H, Cp*), 1.60 (m, 22H, PCH_3 and -NCH$_2$CH_2CH_2CH$_2$-). $^{31}P\{^1H\}$ NMR (202.3 MHz, C_6D_6, 22°C): 106.5 (br s, –*P*(pyr)$_2$Me). VT $^{31}P\{^1H\}$ NMR (202.3 MHz; CD_2Cl_2, - 49°C): 101.1, 111.0 (dd, J = 68.8 Hz, –*P*(pyr)$_2$Me).

3.3.2 Method B

To a THF (10 mL) solution of [Cp*RuCl$_2$]$_2$ (0.050 g, 0.0814mmol) a 0.5M diethyl ether solution of Me(pyr)$_2$P (0.651 mL, 0.326 mmol) was added, followed by a ten-fold excess of zinc powder (0.053 g, 0.814 mmol) against a positive flow of nitrogen gas. The mixture was allowed to stir for 30 minutes, at which time the volatiles were removed *in vacuo* yielding a yellow/green oily solid. These solids were dissolved in CH_2Cl_2 (7 mL) and filtered through Celite. Upon removing the volatiles under reduced pressure, a bright orange oily solid was obtained. These solids were redissolved in diethyl ether (4 mL) and placed into a cold bath (~ -60°C) to facilitate precipitation. After standing for several minutes, a microcrystalline bright orange solid had deposited. The supernatant was cannulated off, and the product was dried under reduced pressure. Yield: 0.156 g (74.3%). The NMR spectroscopic data of the orange solid were identical to the product isolated using Method A.

3.3.3 Structural Characterization of 1 via X-ray Crystallography

Crystals of compound **1** were grown by slow evaporation of a concentrated diethyl ether solution over several days at room temperature. The crystal structure data were collected and processed by Dr. Ruiyao Wang of the Department of Chemistry, Queen's University. The crystals were mounted on a glass fibre with grease and cooled to -93°C in a stream of nitrogen gas controlled with a Cryostream Controller 700. Data collection was performed on a Bruker SMART APEX II X-ray diffractometer with graphite-monochromated Mo K_α radiation (λ = 0.71073 Å), operating at 50 kV and 30 mA over 2θ ranges of 3.46 ~ 52.00º. No significant decay was observed during the data collection in all cases. Data were processed using the Bruker AXS Crystal Structure Analysis Package[31]: Data collection: APEX2; cell refinement: SAINT; data reduction: SAINT; structure solution: XPREP and SHELXTL; structure refinement: SHELXTL. Neutral atom scattering factors were taken from Cromer and Waber.[32] The structures were solved by direct methods. Full-matrix least-square refinements minimizing the function $\Sigma w\,(F_o^2 - F_c^2)^2$ were applied to each compound. All non-hydrogen atoms were refined anisotropically. All of the H atoms were placed in geometrically calculated positions.

Table 3.1: Crystal data and structural refinement for 1

Empirical formula	$C_{28}H_{53}ClN_4P_2Ru$	
Formula weight	644.20	
Temperature	180(2) K	
Wavelength	0.71073 Å	
Crystal system	Monoclinic	
Space group	P2(1)/c	
Unit cell dimensions	a = 10.6418(4) Å	α= 90°
	b = 15.2543(5) Å	β= 103.287(2)°
	c = 19.1045(7) Å	γ = 90°
Volume	3018.28(19) $Å^3$	
Z	4	
Density (calculated)	1.418 Mg/m^3	
Absorption coefficient	0.738 mm^{-1}	
F(000)	1360	
Crystal size	0.15 × 0.10 × 0.06 mm^3	
Theta range for data collection	1.73 to 26.00°	
Index ranges	-13<=h<=10, -18<=k<=14, -23<=l<=23	
Reflections collected	25306	
Independent reflections	5922 [R(int) = 0.0225]	
Completeness to theta = 26.00°	100.0%	
Absorption correction	Multi-scan	
Max. and min. transmission	0.9570 and 0.8973	
Refinement method	Full-matrix least-squares on F^2	
Data / restraints / parameters	5922 / 0 / 331	
Goodness-of-fit on F^2	1.035	
Final R indices [I>2sigma(I)]	R1 = 0.0228, wR2 = 0.0604	
R indices (all data)	R1 = 0.0252, wR2 = 0.0622	
Largest diff. peak and hole	0.559 and -0.471 e.$Å^{-3}$	

3.4 Synthesis of [Cp*RuCl(dpyrpe)], 2

3.4.1 Method A

$(Cp^*RuCl)_4$ (0.175 g, 0.161 mmol) was dissolved in hexanes (10 mL). Next, the ligand dpyrpe (0.262 g, 0.708 mmol) in diethyl ether was added via syringe to the hexanes solution, and the mixture was allowed to stir for 1 hour. Next, the mixture was evaporated to dryness under reduced pressure, and then the orange product was washed with a small volume of hexanes (~2-3 mL). Yield: 0.372 g (90%). Anal. Calcd. for $C_{28}H_{51}ClN_4P_2Ru$: C, 52.4; H, 8.00; N, 8.72. Found:

C, 52.7; H, 7.80; N, 8.61. ^{1}H NMR (499.9 MHz, C_6D_6, 22°C): 3.18 (m, 8H, -CH_2NCH_2-), 3.11 (m, 4H, -PCH_2CH_2P-), 2.92 (m, 8H, -CH_2NCH_2-), 1.77-1.71 (m, 16H, -$NCH_2CH_2CH_2CH_2$-), 1.66 (s, 15H, Cp*). $^{31}P\{^{1}H\}$ NMR (202.3 MHz, C_6D_6, 22°C): 144.4 (s, -PCH_2CH_2P-).

3.4.2 Method B

$(Cp^*RuCl_2)_2$ (0.200 g, 0.325 mmol) was dissolved in THF (15 mL). Next, dpyrpe (0.241 g, 0.650 mmol) in diethyl ether was added via syringe, followed by excess zinc powder (0.200 g). The mixture was stirred for 30 minutes, and slowly became orange. The volatiles were then removed under reduced pressure, and the product was extracted with CH_2Cl_2 (2 × 10 mL) and filtered through Celite. Removal of the volatiles under reduced pressure yielded an orange solid. Yield: 0.381 g (91%). The NMR spectroscopic data of the orange solid were identical to the product isolated using Method A.

3.5 Synthesis of [CpRuCl(dpyrpe)], 3

$[CpRuCl(PPh_3)_2]$ (0.095 g, 0.131 mmol) was dissolved in toluene (5 mL). The ligand dpyrpe (0.049 g, 0.131 mmol) in diethyl ether was added via syringe, and the solution was refluxed for 2 hours. The yellow-orange solution was allowed to cool to room temperature, and then it was cannulae transferred to a second flask in order to separate it from a small amount of dark brown material that had deposited. The volatiles were removed under reduced pressure, and then the orange residue was redissolved in diethyl ether (4 mL). The solution was cooled to -78°C for several hours, after which time small orange microcrystals had deposited. The supernatant was cannulated off, and the crystals were dried under reduced pressure. Yield: 0.042 g (56%). Anal. Calcd. for $C_{23}H_{41}ClN_4P_2Ru$: C, 48.3; H, 7.22; N, 9.79. Found: C, 48.8; H, 6.95; N, 10.0. ^{1}H NMR (499.9 MHz, C_6D_6, 22°C): 4.85 (s, 5H, Cp), 3.51, 3.34, 2.84, 2.74 (4 × m, 16H, -CH_2NCH_2-), 2.28 (m, 4H, -PCH_2CH_2P-), 1.79, 1.50 (2 × m, 16H, -$NCH_2CH_2CH_2CH_2$-). $^{31}P\{^{1}H\}$ NMR (202.3 MHz, C_6D_6, 22°C): 149.8 (s, -PCH_2CH_2P-).

3.5.1 Structural Characterization of 3 via X-ray Crystallography

Crystals of compound **3** were grown or by slow evaporation of a concentrated diethyl ether solution over several days at room temperature. The crystal structure data were collected and processed by Dr. Ruiyao Wang of the Department of Chemistry, Queen's University. A crystal of the compound (orange, plate-shaped, size 0.25 x 0.15 x 0.08 mm) was mounted on a glass fibre with grease and cooled to -93 °C in a stream of nitrogen gas controlled with Cryostream Controller 700. Data collection was performed on a Bruker SMART APEX II X-ray diffractometer with graphite-monochromated Mo K_α radiation (λ = 0.71073 Å), operating at 50 kV and 30 mA over 2θ ranges of 4.02 ~ 52.00º. No significant decay was observed during the data collection. Data were processed on a PC using the Bruker AXS Crystal Structure Analysis Package:[31] Data collection: APEX2 (Bruker, 2006); cell refinement: SAINT (Bruker, 2005); data reduction: SAINT (Bruker, 2005); structure solution: XPREP (Bruker, 2005) and SHELXTL (Bruker, 2000); structure refinement: SHELXTL; molecular graphics: SHELXTL; publication materials: SHELXTL. Neutral atom scattering factors were taken from Cromer and Waber.[32] The crystal is monoclinic space group *C*2/c, based on the systematic absences, *E* statistics and successful refinement of the structure. The structure was solved by direct methods. Full-matrix least-square refinements minimizing the function $\sum w\,(F_o^2 - F_c^2)^2$ were applied to the compound. All non-hydrogen atoms were refined anisotropically. All H atoms were placed in geometrically calculated positions, with C-H = 0.95 (aromatic), and 0.99(CH_2) Å, and refined as riding atoms, with Uiso(H) = 1.2 UeqC. Convergence to final R_1 = 0.0240 and wR_2 = 0.0594 for 4495 (I>2σ(I)) independent reflections, and R_1 = 0.0269 and wR_2 = 0.0616 for all 4895 (R(int) = 0.0178) independent reflections, with 280 parameters and 0 restraints, were achieved.[33] The largest residual peak and hole to be 0.547 and – 0.401 e/Å^3, respectively.

Table 3.2: Crystal data and structural refinement for 3

Empirical formula	$C_{23}H_{41}ClN_4P_2Ru$	
Formula weight	572.06	
Temperature	180(2) K	
Wavelength	0.71073 Å	
Crystal system	Monoclinic	
Space group	C2/c	
Unit cell dimensions	a = 30.637(4) Å	α= 90°
	b = 10.7422(15) Å	β= 93.063(2)°
	c = 15.205(2) Å	γ = 90°
Volume	4996.9(12) Å^3	
Z	8	
Density (calculated)	1.521 Mg/m^3	
Absorption coefficient	0.882 mm^{-1}	
F(000)	2384	
Crystal size	0.25 × 0.15 × 0.08 mm^3	
Theta range for data collection	2.01 to 26.00°	
Index ranges	-34<=h<=37, -13<=k<=12, -18<=l<=18	
Reflections collected	12172	
Independent reflections	4895 [R(int) = 0.0178]	
Completeness to theta = 26.00°	99.8%	
Absorption correction	Multi-scan	
Max. and min. transmission	0.9328 and 0.8097	
Refinement method	Full-matrix least-squares on F^2	
Data / restraints / parameters	4895 / 0 / 280	
Goodness-of-fit on F^2	1.045	
Final R indices [I>2sigma(I)]	R1 = 0.0240, wR2 = 0.0594	
R indices (all data)	R1 = 0.0269, wR2 = 0.0616	
Largest diff. peak and hole	0.547 and -0.401 e.Å^{-3}	

3.6 Synthesis of [Cp*Ru(^{t}Bu(pyr)$_2$P)Cl], 4

To a 50 mL Schlenk tube [Cp*RuCl]$_4$ (0.040 g, 3.68×10^{-5} mol) was added and suspended in hexanes (5 mL). To this red brown mixture a 0.40M diethyl ether solution of ^{t}Bu(pyr)$_2$P (0.368 mL, 1.47×10^{-4} mol) was added and the blue solution stirred for 20 minutes. Following this time the volatiles were removed *in vacuo* from the solution leaving an indigo-blue solid. ^{31}P{^{1}H} NMR analysis revealed one main signal at δ = 98.8 ppm, representing ~70% of the mixture. The instability of **4**, leading to decomposition, precluded any attempts to purify. ^{1}H NMR (499.9 MHz; C_6D_6, 22°C): 2.85(m, 16H, -CH_2NCH_2-), 1.27 (m, 16H, -NCH$_2$CH_2CH_2CH$_2$-), 0.96 (s, 15H, Cp*), 0.94 (s, 9H, -PC(CH_3)$_3$). ^{31}P{^{1}H} NMR (202.3 MHz; CD_2Cl_2, 22°C): 98.8 (s, –*P*(pyr)$_2$^{t}Bu).

3.7 Synthesis of [Cp*Ru(MeCN)(Me(pyr)$_2$P)$_2$][BAr$^{f}_{4}$], 5a

Complex **1** (0.100 g, 0.155 mmol) and NaBAr$^{f}_{4}$ (0.138 g, 0.155 mmol) were combined and dissolved in mixture of diethyl ether (5 mL) and MeCN (5 mL). The mixture was allowed to stir for 1 hour, at which time the volatiles were removed *in vacuo* yielding a pale yellow solid. The solid was redissolved in CH_2Cl_2 (7 mL) and filtered through Celite. Upon removing the volatiles under reduced pressure, a light yellow solid was produced. The solid was triturated in hexanes (15 mL) for 1 hour. After standing for several minutes, a microcrystalline pale yellow solid had deposited. The supernatant was cannulated off, and the product was dried under reduced pressure. Yield: 0.202 g (86%). Anal. Calcd. For $C_{62}H_{68}BF_{24}N_5P_2RuCCH_2Cl_2$: C, 47.35; H, 4.42; N, 4.38. Found: C, 47.08; H, 4.23; N, 3.94. ^{1}H NMR (499.9 MHz; CD_3CN, 22°C): 7.64 (s, 8H, *o*-H of Ar^{f}), 7.48 (s, 4H, *p*-H of Ar^{f}), 3.08, 3.00, 2.78 (3 × m, 16H, -CH_2NCH_2-), 2.35 (s, 3H, CH_3CN), 1.86, 1.77, 1.70 (3 × m, 16H, -NCH$_2$CH_2CH_2CH$_2$-), 1.50 (s, 15H, Cp*), 1.42 (m, 6H, PCH_3). ^{31}P{^{1}H} NMR (202.3 MHz, CD_3CN, 22°C): 103.5 (s, *P*(pyr)$_2$Me).

3.8 Synthesis of [Cp*Ru(CO)(Me(pyr)$_2$P)$_2$][BAr$^{f}_{4}$], 5b

Complex **1** (0.100 g, 0.155 mmol) and NaBAr$^{f}_{4}$ (0.138 g, 0.155 mmol) were combined and suspended in hexanes (10 mL). The mixture was allowed to stir for 1 hour under CO, at which time the volatiles were removed *in vacuo* yielding an off-white solid. The solid was redissolved in CH_2Cl_2 (7 mL) and the solution was filtered through Celite. Upon removing the volatiles under reduced pressure, an off-white solid was produced. The solid was triturated in hexanes (15 mL) for 1 hour. After standing for several minutes, a microcrystalline solid had deposited. The supernatant was cannulated off, and the product was dried under reduced pressure. Yield: 0.200 g (85.8%). Anal. Calcd. For $C_{61}H_{65}BF_{24}N_4OP_2Ru$: C, 48.84; H, 4.37; N, 3.74. Found: C, 48.55; H, 4.38; N, 3.62. IR (Nujol, NaCl): ν(CO) = 1956.6 cm^{-1}. ^{1}H NMR (499.9 MHz; $CDCl_3$, 22°C): 7.62 (s, 8H, *o*-H of Ar^{f}), 7.45 (s, 4H, *p*-H of Ar^{f}), 2.98, 2.86 (2 × m, 16H, -

CH_2NCH_2-), 1.79 (m, 16H, -$NCH_2CH_2CH_2CH_2$-), 1.69 (s, 15H, Cp*), 1.59 (s, 6H, PCH_3).
$^{31}P\{^1H\}$ NMR (202.3 MHz, C_6D_6, 22°C) δ_P 100.3 (s, –P(pyr)$_2$Me).

3.9 Synthesis of [Cp*Ru(N$_2$)(Me(pyr)$_2$P)$_2$][BAr$^f_4$], 5c

Complex **1** (0.015 g, 0.0233 mmol) and NaBAr$^f_4$ (0.0.20 g, 0.0233 mmol) were combined in a sealable NMR tube and dissolved in C_6D_6 (0.5 mL) under N_2. The mixture was agitated for over a minute, after which time the yellow-orange contents were analyzed via ^{31}P and ^1H NMR spectroscopy. ^1H NMR (499.9 MHz; C_6D_6, 22°C): 7.58 (s, 8H, *o*-H of Ar^f), 7.42 (s, 4H, *p*-H of Ar^f) 2.94, 2.76 (2 × m, 16H, -CH_2NCH_2-), 1.72, 1.67 (2 × m, 16H, -$NCH_2CH_2CH_2CH_2$-), 1.50 (s, 15H, Cp*), 1.44 (m, 6H, PCH_3). $^{31}P\{^1H\}$ NMR (202.3 MHz, C_6D_6, 22°C): 98.5 (s, –P(pyr)$_2$Me).

3.10 Synthesis of [Cp*Ru(NCMe)(dpyrpe)][BAr$^f_4$], 6a

Complex **2** (0.103 g, 0.160 mmol) and NaBAr$^f_4$ (0.142 g, 0.160 mmol) were combined and dissolved in a mixture of CH_2Cl_2 (5 mL) and MeCN (5 mL). The mixture was allowed to stir for 2 hours. After this time, the cloudy, pale yellow mixture was filtered through Celite. Upon removing the volatiles under reduced pressure, a pale yellow solid was produced. The solid was redissolved in CH_2Cl_2 (~2 mL) and excess hexanes (20 mL) were added. After standing for several minutes, a microcrystalline yellow solid had deposited. The supernatant was cannulated off, and the product was dried under reduced pressure. Yield: 0.196 g (81%). Anal. Calcd. for $C_{62}H_{66}BF_{24}N_5P_2Ru\bullet 2CH_2Cl_2$: C, 45.7; H, 4.20; N, 4.17. Found: C, 45.5; H, 3.92; N, 4.10. ^1H NMR (499.9 MHz, $CDCl_3$, 22°C): 7.72 (s, 8H, *o*-H of Ar^f), 7.55 (s, 4H, *p*-H of Ar^f), 3.14 (br m, 4H, -PCH_2CH_2P-), 3.09, 3.00, 2.87 (3 × m, 16H, -CH_2NCH_2-), 2.11 (s, 3H, CH_3CN), 1.78 (m, 16H, -$NCH_2CH_2CH_2CH_2$-), 1.66 (s, 15H, Cp*). $^{31}P\{^1H\}$ NMR (202.3 MHz, $CDCl_3$, 22°C): 136.4 (s, -PCH_2CH_2P-).

3.10.1 Structural Characterization of 6a via X-ray Crystallography

Crystals of compound **6a** were grown by slow diffusion of hexanes into a concentrated CH_2Cl_2 solution over several days at room temperature. The crystal structure data were collected and processed by Dr. Ruiyao Wang of the Department of Chemistry, Queen's University. A crystal of the compound (yellow, block-shaped, size 0.30 x 0.25 x 0.15 mm) was mounted on a glass fibre with grease and cooled to -93 °C in a stream of nitrogen gas controlled with Cryostream Controller 700. Data collection was performed on a Bruker SMART APEX II X-ray diffractometer with graphite-monochromated Mo K_α radiation (λ = 0.71073 Å), operating at 50 kV and 30 mA over 2θ ranges of 4.28 ~ 52.00º. No significant decay was observed during the data collection. Data were processed on a PC using the Bruker AXS Crystal Structure Analysis Package:[31] Data collection: APEX2 (Bruker, 2006); cell refinement: SAINT (Bruker, 2005); data reduction: SAINT (Bruker, 2005); structure solution: XPREP (Bruker, 2005) and SHELXTL (Bruker, 2000); structure refinement: SHELXTL; molecular graphics: SHELXTL; publication materials: SHELXTL. Neutral atom scattering factors were taken from Cromer and Waber.[32] The crystal is monoclinic space group $P2_1$, based on the systematic absences, E statistics and successful refinement of the structure. The structure was solved by direct methods. Full-matrix least-square refinements minimizing the function $\sum w\,(F_o^2 - F_c^2)^2$ were applied to the compound. All non-hydrogen atoms were refined anisotropically. All H atoms were placed in geometrically calculated positions, with C-H = 0.95 (aromatic), and 0.99(CH_2) Å, and refined as riding atoms, with Uiso(H) = 1.5UeqC(CH_3) or 1.2 UeqC(other C). The phosphine ligand and the -CF_3 groups of the anion are disordered. SHELX commands, EADP, DFIX, EXYZ and SUMP were used to resolve the disorder. Convergence to final R_1 = 0.0442 and wR_2 = 0.1147 for 11960 ($I>2\sigma(I)$) independent reflections, and R_1 = 0.0482 and wR_2 = 0.1189 for all 12798 (R(int) = 0.0190) independent reflections, with 870 parameters and 22 restraints, were achieved.[34] The largest residual peak and hole to be 0.496 and – 0.494 e/Å^3, respectively.

Table 3.3: Crystal data and structural refinement for 6a

Empirical formula	$C_{62}H_{66}BF_{24}N_5P_2Ru$	
Formula weight	1511.02	
Temperature	180(2) K	
Wavelength	0.71073 Å	
Crystal system	Monoclinic	
Space group	P2(1)	
Unit cell dimensions	*a* = 12.8983(2) Å	α= 90°
	b = 13.5429(2) Å	β= 103.2460(10)°
	c = 19.4856(19) Å	γ = 90°
Volume	3313.20(9) $Å^3$	
Z	2	
Density (calculated)	1.515 Mg/m^3	
Absorption coefficient	0.396 mm^{-1}	
F(000)	1536	
Crystal size	0.30 × 0.25 × 0.15 mm^3	
Theta range for data collection	2.14 to 26.00°	
Index ranges	-15<=h<=11, -16<=k<=16, -24<=l<=24	
Reflections collected	30911	
Independent reflections	12798 [R(int) = 0.0190]	
Completeness to theta = 26.00°	99.9%	
Absorption correction	Multi-scan	
Max. and min. transmission	0.9430 and 0.8905	
Refinement method	Full-matrix least-squares on F^2	
Data / restraints / parameters	12798 / 22 / 870	
Goodness-of-fit on F^2	1.013	
Final R indices [I>2sigma(I)]	R1 = 0.0442, wR2 = 0.1147	
R indices (all data)	R1 = 0.0482, wR2 = 0.1189	
Absolute structure parameter	0.02(2)	
Largest diff. peak and hole	0.496 and -0.494 e.$Å^{-3}$	

3.11 Synthesis of [Cp*Ru(CO)(dpyrpe)][BAr^f_4], 6b

Complex **2** (0.154 g, 0.240 mmol) and $NaBAr^f_4$ (0.213 g, 0.240 mmol) were combined and dissolved in diethyl ether (10 mL) under CO. The mixture was allowed to stir for 1 hour under CO, and then it was filtered through Celite. Removal of the volatiles under reduced pressure yielded a pale yellow solid. Yield: 0.289 g (80%). Analytically pure samples were prepared by recrystallizing the solid from diethyl ether/hexanes via slow diffusion. Anal. Calcd. for $C_{61}H_{63}BF_{24}N_4OP_2Ru$: C, 48.9; H, 4.24; N, 3.74. Found: C, 48.9; H, 4.31; N, 3.59. IR (Nujol, NaCl): ν(CO) = 1960 cm^{-1}. ^{1}H NMR (499.9 MHz, $CDCl_3$, 22°C): 7.63 (s, 8H, *o*-H of Ar^f), 7.45 (s, 4H, *p*-H of Ar^f), 3.20 (br m, 4H, -$PC\mathit{H_2}C\mathit{H_2}P$-), 3.01, 2.94, 2.82 (3 × m, 16H, -$C\mathit{H_2}NC\mathit{H_2}$-), 1.90 (m, 8H, -$NCH_2C\mathit{H_2}C\mathit{H_2}CH_2$-), 1.81 (s, 15H, Cp*), 1.73 (m, 8H, -$NCH_2C\mathit{H_2}C\mathit{H_2}CH_2$-). ^{31}P{^{1}H} NMR (202.3 MHz, $CDCl_3$, 22°C): 130.4 (s, -$\mathit{P}CH_2CH_2\mathit{P}$-).

3.12 Synthesis of [Cp*Ru(N_2)(dpyrpe)][BAr^f_4], 6c

Complex **2** (0.085 g, 0.132 mmol) and $NaBAr^f_4$ (0.117 g, 0.132 mmol) were combined, dissolved in diethyl ether (10 mL) and stirred under N_2 for 30 minutes. The mixture was then filtered through Celite, and the volatiles were removed under reduced pressure to yield a yellow-orange solid. Yield: 0.144 g (73%). All attempts to recrystallize the product resulted in dinitrogen loss. IR (Nujol, NaCl): ν(N_2) = 2148 cm^{-1}. ^{1}H NMR (499.9 MHz, CD_2Cl_2, 22°C): 7.64 (s, 8H, *o*-H of Ar^f), 7.48 (s, 4H, *p*-H of Ar^f), 3.03 (m, 8H, -$C\mathit{H_2}NC\mathit{H_2}$-), 2.90 (m, 4H, -$PC\mathit{H_2}C\mathit{H_2}P$-), 2.79 (m, 8H, -$C\mathit{H_2}NC\mathit{H_2}$-), 1.80 (m, 8H, -$NCH_2C\mathit{H_2}C\mathit{H_2}CH_2$-), 1.73 (m, 8H, -$NCH_2C\mathit{H_2}C\mathit{H_2}CH_2$-), 1.68 (s, 15H, Cp*). ^{31}P{^{1}H} NMR (202.3 MHz, $CDCl_3$, 22°C): 131.2 (s, -$\mathit{P}CH_2CH_2\mathit{P}$-).

3.13 Synthesis of [Cp*RuH_2(dpyrpe)][BAr^f_4], 6d

Compound **2** (0.020 g, 0.0311 mmol) and $NaBAr^f_4$ (0.028 g, 0.0311 mmol) were combined in an NMR tube fitted with a rubber septum. The contents of the tube were evacuated and purged with H_2, and then Ar-purged CD_2Cl_2 (0.5 mL) was added via syringe. The mixture was allowed to mix (tumbling) for 30 minutes. NMR spectroscopy revealed clean and quantitative conversion to compound **6d**. ^{1}H NMR (499.9 MHz, CD_2Cl_2, 22°C): 7.72 (s, 8H, *o*-H of Ar^f), 7.55 (s, 4H, *p*-H of Ar^f), 3.15 (br m, 4H, -$PC\mathit{H_2}C\mathit{H_2}P$-), 3.02-2.93 (br m, 16H, -$C\mathit{H_2}NC\mathit{H_2}$-), 2.03 (s, 15H, Cp*), 1.91-1.83 (br m, 16H, -$NCH_2C\mathit{H_2}C\mathit{H_2}CH_2$-), -9.76 (t, $^2J_{PH}$ = 29 Hz, 2H, Ru-*H*). ^{31}P{^{1}H} NMR (202.3 MHz, CD_2Cl_2, 22°C): 135.6 (s, -$\mathit{P}CH_2CH_2\mathit{P}$-).

3.14 Synthesis of [Cp*Ru(CO)($MePPh_2$)$_2$][BAr^f_4], 7a

Cp*RuCl(PPh_3)$_2$ (0.100 g, 0.125 mmol) was dissolved in C_6H_6 (10 mL). To this solution, Ph_2PMe (47 μL, 0.250 mmol) was added via syringe. The mixture was then stirred for 1.5 hours.

After this time, the volatiles were stripped away under reduced pressure, $NaBAr^f_4$ (0.111 g, 0.125 mmol) was added, and then the flask was evacuated/purged with CO. Next, diethyl ether (10 mL) was added and the mixture was allowed to stir under CO for 1 hour. The murky, pale yellow mixture was then filtered through Celite and then the volatiles were stripped from the filtrate under reduced pressure. The product was triturated with hexanes (10 mL) for ~ 5 minutes yielding a pale yellow solid. Yield: 0.132 g (69%). An analytically pure sample was prepared by recrystallizing the product from diethyl ether/hexanes. Anal. Calcd. for $C_{69}H_{53}BF_{24}OP_2Ru{\bullet}Et_2O$: C, 54.7; H, 3.96. Found: C, 54.7; H, 3.53. IR (Nujol, NaCl): ν(CO) = 1951 cm^{-1}. ^{1}H NMR (499.9 MHz, $CDCl_3$, 22°C): 7.75 (s, 8H, *o*-H of Ar^f), 7.61-7.25 (m, 16H, Ph), 7.54 (s, 4H, *p*-H of Ar^f), 6.81 (m, 4H, Ph), 1.50 (s, 15H, Cp*), 1.37 (m, 6H, $PC\mathit{H_3}$). ^{31}P{^{1}H} NMR (202.3 MHz, $CDCl_3$, 22°C): 26.3 (s, $Ph_2\mathit{P}Me$).

3.15 Synthesis of [Cp*Ru(CO)(dppe)][BAr^f_4], 7b

Cp*RuCl(PPh_3)$_2$ (0.100 g, 0.125 mmol) and dppe (0.050 g, 0.125 mmol) were combined and stirred in C_6H_6 (10 mL) for 1.5 hours. After this time, the volatiles were stripped away under reduced pressure, $NaBAr^f_4$ (0.111 g, 0.125 mmol) was added, and then the flask was evacuated/purged with CO. Next, diethyl ether (10 mL) was added and the mixture was allowed to stir under CO for 1 hour. The murky, pale yellow mixture was then filtered through Celite and then the volatiles were stripped from the filtrate under reduced pressure. The product was triturated with hexanes (10 mL) for ~ 5 minutes yielding a pale yellow solid. Yield: 0.149 g (78%). An analytically pure sample was prepared by recrystallizing the product from diethyl ether/hexanes. Anal. Calcd. for $C_{69}H_{51}BF_{24}OP_2Ru$: C, 54.3; H, 3.37. Found: C, 54.5; H, 3.34. IR (Nujol, NaCl): ν(CO) = 1961 cm^{-1}. ^{1}H NMR (499.9 MHz, $CDCl_3$, 22°C): 7.73 (s, 8H, *o*-H of Ar^f), 7.56-747 (m, 20H, *p*-H of Ar^f and Ph), 7.18-7.15 (m, 4H, Ph), 2.57 (m, 4H, -$PC\mathit{H_2}C\mathit{H_2}P$-), 1.59 (s, 15H, Cp*). ^{31}P{^{1}H} NMR (202.3 MHz, $CDCl_3$, 22°C): 71.8 (s, -$\mathit{P}CH_2CH_2\mathit{P}$-).

3.16 Synthesis of [(*p*-cymene)Ru(Me(pyr)$_2$P)Cl_2], 8

To a CH_2Cl_2 (15 mL) solution of [(*p*-cymene)RuCl_2]$_2$ (0.300 g, 0.49 mmol) was added a 0.51 M diethyl ether solution of Me(pyr)$_2$P (1.92 mL, 0.98 mmol). The reaction was allowed to stir for 1 hour, after which time the volatiles were removed *in vacuo* yielding a red oily solid. The solid was triturated in hexanes (3 × 15 mL). After standing to allow for the settling of any suspended solids the supernatant was cannulated off and the light red product was dried under reduced pressure. Yield: 0.449 g (93%). Despite several attempts, satisfactory analyses could not be obtained. ^{1}H NMR (499.9 MHz; C_6D_6, 22°C): 5.31, 5.10 (2 × m, 4H, *H* of *p*-Cy), 3.11 (m, 8H, -C*H*$_2$NC*H*$_2$-), 2.93 (sept, 1H –C*H*(CH_3)$_2$ of *p*-Cy), 1.82 (s, 3H, -C*H*$_3$ of *p*-Cy), 1.78 (d, 3H, PC*H*$_3$), 1.54 (m, 8H, -NCH_2C*H*$_2$C*H*$_2$$CH_2$-), 1.15 (s, 6H –CH(C*H*$_3$)$_2$ of *p*-Cy). ^{31}P{^{1}H} NMR (202.3 MHz, C_6D_6, 22°C): 91.4 (s, –*P*(pyr)$_2$Me).

3.17 Synthesis of [(*p*-cymene)Ru(^{t}Bu(pyr)$_2$P)Cl$_2$], 9

To a CH_2Cl_2 (15 mL) solution of [(*p*-cymene)RuCl_2]$_2$ (0.250 g, 0.410 mmol) was added a 0.248 M diethyl ether solution of ^{t}Bu(pyr)$_2$P (3.3 mL, 0.82 mmol). The reaction was allowed to stir for 1 hour, after which time the volatiles were removed *in vacuo* yielding a dark red solid. The solid was washed with hexanes (3 × 15 mL). After standing to allow for the settling of any suspended solids the supernatant was cannulated off and the red product was dried under reduced pressure. Yield: 0.390 g (89%). Anal. Calcd. for $C_{22}H_{39}Cl_2N_2PRu$: C, 49.44; H, 7.35; N, 5.24. Found: C, 48.83; H, 6.71; N, 4.77. ^{1}H NMR (499.9 MHz; C_6D_6, 22°C): 5.58, 5.47 (2 × m, 4H, *H* of *p*-Cy), 3.34, 3.24 (2 × m, 8H, -C*H*$_2$NC*H*$_2$-), 2.81 (sept, 1H –C*H*(CH_3)$_2$ of *p*-Cy), 2.10 (s, 3H, -C*H*$_3$ of *p*-Cy), 1.72 (m, 8H, -NCH_2C*H*$_2$C*H*$_2$$CH_2$-), 1.39 (d, 9H, PC(C*H*$_3$)$_3$), 1.32 (d, 6H –CH(C*H*$_3$)$_2$ of *p*-Cy). ^{31}P{^{1}H} NMR (202.3 MHz, C_6D_6, 22°C): 105.88 (s, –*P*(pyr)$_2$^{t}Bu).

3.18 Synthesis of [(*p*-cymene)Ru(Me(pyr)$_2$P)(MeCN)$_2$][BAr$^f_4$]$_2$, 10

Complex **8** (0.150 g, 0.305 mmol) and NaBAr$^f_4$ (0.540 g, 0.610 mmol) were combined and dissolved in diethyl ether (5 mL) followed by the addition of MeCN (5 mL). The mixture was allowed to stir for 1 hour, after which time the orange solution was filtered through Celite. Following this the volatiles were removed *in vacuo* yielding an orange oily solid. The solid was triturated in hexanes (3 × 15 mL). The supernatant was cannulated off and the less oily orange red product was dried under reduced pressure. Yield: 0.60 g (88.2%). Anal. Calcd. for $C_{87}H_{63}B_2F_{48}N_4PRu$: C, 46.86; H, 2.85; N, 2.51. Found: C, 45.02; H, 3.17; N, 2.49. ^{1}H NMR (499.9 MHz; CD_3CN, 22°C): 7.62 (s, 8H, *o-H* of Ar^f), 7.59 (s, 4H, *p-H* of Ar^f), 5.80, 5.68, 5.61 (3 × m, 4H, *H* of *p*-Cy), 3.05, 2.98 (2 × m, 8H, -C*H*$_2$NC*H*$_2$-), 2.61 (sept, 1H –C*H*(CH_3)$_2$ of *p*-Cy), 2.17 (s, 6H, -NCC*H*$_3$), 1.97 (s, 3H, -C*H*$_3$ of *p*-Cy), 1.87 (d, 3H, PC*H*$_3$), 1.74 (m, 8H, -

$NCH_2C\mathit{H_2}C\mathit{H_2}CH_2$-), 1.16 (s, 6H –$CH(C\mathit{H_3})_2$ of *p*-Cy). $^{31}P\{^1H\}$ NMR (202.3 MHz, CD_3CN, 22°C): 86.40 (s, –*P*$(pyr)_2$Me).

3.19 Synthesis of [(*p*-cymene)Ru(^{t}Bu(pyr)$_2$P)(MeCN)$_2$][BAr$^f_4$]$_2$, 11

Complex **9** (0.075 g, 0.14 mmol) and $NaBAr^f_4$ (0.248 g, 0.28 mmol) were combined and dissolved in diethyl ether (5 mL) followed by the addition of MeCN (5 mL). The mixture was allowed to stir for 1 hour, after which time the orange solution was filtered through Celite. Following this the volatiles were removed *in vacuo* yielding an orange oily solid. The solid was triturated in hexanes (3 × 15 mL). The supernatant was cannulated off, and the less oily orange product was dried under reduced pressure. Yield: 0.254 g (80%). Anal. Calcd. for $C_{90}H_{69}B_2F_{48}N_4PRu$: C, 47.57; H, 3.06; N, 2.47. Found: C, 46.14; H, 3.17; N, 2.05. ^1H NMR (499.9 MHz; $CDCl_3$, 22°C): 7.70 (s, 8H, *o-H* of Ar^f), 7.54 (s, 4H, *p-H* of Ar^f), 5.87, 5.68, 5.49 (3 × m, 4H, *H* of *p*-Cy), 3.27, 3.14, 3.08, 3.01 (3 × m, 8H, -$C\mathit{H_2}NC\mathit{H_2}$-), 2.59 (sept, 1H –$C\mathit{H}(CH_3)_2$ of *p*-Cy), 2.37 (s, 3H, -$C\mathit{H_3}$ of *p*-Cy), 1.88 (s, 6H, 2 -$NCC\mathit{H_3}$), 1.79, 1.72 (2 × m, 8H, -$NCH_2C\mathit{H_2}C\mathit{H_2}CH_2$-), 1.35, 1.32 (d, 9H, $PC(C\mathit{H_3})_3$), 1.25 (m, 6H –$CH(C\mathit{H_3})_2$ of *p*-Cy). $^{31}P\{^1H\}$ NMR (202.3 MHz, C_6D_6, 22°C): 110.27 (s, 2 –*P*$(pyr)_2{}^t$Bu).

3.19.1 Structural Characterization of 11 via X-ray Crystallography

Crystals of **11** were grown in an NMR spectroscopy tube through slow evaporation of the mother liquor, CD_3Cl, over several days at room temperature. The crystal structure data were collected and processed by Dr. Ruiyao Wang of the Department of Chemistry, Queen's University. A crystal of the compound (yellow, plate-shaped, size 0.20 x 0.20 x 0.06 mm) was mounted on a glass fibre with grease and cooled to -93 °C in a stream of nitrogen gas controlled with Cryostream Controller 700. Data collection was performed on a Bruker SMART APEX II X-ray diffractometer with graphite-monochromated Mo K_α radiation (λ = 0.71073 Å), operating at 50 kV and 30 mA over 2θ ranges of 3.38 ~ 51.00º. No significant decay was observed during the data collection.

Data were processed on a PC using the Bruker AXS Crystal Structure Analysis Package:[31] Data collection: APEX2 (Bruker, 2006); cell refinement: SAINT (Bruker, 2005); data reduction: SAINT (Bruker, 2005); structure solution: XPREP (Bruker, 2005) and SHELXTL (Bruker, 2000); structure refinement: SHELXTL; molecular graphics: SHELXTL; publication materials: SHELXTL. Neutral atom scattering factors were taken from Cromer and Waber.[32] The crystal is triclinic space group P-1, based on the systematic absences, E statistics and successful refinement of the structure. The structure was solved by direct methods. Full-matrix least-square refinements minimizing the function $\sum w\,(F_o^2 - F_c^2)^2$ were applied to the compound. All H atoms were placed in geometrically calculated positions, with C-H = 0.95 (aromatic), 1.00 (aliphatic CH), 0.99(CH_2) and 0.98 (methyl) Å, and refined as riding atoms, with Uiso(H) = 1.5 Ueq(C) (methyl), and 1.2 Ueq(other C). The structure is severely disordered with the metal complex tilted in two ways(~66% to ~34%), and all of the -CF_3 groups and the solvent molecule $CHCl_3$ are also disordered. SHELX command PART, EADP, DFIX, SADI, SUMP and DELU were applied to resolve the disorder. Due to the disorder, some of the non-hydrogen atoms were refined isotropically, and the SQUEEZE subroutine of the PLATON[35] was used to squeeze out the disordered $CDCl_3$ solvent, which was present from the NMR spectroscopic analysis. One solvent accessible void per lattice was found, comprising a total volume of 256 $Å^3$ and contributing a total of 78 electrons. The void was thus assigned to 1.5 disordered chloroform, which contributes 1.5×58 = 87 electrons, and occupies about 120 $Å^3$ in space. The larger volume and the smaller electron density of the void may be a result of the disorder. The contributions have been included in all derived crystal quantities although the precise composition of the lattice solvate is somewhat speculative. Convergence to final R_1 = 0.1129 and wR_2 = 0.3140 for 8997 (I>2σ(I)) independent reflections, and R_1 = 0.1838 and wR_2 = 0.3631 for all 18356 (R(int) = 0.0900) independent reflections, with 1373 parameters and 1062 restraints, were achieved.[36] The largest residual peak and hole to be 1.137 and – 0.683 e/$Å^3$, respectively.

Table 3.4: Crystal data and structural refinement for 11

Empirical formula	$C_{90.75}H_{69.75}B_2Cl_{2.25}F_{48}N_4PRu$	
Formula weight	2361.68	
Temperature	180(2) K	
Wavelength	0.71073 Å	
Crystal system	Triclinic	
Space group	P-1	
Unit cell dimensions	a = 13.3368(5) Å	α= 84.521(2)°.
	b = 13.7235(5) Å	β= 89.077(2)°.
	c = 27.1327(9) Å	γ = 89.307(2)°.
Volume	4942.4(3) $Å^3$	
Z	2	
Density (calculated)	1.587 Mg/m^3	
Absorption coefficient	0.373 mm^{-1}	
F(000)	2363	
Crystal size	0.20 × 0.20 × 0.06 mm^3	
Theta range for data collection	1.69 to 25.50°	
Index ranges	-11<=h<=16, -16<=k<=16, -32<=l<=32	
Reflections collected	56457	
Independent reflections	18356 [R(int) = 0.0900]	
Completeness to theta = 25.50°	99.8%	
Absorption correction	Multi-scan	
Max. and min. transmission	0.9779 and 0.9291	
Refinement method	Full-matrix least-squares on F^2	
Data / restraints / parameters	18356 / 1062 / 1373	
Goodness-of-fit on F^2	1.094	
Final R indices [I>2sigma(I)]	R1 = 0.1129, wR2 = 0.3140	
R indices (all data)	R1 = 0.1838, wR2 = 0.3631	
Largest diff. peak and hole	1.137 and -0.683 e.$Å^{-3}$	

3.20 Synthesis of [(*p*-cymene)Ru(Me(pyr)$_2$P)(CO)Cl][BAr$^f_4$], 12

Complex **8** (0.050 g, 0.102 mmol) and NaBAr$^f_4$ (0.090 g, 0.102 mmol) were combined and purged with CO. These solids were dissolved in diethyl ether (10 mL) and the mixture was allowed to stir for 45 minutes under CO, after which time the orange-yellow mixture was filtered through Celite. Following this the volatiles were removed *in vacuo* yielding a bright orange yellow oily solid. The solid was triturated in hexanes (3 × 15 mL). The supernatant was cannulated off and the waxy orange yellow product was dried under reduced pressure. Yield: 0.107 g (77.8%). Despite several attempts, satisfactory analyses could not be obtained. ^{1}H NMR (499.9 MHz; $CDCl_3$, 22°C): 7.61 (s, 8H, *o-H* of Ar^f), 7.45 (s, 4H, *p-H* of Ar^f), 6.40, 6.12, 5.97, 5.88 (4 × d, 4H, *H* of *p*-Cy), 3.03, 2.96 (2 × m, 8H, -CH_2NCH_2-), 2.60 (sept, 1H –$CH(CH_3)_2$ of *p*-Cy), 2.09 (s, 3H, -CH_3 of *p*-Cy), 1.90 (d, 3H, PCH_3), 1.76 (m, 8H, -$NCH_2CH_2CH_2CH_2$-), 1.22, 1.15 (2 × d, 6H –$CH(CH_3)_2$ of *p*-Cy). Selected $^{13}C\{^{1}H\}$ NMR (125.7 MHz, CD_2Cl_2, 22°C): 193.38 (d, $^{2}J_{PC}$ = 27.78 Hz, Ru-*C*O). $^{31}P\{^{1}H\}$ NMR (202.3 MHz, $CDCl_3$, 22°C): 86.10 (s, –*P*$(pyr)_2$Me).

3.21 Synthesis of [(*p*-cymene)Ru(^{t}Bu(pyr)$_2$P)(CO)Cl][BAr$^{f}_{4}$], 13

Complex **9** (0.075 g, 0.14 mmol) and NaBAr$^{f}_{4}$ (0.124 g, 0.14 mmol) were combined and purged with CO. These solids were dissolved in diethyl ether (10 mL) and the mixture was allowed to stir for 45 minutes under CO, after which time the orange solution was filtered through Celite. Following this the volatiles were removed *in vacuo* yielding a bright orange oily solid. The solid was triturated in hexanes (3 × 15 mL). The supernatant was cannulated off and the waxy orange product was dried under reduced pressure. Yield: 0.099 g (76.2%). Despite several attempts, satisfactory analyses could not be obtained. ^{1}H NMR (499.9 MHz; $CDCl_3$, 22°C): 7.58 (s, 8H, *o-H* of Ar^f), 7.41 (s, 4H, *p-H* of Ar^f), 6.54, 6.20, 5.96, 5.88 (4 × d, 4H, *H* of *p*-Cy), 3.21, 3.02, 2.91 (3 × m, 8H, -CH_2NCH_2-), 2.51 (sept, 1H –$CH(CH_3)_2$ of *p*-Cy), 2.07 (s, 3H, -CH_3 of *p*-Cy), 1.72 (m, 8H, -$NCH_2CH_2CH_2CH_2$-), 1.17, 1.13 (d, 9H, $PC(CH_3)_3$), 1.25, 1.11 (2 × d, 6H –$CH(CH_3)_2$ of *p*-Cy). Selected $^{13}C\{^{1}H\}$ NMR (125.7 MHz, CD_2Cl_2, 22°C): 195.52 (d, $^{2}J_{PC}$ = 24.76 Hz, Ru-*C*O). $^{31}P\{^{1}H\}$ NMR (202.3 MHz, $CDCl_3$, 22°C): 115.64 (s, –*P*$(pyr)_2{}^{t}$Bu).

3.22 Catalytic Transfer Hydrogenation Reactions, Using Complex 10 and 11

The following describes a typical procedure used for the transfer hydrogenation of ketones using **10** and **11** as a catalyst. The catalyst (8 μmol, 0.2 mol %) was added to a flask under nitrogen. Next, 2-propanol (8 mL) was added via syringe, followed by the ketone (4 mmol). The mixture was heated to 86 ± 2 °C, and then it was treated with 0.1 M KOH in 2-propanol (2 mL), initiating the reaction (*t* = 0). At specific time intervals, an aliquot (200 μL) was removed from the mixture via syringe and filtered through a short pad of silica, using diethyl ether as an eluent. The eluate was spiked with 2-phenylethanol (4.8 μL) as a standard, and diluted to the mark in a volumetric flask (10 mL) using diethyl ether. The sample was then analyzed via GC. Each catalytic run was performed at least in duplicate.

4. Results and Discussion

The search for strongly donating phosphines is a common focus of many research groups, including the Spivak laboratory. One limitation often associated with this feature is the steric contribution. Some of the most strongly donating, conventional phosphines (*e.g.*, $^{t}Bu_3P$ or Cy_3P, and their bidentate equivalents) often also require a large volume of space in order to impart effectively their electronic properties. Alternatively, the pyrrolidinyl substituted phosphine ligands bis(pyrrolidinyl)alkylphosphine (**I**) and 1,2-bis(dipyrrolidinylphosphino)ethane (**II**) (**Scheme 4.1**) have shown promising electronic properties with only modest steric bulk. This is accomplished through the use of the pyrrolidinyl substituents on the phosphorus which enhance the Lewis basicity of the phosphine, most likely through an additional contribution of the nitrogen lone pair (*vide infra*), but still possess a steric characteristic similar to that of a phenyl substituent.[1b,c] Two alkyl variations of ligand **I** ($Me(pyr)_2P$ = **Ia**; $^{t}Bu(pyr)_2P$ = **Ib**; pyr = pyrrolidinyl) were examined in this project in order to monitor the effect of alkyl group size on the synthesis and chemistry of the ruthenium complexes to which they are coordinated. Since both the Me and ^{t}Bu substituents contribute somewhat similar electronic properties to the phosphine, it is expected that both **Ia** and **Ib** will also possess close Lewis basicities. This allows for a better assessment of the steric demand of these phosphines and their role in the chemistry of the Cp* and *p*-cymene containing Ru-complexes examined in this project. In addition, ligand **II**, $(pyr)_2PCH_2CH_2P(pyr)_2$ (1,2-bis(dipyrrolidinylphosphino)ethane, abbreviated *dpyrpe*) was prepared as the bidentate equivalent of ligand **Ia** in order to compare and contrast the chemistry observed for a bis(monophosphine) complex and its bidentate analogue.

Through a modification of an established procedure[1c] the pyrrolidinylalkylphosphine ligands were synthesized in excellent yields. Ligand **I** was prepared by adding excess pyrrolidine (5 equivalents) to a diethyl ether solution of the respective dichloroalkylphosphine ($MePCl_2$ or $^{t}BuPCl_2$). The pyrrolidine serves as a source of the pyrrolidinyl substituent, and also to remove the HCl (as pyrrolidinium chloride) that is generated during the reaction. Upon work-up, viscous, extremely air-sensitive oils are obtained in yields of 87% (**Ia**) and 84% (**Ib**). Similarly, ligand **II** (dpyrpe) was synthesized from $Cl_2PCH_2CH_2PCl_2$ and 10 equivalents of pyrrolidine, producing a free-flowing, extremely air-sensitive white solid, in 85% yield. Despite the extreme air- and moisture-sensitivity, ligands **I** and **II** are stable indefinitely under an inert atmosphere.

Scheme 4.1: Synthesis of ligands I and II[1c]

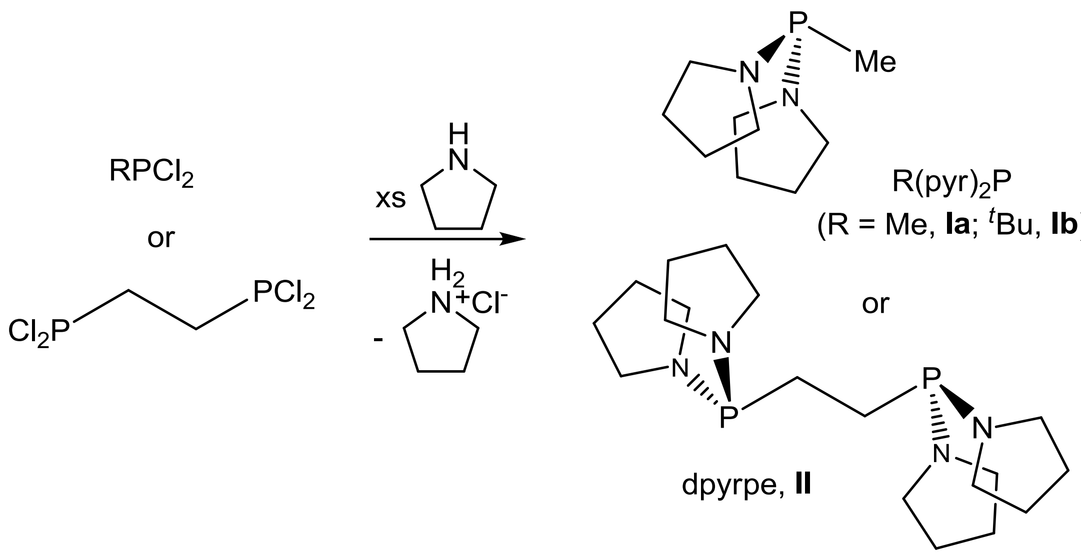

The $^{31}P\{^1H\}$ NMR spectra of ligands **Ia**, **Ib** and **II** reveal sharp singlets at δ = 74.1 , 99.4 and 72.8 ppm, respectively. The $^{31}P\{^1H\}$ NMR chemical shifts of the analogous, more conventional phosphines $MePh_2P$, $^tBuPh_2P$, and dppe (see section **4.1.2**) are quite different from the bis(pyrrolidinyl)alkylphosphines at δ = 26 ppm,[37a] -17.1 ppm,[37a] and -12.6 ppm,[37b] respectively, suggesting the pyrrolidinyl substituents impart a strong electronic effect on the phosphorus. The chemical shifts observed for ligands **Ia** and **II** are quite similar, differing only by 1.3 ppm, which perhaps is not surprising considering **II** is essentially two units of **Ia** joined through the methyl substituents (*i.e.*, the ethane bridge). In stark contrast, the chemical shift of $MePPh_2$ differs from its bidentate equivalent dppe by almost 39 ppm. Additional similarities have also been observed between **Ia** and **II** in their ^1H NMR spectra. For example, ligand **Ia** reveals signals at δ = 2.82 and 1.30 ppm for the pyrrolidine ring hydrogens in positions C-2/C-5 and C-3/C-4, respectively,[1c] while for ligand **II** these same signals appear at δ = 3.15 and 1.52. For ligand **Ib** the pyrrolidinyl hydrogen atoms appear slightly downfield (δ = 3.42 and 1.92 ppm).[1c] The extreme sensitivity of these ligands to moisture and air made it difficult to obtain microanalytical data. Nonetheless, the ligands were routinely obtained in high spectroscopic purity.

Further examination of their steric and electronic contributions was achieved through the synthesis of a series of ruthenium piano-stool complexes incorporating either Cp*,Cp or *p*-

cymene as ancillary ligands. Analysis of these compounds through ^{1}H and $^{31}P\{^{1}H\}$ NMR spectroscopy and, where possible, X-ray crystallography was fundamental in understanding the properties of these phosphines.

4.1 Synthesis of [Cp*Ru(PP)Cl], (PP = $[Me(pyr)_2P]_2$, 1; dpyrpe, 2)

The coordination chemistry of ligands **I** and **II** was examined through the synthesis of a series of ruthenium piano-stool complexes beginning with conveniently available starting complexes. For example the introduction of appropriate equivalents of ligand **Ia** or **II** to a hexane suspension of $[Cp^*RuCl]_4$[27] resulted in cleavage of the chloride bridge of the tetrameric starting material, yielding spectroscopically pure, moderately air stable, orange solids of $[Cp^*Ru(Me(pyr)_2P)_2Cl]$ (**1**) and [Cp*Ru(dpyrpe)Cl] (**2**) upon workup, in yields of 76% and 90%, respectively (**Scheme 4.2**).

Scheme 4.2: Strategies utilized in synthesizing complexes 1 and 2

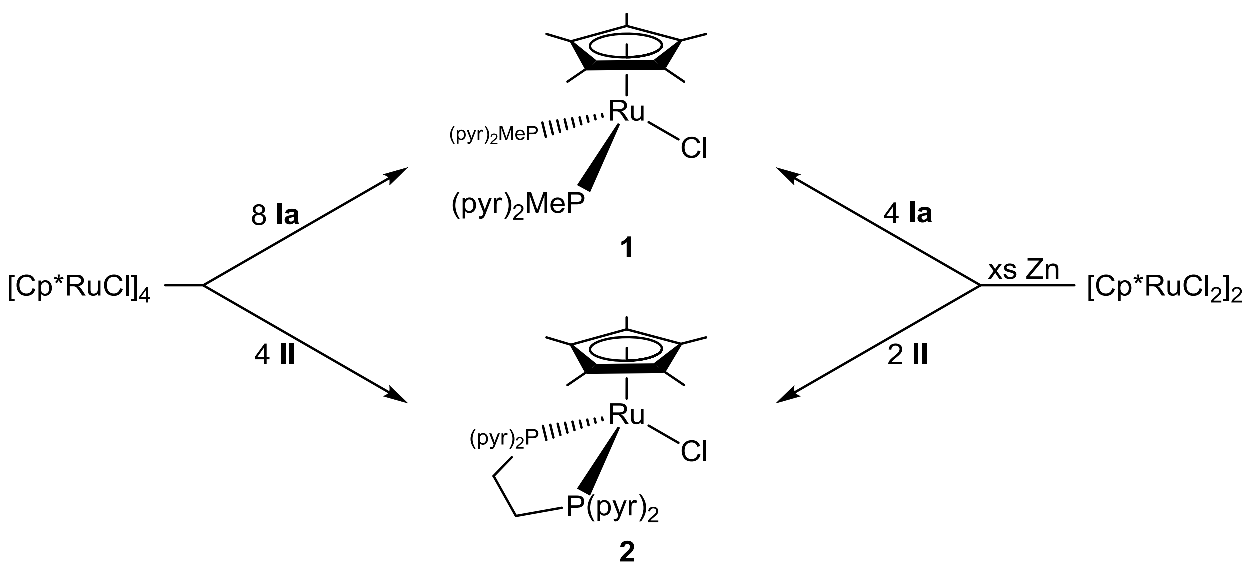

An alternative synthetic route was also explored (**Scheme 4.2**) in an effort to find perhaps a more convenient, and better yielding synthetic route to complexes **1** and **2**. Thus, reducing the dimeric complex $[Cp^*RuCl_2]_2$ using excess zinc[38] in the presence of either ligand **Ia** or **II** does lead to the desired products **1** and **2**, respectively, in slightly better yields. However, the products obtained through this particular method proved to be far less stable, and turned brown within days, even when stored under reduced pressure. Despite being spectroscopically pure, elemental analyses of the products synthesized via this alternate route often revealed they were not analytically pure, despite attempts to purify them. One possible explanation is the presence of additional zinc containing impurities which could not be removed through extraction or recrystallization during workup.[38]

The $^{31}P\{^{1}H\}$ NMR spectrum of complex **1** revealed a broad singlet centred at $\delta = 106.5$ ppm (**Figure 4.1**) whereas **2** showed a sharp singlet at $\delta = 144.4$ ppm, both of which are far downfield from the corresponding free phosphine chemical shifts of $\delta = 74.1$ and 72.8 ppm, respectively.[1] The broadness of the signal in the $^{31}P\{^{1}H\}$ NMR spectrum of **1** suggests the presence of a dynamic process about the complex (see Section **4.1.1**). The ^{1}H NMR spectra of **1** revealed pyrrolidinyl signals between $\delta = 2.90$-3.20 ppm corresponding to the hydrogens on positions C-2 and C-5 of the pyrrolidinyl rings, and at $\delta = 1.60$ ppm, corresponding to the hydrogens on positions C-3 and C-4; the latter signal overlapped the signal pertaining to the methyl group on the phosphine. The Cp* signal appeared at $\delta = 1.67$ ppm (sharp singlet). The ^{1}H NMR spectrum of **2** was similar, with the C-2 and C-5 hydrogens appearing between $\delta = 2.92$-3.18 ppm, and the C-3 and C-4 hydrogens appearing between $\delta = 1.71$-1.77 ppm. The Cp* signal appeared at $\delta = 1.67$ ppm (sharp singlet), while the hydrogens of the ethane bridge were identified as a multiplet further downfield at $\delta = 3.11$ ppm. Elemental analyses were acquired for **1** and **2**, which confirmed the elemental composition for both.

Figure 4.1: $^{31}P\{^1H\}$ NMR spectrum of complex 1 (broad signal)

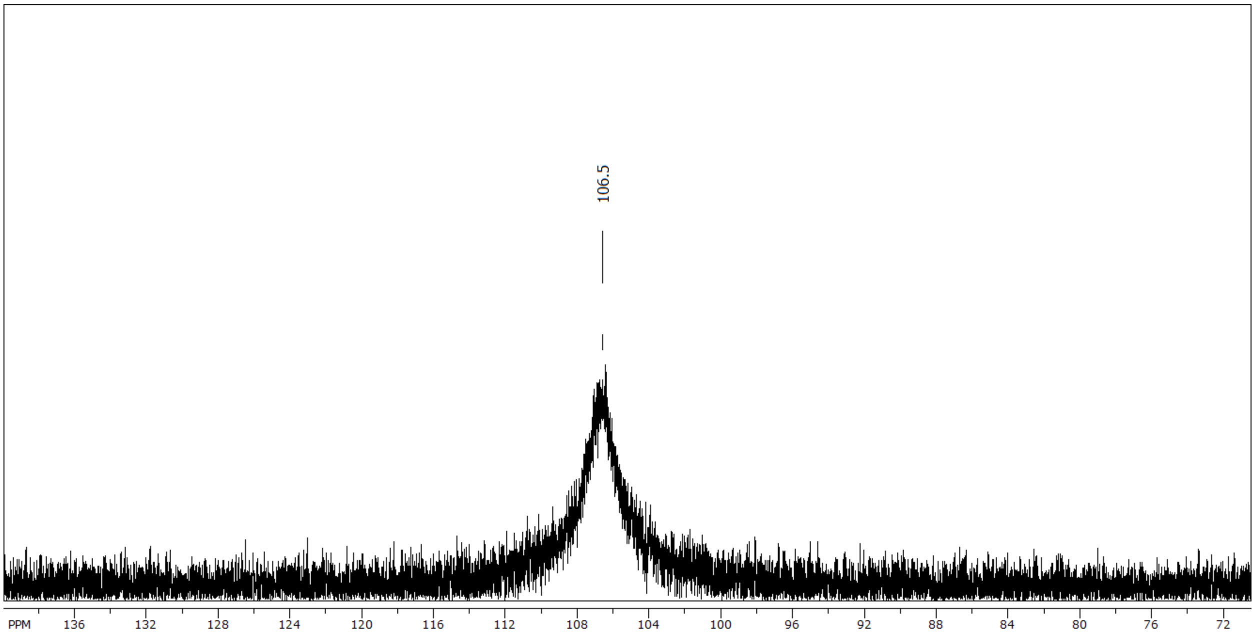

4.1.1 Variable Temperature NMR Analysis of 1

The broad signal present in the $^{31}P\{^1H\}$ NMR spectrum of **1** was intriguing. In order to further understand the origin of the broadness of this signal, variable temperature NMR analysis was employed. At room temperature the $^{31}P\{^1H\}$ NMR spectrum of **1** shows a broad signal at δ = 106.5 ppm (**Figure 4.1**), however, as the temperature is decreased the peak begins to broaden. By -10 °C the signal begins to decoalesce into two broad signals. As the temperature is decreased further a greater separation and increased definition of the signals is observed. Finally, at -49 °C an AB spin pattern consisting of two equally intense sharp doublets at δ = 111.0 ppm and δ = 101.1 ppm ($^2J_{PP}$ = 69 Hz) is observed. When the temperature is slowly increased back to room temperature and eventually up to 60 °C, the signals once again merge, producing a sharp singlet at δ = 106.8 ppm at elevated temperatures (**Figure 4.2**).

These results are consistent with hindered rotation about the M-P bonds on the NMR time scale,[39] giving rise to rotational isomers at lower temperatures. At low temperatures, each phosphine ligand adopts a different conformation, such as those illustrated in **Figure 4.3** (rotamers **A/A'** of **1**), thus producing an AB spin pattern in the $^{31}P\{^1H\}$ NMR spectrum.

Figure 4.2: Variable Temperature $^{31}P\{^1H\}$ NMR spectrum of 1

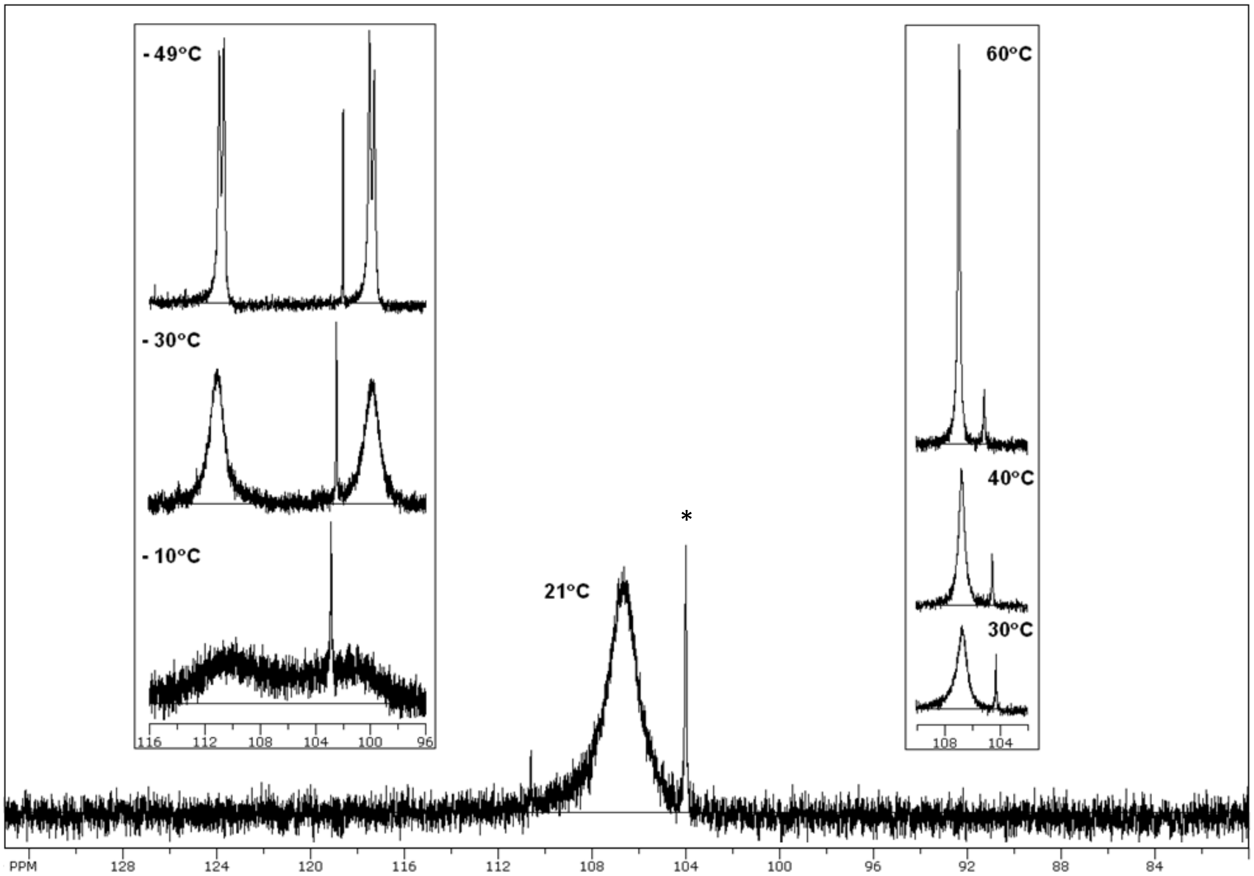

*Signal at δ = 104 ppm is a residual impurity.

Figure 4.3: Possible rotamers A/A' or 1 present at lower temperatures

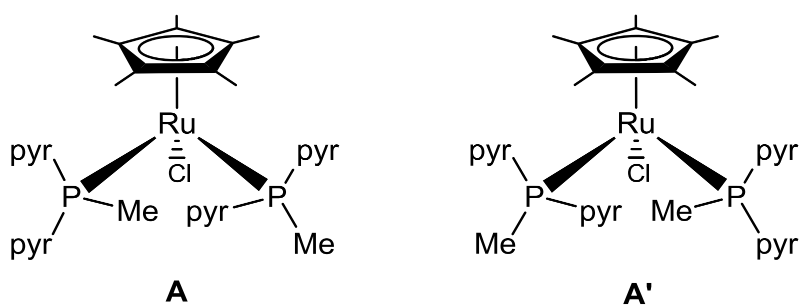

4.1.2 Synthesis of [CpRuCl(dpyrpe)], 3, and X-ray Structural Analyses of 1 and 3

To further understand the geometric nature of these phosphines, an X-ray crystallographic study of single crystals of **1** was conducted. Crystals of **1** were acquired through the slow evaporation of a concentrated diethyl ether solution over several days at room temperature. Dr. Ruiyao Wang of the Department of Chemistry at Queen's University acquired the X-ray crystallographic data, and solved the structure. The solid state structure of **1** is illustrated in **Figure 4.4** and selected bond lengths and angles are given in **Table 4.1**.

Complex **1** displays the typical piano-stool structure observed for ruthenium-Cp and -Cp* complexes. The substituents on each phosphine ligand are staggered asymmetrically with respect to one another, similar to the rotamers **A/A'** illustrated in **Figure 4.3**. The four pyrrolidinyl substituents of the phosphine atoms are positioned around their respective P-N bond in a staggered fashion, such that the nitrogen lone pair is directed away from the phosphorus lone pair (*i.e.*, the Ru-P bond).

Figure 4.4: Solid state X-ray structure of 1 (hydrogens omitted for clarity)

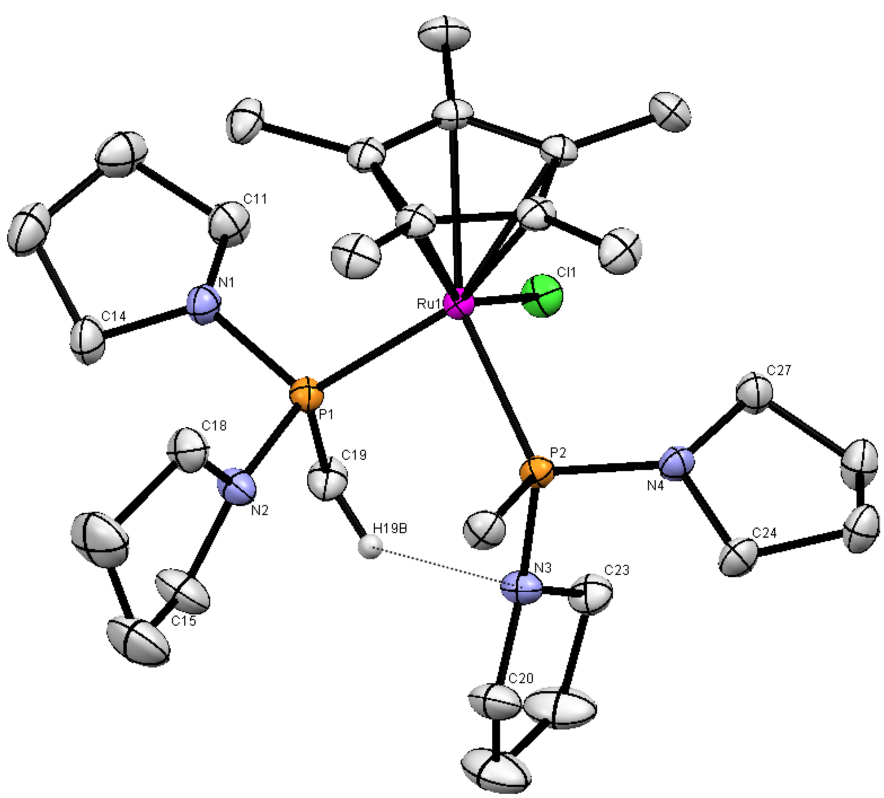

Table 4.1: Selected bond lengths and angles for 1

Selected Bond Lengths (Å)		Selected Bond Angles (°)	
Ru(1)-P(1)	2.2893(4)	P(1)-Ru(1)-P(2)	89.78(2)
Ru(1)-P(2)	2.2797(5)	P(1)-N(1)-C(11)	118.6(1)
Ru(1)-Cl(1)	2.4530(5)	P(1)-N(1)-C(14)	123.1(1)
P(1)-N(1)	1.707(2)	C(11)-N(1)-C(14)	104.8(2)
P(1)-N(2)	1.683(2)	P(1)-N(2)-C(15)	126.1(1)
P(2)-N(3)	1.709(2)	P(1)-N(2)-C(18)	120.2(1)
P(2)-N(4)	1.691(1)	C(18)-N(2)-C(15)	110.3(2)
N(3)-C(19)	3.263(2)	P(2)-N(4)-C(24)	122.0(1)
N(3)-H(19B)	2.510*	P(2)-N(4)-C(27)	122.8(1)
Ru(1)-centroid	1.899*	C(24)-N(4)-C(27)	109.8(1)
		P(2)-N(3)-C(20)	126.5(1)
		P(2)-N(3)-C(23)	118.0(1)
		C(20)-N(3)-C(23)	108.5(2)

*Calculated

Among the pyrrolidinyl rings, three display nitrogens approaching planarity (N(2), N(3), and N(4)), with the sum of the angles about each nitrogen ranging between 353-357°. The proximity of N(3) and the methyl substituent on the adjacent phosphine ligand, specifically the C(19) and H(19B) atoms, indicate the presence of a possible weak intramolecular hydrogen bond. Looking at both the N(3)-C(19) distance (3.263(2) Å) and the N(3)-H(19B) distance (calculated at 2.510 Å), it is evident that they are both shorter than the sum of the van der Waal radii for nitrogen-carbon (3.41 Å) and nitrogen-hydrogen (2.74 Å), indicating an intramolecular interaction.[40] This additional interaction likely contributes to the hindered rotation of the phosphine ligands (see **Section 4.1.1** above). The fourth nitrogen, N(1), however, reveals some distortion towards a geometry intermediate between tetrahedral and planar (sum of the angles around N(1) = 347°). It was expected that this may be a result of an intramolecular interaction, as seen with N(3), however, the shortest intramolecular N-H contact distance between this nitrogen, N(1), and the nearest non-pyrrolidinyl hydrogen atom, is 2.81 Å, which is greater than the sum of the van der Waal radii for nitrogen and hydrogen. Thus, the pyramidalization of N(1) in the solid state is likely not due to any secondary N-H interaction. The nearly planar geometries about N(2), N(3), and N(4) of the pyrrolidinyl rings may be the result of an additional dative bond or π-donation of the nitrogen lone pair into a vacant phosphorus-based orbital, as illustrated in **Figure 4.5**.

Figure 4.5: Possible additional bonding modes in P-N of pyrrolidinyl substituents

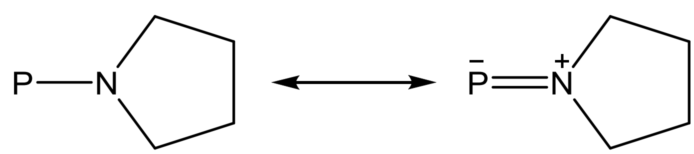

B C

The distances observed in the four P-N bonds of the pyrrolidinyl substituents range between 1.6833(16)-1.7087(16) Å, with the more planar nitrogen atoms yielding the shorter distances. Thus, a decrease in the tetrahedral nature of the nitrogen may allow an additional interaction with vacant phosphorus-based orbitals. Other systems bearing analogous ligands have also exhibited similar phenomena.[1] These results may suggest that this type of ligand, and hybrid aminoalkylphosphine ligands in general, possess greater Lewis basicities in relation to their hydrocarbyl counterparts. Sterically, $Me(pyr)_2P$ displays similarities to aryl containing phosphines. The Ru-P distances, at 2.2893(4) Å and 2.2797 (5) Å and P-Ru-P bond angle of 89.78(2)° in **1** are comparable to those determined for [Cp*RuCl(Ph_2PH)$_2$] (2.282(1) Å and 2.277(1) Å), 90.68(4)°,[41] suggesting that the steric contribution of the pyrrolidinyl group is similar to that of the phenyl group.[15] The cone angle of $Me(pyr)_2P$ has been estimated to be similar to that of $MePh_2P$, at 136°,[1c] whereas the cone angle of HPh_2P has been estimated to be 128°,[5] thus the cone angle of ligand **Ia** likely falls within this range.

Attempts were also made to grow single crystals of complex **2** so that comparisons could be made with ligand **II**; however, the high solubility of **2** in even the most non-polar solvents thwarted our efforts. Alternatively, the Cp analogue of **2** was readily prepared via thermal displacement of the PPh_3 ligands in CpRuCl(PPh_3)$_2$ to yield [CpRuCl(dpyrpe)], **3** (**Scheme 4.3**).

Scheme 4.3: Synthesis of complex 3

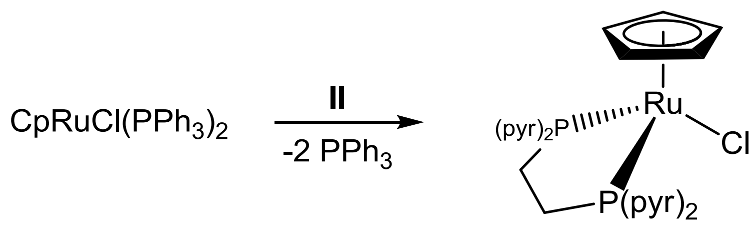

The identity of **3** was confirmed through NMR spectroscopic analysis and microanalytical data. A sharp singlet was observed in the $^{31}P\{^1H\}$ NMR spectrum of **3** at δ = 149.8 ppm, which again is far downfield from the corresponding free phosphine chemical shift at δ = 72.8 ppm. The ^1H NMR spectrum of **3** revealed the Cp signal at δ = 4.85 ppm (sharp singlet). The pyrrolidinyl signals appeared as multiplets between δ = 3.51-2.74 ppm corresponding to the hydrogens on positions C-2 and C-5 of the pyrrolidinyl rings, and at δ = 1.79 and 1.50 ppm, corresponding to the hydrogens on positions C-3 and C-4. Finally, the hydrogens of the ethane bridge were identified as a multiplet at δ = 2.28 ppm.

Single crystals of **3** were grown via slow evaporation of a concentrated diethyl ether solution at room temperature. The X-ray crystallographic data were collected, and the solid state structure was solved by Dr. Ruiyao Wang in the Department of Chemistry at Queen's University. The solid state crystal structure is illustrated in **Figure 4.6** and selected bond lengths and angles are given in **Table 4.2**.

Figure 4.6: Solid state X-ray structure of 3 (hydrogens omitted for clarity)

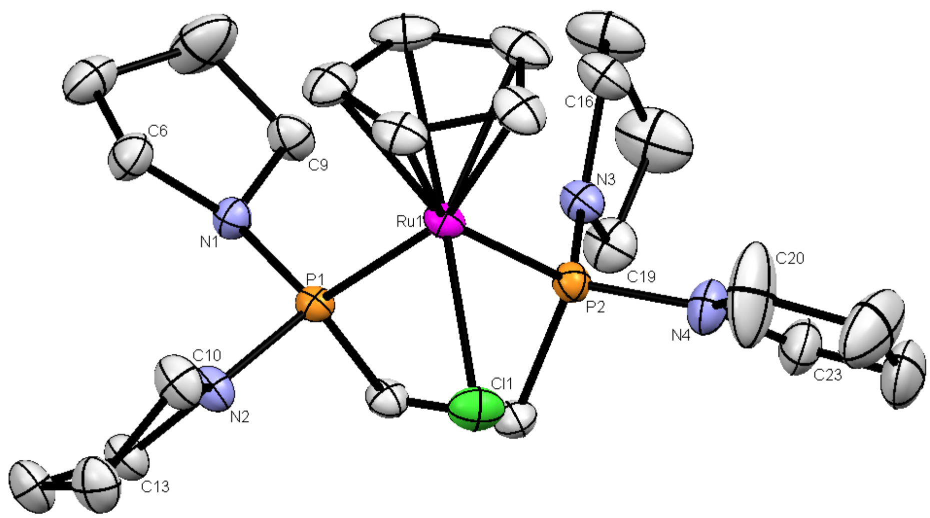

Table 4.2: Selected bond lengths and angles for 3

Selected Bond Lengths (Å)		Selected Bond Angles (°)	
Ru(1)-P(1)	2.2626(6)	P(1)-Ru(1)-P(2)	81.45(2)
Ru(1)-P(2)	2.2654(6)	P(1)-N(1)-C(6)	118.8(1)
Ru(1)-Cl(1)	2.4334(6)	P(1)-N(1)-C(9)	119.0(1)
P(1)-N(1)	1.715(2)	C(6)-N(1)-C(9)	107.5(2)
P(1)-N(2)	1.671(2)	P(1)-N(2)-C(10)	123.5(1)
P(2)-N(3)	1.682(2)	P(1)-N(2)-C(13)	124.3(1)
P(2)-N(4)	1.669(2)	C(10)-N(2)-C(13)	110.6(2)
Ru(1)-centroid	1.879*	P(2)-N(3)-C(16)	120.6(1)
		P(2)-N(3)-C(19)	126.4(1)
		C(16)-N(3)-C(19)	110.0(2)
		P(2)-N(4)-C(20)	126.7(2)
		P(2)-N(4)-C(23)	122.7(2)
		C(20)-N(4)-C(23)	110.6(2)

*Calculated

The solid state structure of **3** exhibits similar structural features to that of **1**. Again, three of the pyrrolidinyl ring substituents possess nitrogen atoms (N(2), N(3), and N(4)) that display nearly planar geometries, with the sum of the angles around each nitrogen ranging between 357-360°. The fourth nitrogen (N(1)) possesses a greater degree of tetrahedral distortion with a sum of angles totalling 345°, and as with **1**, no significantly short N-H contact distances to suggest an intramolecular interaction. The P-N bond lengths within the phosphine ligand, at 1.669(2)-1.715(2) Å, once again show a correlation between the shortening of the P-N bond length and the increased planarity about the nitrogen of the pyrrolidinyl substituents. The Ru-P distances of **3**, at 2.2654(6) Å and 2.2626(6) Å, and P-Ru-P bond angle, at 81.45(2)°, are only slightly smaller than those observed for the structural analogue, [CpRuCl(dppe)] (2.275(2) Å, 2.282(2) Å, and 83.49(4)°),[42] which suggests the dipyrrolidinylphosphino groups of ligand **II** are perhaps better donors, and also similar in size to that of the diphenylphosphino groups of dppe. The cone angle for dppe has been estimated to be 125°,[5] thus one might expect the cone angle for ligand **II** to be about the same.

4.2 *In situ* Synthesis of [Cp*Ru(^{t}Bu(pyr)$_2$P)Cl], 4

The ^{t}Bu analogue of **I**, ^{t}Bu(pyr)$_2$P, is proposed to be one of the most strongly-donating tertiary phosphines known,[1c,d] yet it is not especially large. We found this particularly intriguing, and set out to examine its coordination chemistry in the synthesis of ruthenium piano-stool complexes. Our primary goal was to determine whether or not the chemistry of the corresponding piano-stool complexes paralleled that observed for the smaller, methyl analogue **I**. It was postulated that the greater steric size of the ^{t}Bu analogue, along with its enhanced donating abilities, would impart different chemical properties on its respective complexes.

When 8 equivalents of ^{t}Bu(pyr)$_2$P were added to a hexane suspension of [Cp*RuCl]$_4$, an extremely air sensitive, steely-blue solid was isolated from a deep, dark blue solution, unlike what is observed in the analogous reaction involving Me(pyr)$_2$P. The extreme air sensitivity, and intense blue colour were reminiscent of coordinatively unsaturated, 16-electron complexes of the type [Cp*RuCl(PR$_3$)][43] where PR$_3$ is a bulky phosphine. Furthermore, ^{31}P{^{1}H} NMR spectroscopic analysis (in CD_2Cl_2) of the blue solid after several minutes revealed a number of signals; however, one main signal appeared at δ = 98.8 ppm, and represented approximately 50% of the content of the sample, based on approximate NMR spectrum integrations. The intense blue colour of the product suggested that the 16-electron, coordinatively unsaturated complex, [Cp*RuCl(^{t}Bu(pyr)$_2$P)] was the dominant product of this reaction. With this information in hand, subsequent attempts to isolate the species at δ = 98.8 ppm were made by first adjusting the stoichiometry of the reaction. Thus, ^{t}Bu(pyr)$_2$P and [Cp*RuCl]$_4$ were reacted together in hexanes in a 4:1 ratio, which again yielded the deep, dark blue solution as expected, and from which a deep, dark blue solid was isolated. The $^{31}P\{^1H\}$ NMR spectrum of the solid in C_6D_6 was acquired immediately, and showed the species at δ = 98.8 ppm was now the dominant product in solution (~70%). Unfortunately, this complex proved to be very unstable, and considerable decomposition was observed after only 30 minutes; within 24 hours, it had completely decomposed to multiple products that were not characterized. Thus, the inability of two **Ib** ligands to coordinate (unlike **Ia**) suggest **Ib** is (perhaps unexpectedly) larger than was originally anticipated.

4.3 Substitution Chemistry of 1 and 2 to Afford [Cp*RuL(PP)Cl], (PP = [Me(pyr)$_2$P]$_2$; L = MeCN, 5a; CO, 5b; N$_2$, 5c; PP = dpyrpe; L = MeCN, 6a; CO, 6b; N$_2$, 6c; H$_2$, 6d)

Some attention was given to screening the substitution chemistry of complexes **1** and **2** (**Scheme 4.4**). The results were, in a number of ways, typical of the substitution chemistry often observed in Cp*-ruthenium piano-stool complexes. All complexes were characterized by NMR spectroscopy and through the acquisition of microanalytical data. In all cases, chloride ligand removal from either **1** or **2** in the presence of ligand L was facilitated with NaBAr$^f_4$ (Ar^f = 3,5-bis(trifluoromethyl)phenyl), and allowed for the subsequent isolation of [Cp*Ru(L)(Me(pyr)$_2$P)$_2$][BAr$^f_4$] (L = MeCN, **5a**; CO, **5b**; N$_2$, **5c**) and [Cp*Ru(L)(dpyrpe)][BAr$^f_4$] (L = MeCN, **6a**; CO, **6b**; N$_2$, **6c**). Reactions of **2** with NaBAr$^f_4$ under H$_2$ gave the oxidative addition product [Cp*RuH$_2$(dpyrpe)][BAr$^f_4$], **6d**.

Scheme 4.4: Synthetic strategy for obtaining substitution adduct of complex 1 and 2

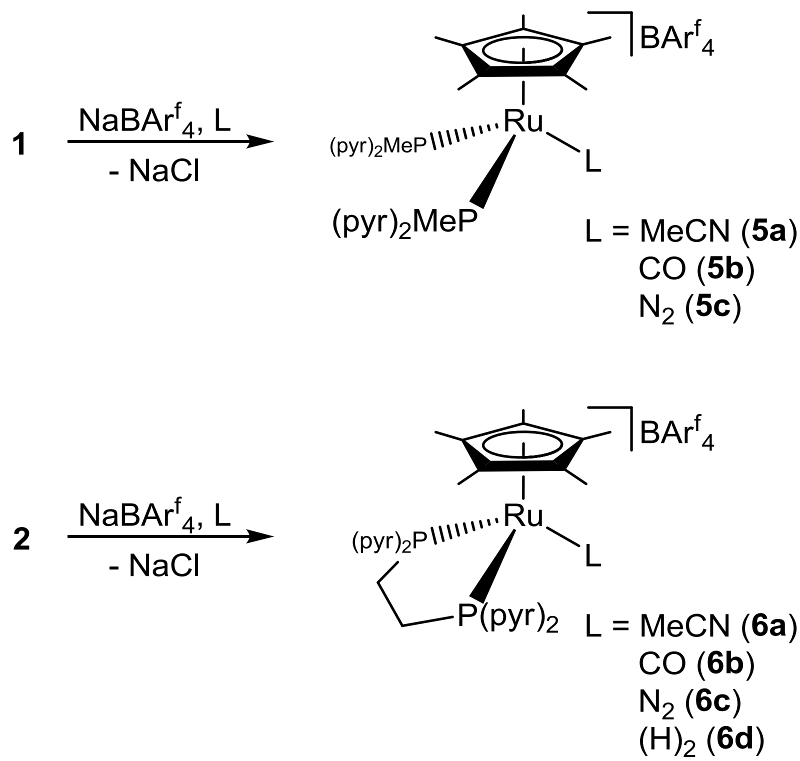

4.3.1 The MeCN Complexes 5a and 6a

An upfield shift in the $^{31}P\{^1H\}$ NMR spectrum from the parent chloride species **1** and **2** was observed for both **5a** and **6a**, with each displaying sharp signals at δ = 103.5 ppm and 136.4 ppm, respectively. Complex **6a** displayed a greater upfield shift compared to **5a**. The sharp signal observed for **5a** contrasts what is observed for complex **1**, suggesting phosphine rotation is not as hindered in **5a**. Complexes **5a** and **6a** form very quickly. For example, complex **1** and $NaBAr^f_4$ were dissolved in C_6D_6 and the sample was monitored via NMR spectroscopy. The subsequent addition of CD_3CN and NMR spectral analysis showed that [Cp*Ru($NCCD_3$)(Me(pyr)$_2$P)$_2$][BAr^f_4]), **5a'**, was cleanly formed within 15 minutes.

4.3.1.1 X-ray Crystal Structure Analysis of 6a

Crystals of **6a** were acquired through the slow diffusion of hexanes into a concentrated CH_2Cl_2 solution over several days at room temperature. The X-ray crystallographic data were acquired, and the structure solved by Dr. Ruiyao Wang in the Department of Chemistry at

Queen's University. All attempts to grow crystals of **5a** for further X-ray crystallographic analysis, however, proved unsuccessful. The X-ray structure of **6a** is illustrated in **Figure 4.7**, and selected bond lengths and angles are listed in **Table 4.3**.

Figure 4.7: Solid state X-ray structure of 6a (hydrogens and counter ion omitted for clarity)

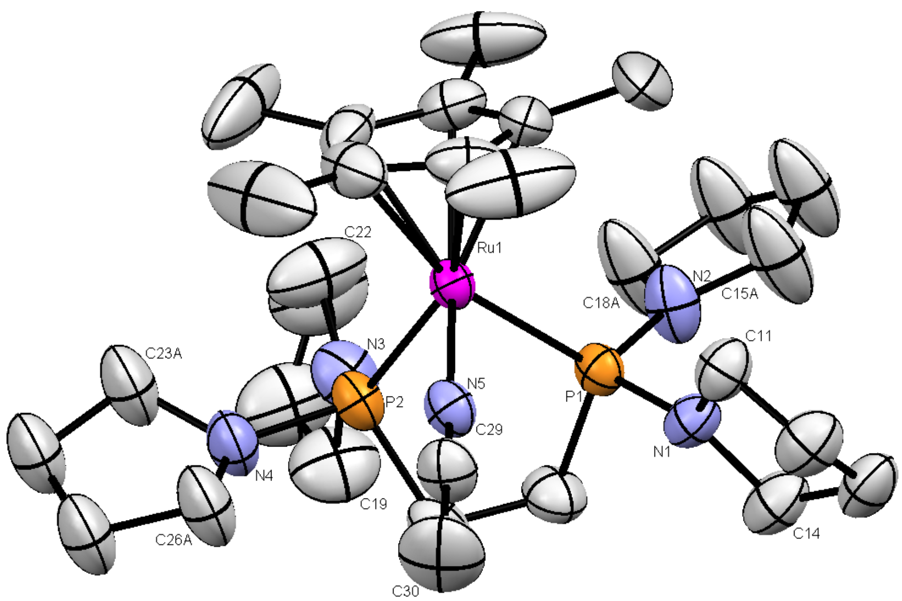

In contrast to the solid state structures of **1** and **3**, all four nitrogens of the pyrrolidinyl ring substituents in **6a** possess a nearly planar geometry with the sum of the angles about the nitrogen ranging between 357-359°. The P-N bond distances for **6a** range between 1.672(4)-1.680(5) Å, which are shorter than those for **1** or **3** (see **Section 4.1.2** above). These results again suggest additional dative or π-donation from the nitrogen lone pair into a vacant phosphorus-based orbital. The acetonitrile ligand displays a nearly linear geometry at 173.3(4)°. Finally, the Ru-P bond distances at 2.2967(9) Å and 2.304(1) Å are slightly shorter than those observed in [Cp*RuCl(dippe)] (2.336(2) Å and 2.331(2) Å; dippe = 1,2-bis(diisopropylphosphino)ethane)[43e] and [Cp*Ru(dippe)][BAr^f_4] (2.331(1) Å and 2.356(1) Å),[43b] suggesting a smaller size of ligand **II** compared to dippe.

Table 4.3: Selected bond lengths and angles for 6a

Selected Bond Lengths (Å)		Selected Bond Angles (°)	
Ru(1)-P(1)	2.304(1)	P(1)-Ru(1)-P(2)	81.34(4)
Ru(1)-P(2)	2.2967(9)	N(5)-C(29)-C(30)	178.5(6)
Ru(1)-N(5)	2.024(4)	P(1)-N(1)-C(11)	124.4(3)
P(1)-N(1)	1.672(4)	P(1)-N(1)-C(14)	123.9(3)
P(1)-N(2)	1.680(5)	C(11)-N(1)-C(14)	109.4(4)
P(2)-N(3)	1.674(5)	P(1)-N(2)-C(15A)	124.9(7)
P(2)-N(4)	1.677(4)	P(1)-N(2)-C(18A)	126.2(7)
Ru(1)-centroid	1.899*	C(15A)-N(2)-C(18A)	107.7(9)
		P(2)-N(3)-C(19)	122.8(4)
		P(2)-N(3)-C(22)	124.0(4)
		C(19)-N(3)-C(22)	111.6(5)
		P(2)-N(4)-C(23A)	122.5(6)
		P(2)-N(4)-C(26A)	127.0(7)
		C(23A)-N(4)-C(26A)	107.0(9)

*Calculated

4.3.2 The CO Complexes 5b and 6b

By utilizing the same synthetic strategy in synthesizing **5a** and **6a**, complexes **5b** and **6b** were prepared (**Scheme 4.4**). $^{31}P\{^{1}H\}$ NMR spectroscopic analysis of these species revealed sharp singlets at δ = 100.3 and 103.4 ppm, respectively. Additional analysis through IR spectroscopy on both species was performed in order to gauge the donor abilities of the pyrrolidinylalkylphosphine ligands. This is one of the simplest methods to use to probe the donor properties of metal-phosphine-CO complexes.[1b-d] In general, these studies have revealed that tertiary phosphines bearing two *N*-bound pyrrolidinyl and one alkyl substituent are stronger electron donating ligands compared to their trialkyl-, triaryl-, tris(pyrrolidinyl)phosphine, or dialkylpyrrolidinylphosphine counterparts. The IR spectrum of **5b** revealed a ν(CO) = 1957 cm^{-1}, while for **6b**, ν(CO) = 1960 cm^{-1}. For comparative purposes, and to establish the relative donor strengths of ligands **I** and **II** when coordinated to $[Cp^*Ru(CO)(PP)]^+$ (PP = bidentate or 2 ×

monodentate phosphines), the complexes $[Cp^*Ru(CO)(MePPh_2)_2][BAr^f_4]$, **7a** and $[Cp^*Ru(CO)(dppe)][BAr^f_4]$, **7b**, were also prepared in a similar manner. The identity of **7a** and **7b** were confirmed through NMR spectroscopic analysis and microanalytical data. Since complexes **7a** and **7b** contain conventional phosphine ligands which sterically resemble ligands **Ia** and **II**, the electronic contributions of **Ia** and **II** can be evaluated. The results obtained were surprisingly less definitive when compared to the observations in similar work.[1b-d] The infrared absorption of the CO ligand in complexes **7a** and **7b**, at ν(CO) = 1951 cm^{-1} and ν(CO) = 1961 cm^{-1}, respectively, suggests that ligands **Ia** and **II** possess very similar, if not slightly *weaker*, donor properties to that of $MePh_2P$ and dppe, despite their very different substituents. In addition, the infrared absorption of the CO ligand in the complex $[Cp^*Ru(CO)(PMe_3)_2][PF_6]$ appears at ν(CO) = 1935 cm^{-1},[44] which is significantly lower than what was observed for **5b**, suggesting PMe_3 is a stronger Lewis base than ligand **Ia**. This is in direct conflict with a separate study that reveals ligand **Ia** to be a better donor ligand when compared to PMe_3, again based on ν(CO) absorption data.[1c] It is unclear why ligands **Ia** and **II** exhibit comparable donor strength to their conventional phosphine analogues in these ruthenium complexes, **5b** and **6b**. One can speculate that the pyrrolidinyl rings experience greater steric strain in complexes **5b** and **6b** compared to the platinum complexes in the previous study, thus the ability of the pyrrolidinyl nitrogen to adopt the proper geometry for effective lone pair donation is impeded.

4.3.3 The N_2 Complexes 5c and 6c

The easy removal of the chloride ligands in **1** and **2** prompted the exploration of the synthesis of coordinatively unsaturated, 16-electron complexes $[Cp^*Ru(PP)]^+$ (PP = dpyrpe or $(Me(pyr)_2 P)_2$). It was expected that such complexes would likely display unique catalytic activity that may be exploited in subsequent studies. The synthesis of complexes **5a**,**b** and **6a**,**b** revealed that these reactive species could at least be trapped using suitable ligands, thus offering indirect evidence of their production. To this end, complex **1** and $NaBAr^f_4$ were combined in an NMR tube (in C_6D_6) under N_2. Interestingly, after mixing for *ca.* 5 minutes a yellow-orange solution was obtained. The $^{31}P\{^1H\}$ NMR spectrum of the solution was very clean, and revealed a signal with a shift at δ = 98.5 ppm as the sole phosphorus containing compound. The ^1H NMR spectrum revealed the pyrrolidinyl signals between δ = 2.94-2.76 ppm, corresponding to the hydrogens on positions C-2 and C-5 of the pyrrolidinyl rings, and at δ = 1.72 and 1.67 ppm, corresponding to the hydrogens on positions C-3 and C-4. The hydrogens pertaining to the Cp* were found at δ = 1.50 ppm and finally, the hydrogens corresponding to the methyl substituent of the phosphine were found at δ = 1.44 ppm. Similarly, when complex **2** was treated with $NaBAr^f_4$ in CD_2Cl_2 a yellow-orange solution was obtained, which exhibited a single peak in the $^{31}P\{^1H\}$ NMR spectrum at δ = 131.2 ppm. The ^1H NMR spectrum revealed signals representing the phosphine ligand, including the hydrogens corresponding to the pyrrolidine ring substituents (multiplets at δ = 3.03-2.79 and 1.80-1.73 ppm, for the C-2 and C-5, and C-3 and C-4 hydrogens, respectively), the hydrogens corresponding to the ethane bridge (multiplet at δ = 2.90 ppm) and the hydrogens corresponding to Cp* (singlet at δ = 1.68 ppm). In both cases, the yellow-orange solution colours were unexpected, as 16-electron $[Cp^*Ru(PR_3)_2]^+$ complexes typically are intensely blue-to-violet in colour.[43] The lack of deep coloured solutions in the synthesis of these new complexes piqued our interest as to their true identity. Infrared spectroscopic analysis of the species isolated beginning with complex **2** revealed an absorption at 2148 cm^{-1}, characteristic of a terminally bound dinitrogen ligand, as seen in other ruthenium-dinitrogen complexes.[43d] Thus, it was concluded that the species formed in this reaction is likely the 18-electron complex $[Cp^*Ru(N_2)(dpyrpe)][BAr^f_4]$, **6c**, rather than the expected 16-electron complex. By analogy to **6c** the product generated from complex **1** was tentatively assigned as $[Cp^*Ru(N_2)(Me(pyr)_2P)_2][BAr^f_4]$, **5c**, since infrared spectroscopic analysis proved problematic, likely as a result of the lability of the dinitrogen ligand. There is precedence in the literature for the formation of similar complexes.[43d] Indeed, the presence of a dinitrogen ligand, and thus coordinative saturation about ruthenium, would explain the color of the solutions. Also, the $^{31}P\{^1H\}$ NMR spectral shifts of **5c** and **6c** are in-line with the other 18-electron substitution complexes prepared as part of this work. The purification of these complexes proved difficult due to the lability of the dinitrogen ligand. This has been noted before in similar complexes.[43d] Performing the same reactions under argon using argon-purged solvents yielded yellow and brown mixtures, which when analyzed via $^{31}P\{^1H\}$ NMR spectroscopy revealed a myriad of complexes with no signals pertaining to **5c** and **6c**, thus indirectly providing proof of their identities.

4.4 Oxidative Addition Reactions involving 1 and 2

In addition to their function as intermediates in substitution chemistry, coordinatively unsaturated, 16-electron complexes $[Cp^*Ru(PP)]^+$ have been observed to activate a variety of different bonds, including C-H, H-H, Si-H, and B-H to name a few.[25] Commonly, sterically demanding, electron rich, phosphines are employed, resulting in an increased stability of these highly reactive species. This increased stability is the product of not only the steric properties of the phosphines, but also the electronic contributions. Naturally, the anticipated electronic properties of these bis(pyrrolidinyl)alkylphosphine ligands, and the possible *in situ* formation of $[Cp^*Ru(PP)]^+$ (where (PP) = 2 × **Ia** or **II**) suggested in the synthesis of complexes **5a,b** and **6a-c**, spurred considerable curiosity as to the potential of these complexes in catalyzing oxidative addition reactions.

For example, it is has been established that introducing dihydrogen to the highly reactive complexes $[Cp^*Ru(PP)]^+$ often lead to the formation of the corresponding Ru(IV) dihydride complexes, $[Cp^*RuH_2(PP)^+]$.[38c,43b,d,45] The Ru(II) side-bound dihydrogen complex, $[Cp^*Ru(H_2)(PP)^+]$, has been known to form in certain cases, typically at reduced temperatures; however, as room temperature is approached these species normally isomerize into the dihydride complexes.[38c,43b,d,45] When complex **2** was treated with 1 equivalent of $NaBAr^f_4$ under an atmosphere of dihydrogen, the dihydride complex $[Cp^*RuH_2(dpyrpe)][BAr^f_4]$, **6d**, forms. Complex **6d** shows a sharp signal in the $^{31}P\{^1H\}$ NMR spectrum at δ = 135.6 ppm. The most diagnostic feature in the ^1H NMR spectrum of **6c** is a triplet centred at δ = -9.76 ppm ($^2J_{PH}$ = 29 Hz), which is indicative of hydride ligands. The ^1H NMR spectral data and the room temperature reaction conditions, strongly suggest the identity of **6c** to be $[Cp^*RuH_2(dpyrpe)][BAr^f_4]$. The literature presents a number of examples of similar metal piano-stool complexes which have been shown to possess a transoid arrangement of the hydride ligands,[38c,43d,46] thus, this is likely also the case for **6c**. Unfortunately, extending the same reaction to include complex **1** was not as clean, and produced a series of unidentified species, as determined by $^{31}P\{^1H\}$ NMR spectral analysis. A variety of other substrates containing E-H bonds were also examined, including Ph_2SiH_2, $PhSiH_3$, Et_3SiH, however the reactions were not selective, and produced a variety of complexes that could not be confidently characterized. Similarly, reactions with select boranes, methyl iodide and allyl bromide yielded mixtures of products, as revealed by NMR spectroscopic analysis. Any additional attempts to purify the crude products resulted in further degradation.

4.5 Synthesis and Chemistry of [(*p*-cymene)Ru(R(pyr)$_2$P)Cl$_2$] (R = Me, 8; ^{t}Bu, 9)

The bis(pyrrolidinyl)alkylphosphine ligand **I** was also used in the synthesis of another series of ruthenium piano-stool complexes, this time incorporating the arene face capping ligand *p*-cymene. Ru-arene complexes are some of the most active catalysts in organic synthesis, and exist in seemingly endless combinations. They are commonly employed in the catalysis of a variety of organic reactions, including hydrogenation, hydrosilylation, dehydrohalogenation, borylation and cycloaddition.[26] The promising electronic properties of the bis(pyrrolidinyl)alkylphosphines led to the desire to explore their chemistry as part of Ru-arene complexes. These compounds were characterized through NMR spectroscopy and X-ray diffraction, in the case of compound **11**, however, publishable elemental analysis results proved difficult to obtain. The synthesis of these complexes was accomplished through the addition of either Me(pyr)$_2$P or ^{t}Bu(pyr)$_2$P to solutions of [(*p*-cymene)RuCl$_2$]$_2$ yielding oily red to dark red solids, which upon work-up gave spectroscopically pure, air stable, red solids, characterized as **8** and **9**, respectively (**Scheme 4.5**).

Scheme 4.5: Synthetic strategy utilized in forming 8 and 9

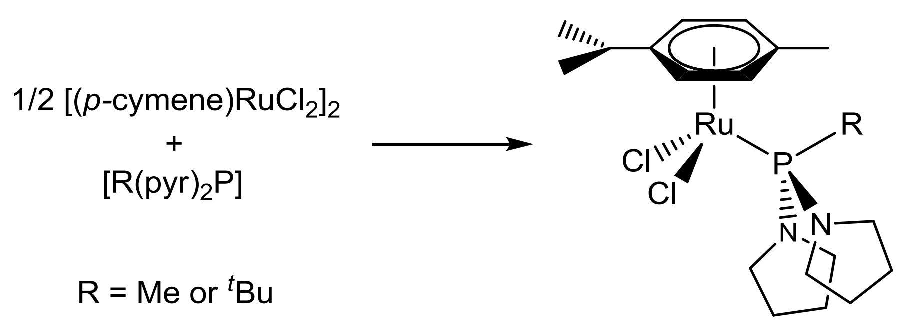

^{31}P{^{1}H} NMR spectroscopic analysis of **8** revealed a singlet at δ = 91.4 ppm whereas **9** showed a sharp singlet at δ = 105.9 ppm. The ^{1}H NMR spectra of **8** and **9** clearly showed signals pertaining to the phosphine and arene ligands. For complex **8** the pyrrolidinyl signals were observed as broad multiplets at δ = 3.11 ppm (C-2 and C-5 hydrogens of the pyrrolidinyl ring), and at δ = 1.54 ppm (C-3 and C-4 hydrogens of the pyrrolidinyl ring). The methyl substituent of the phosphine ligand in **8** was observed at δ = 1.78 ppm (singlet). Finally, the *p*-cymene signals were found at δ = 5.31 and 5.10 ppm (arene), δ = 2.93 ppm (septet; isopropyl methine hydrogen), δ = 1.82 ppm (singlet; methyl) and δ = 1.15 ppm (doublet; isopropyl methyl groups). Similarly, complex **9** revealed the pyrrolidinyl signals at δ = 3.34 and 3.24 ppm (C-2 and C-5 hydrogens of the pyrrolidinyl ring), and at δ = 1.72 ppm (C-3 and C-4 hydrogens of the pyrrolidinyl ring). The tertiary butyl substituent of the phosphine was observed at δ = 1.32 ppm (singlet). Finally, the *p*-cymene hydrogens were found at δ = 5.58 and 5.47 ppm (multiplets), δ = 2.81 ppm (septet; isopropyl methine hydrogen), δ = 2.10 ppm (singlet; methyl), and δ = 1.39 ppm (doublet; isopropyl methyl groups).

4.6 Synthesis and Chemistry of [(*p*-cymene)Ru(R(pyr)$_2$P)(MeCN)$_2$][BAr$^f_4$]$_2$ (R = Me, 10; ^{t}Bu, 11)

As with complexes **1** and **2**, the substitution chemistry of the new complexes **8** and **9** was also explored. Acetonitrile ligands are often labile, thus ruthenium-acetonitrile complexes often serve as convenient catalyst precursors.[47] Thus, by treating diethyl ether solutions of either **8** or **9** with two equivalents of the halide abstracting agent NaBAr$^f_4$ in the presence of an excess of MeCN, the bis(acetonitrile) species [(*p*-cymene)Ru(Me(pyr)$_2$P)(MeCN)$_2$][BAr$^f_4$]$_2$, **10**, and [(*p*-cymene)Ru(^{t}Bu(pyr)$_2$P) (MeCN)$_2$][BAr$^f_4$]$_2$, **11**, were obtained, respectively (**Scheme 4.6**).

Scheme 4.6: Synthesis of Complexes 10 and 11

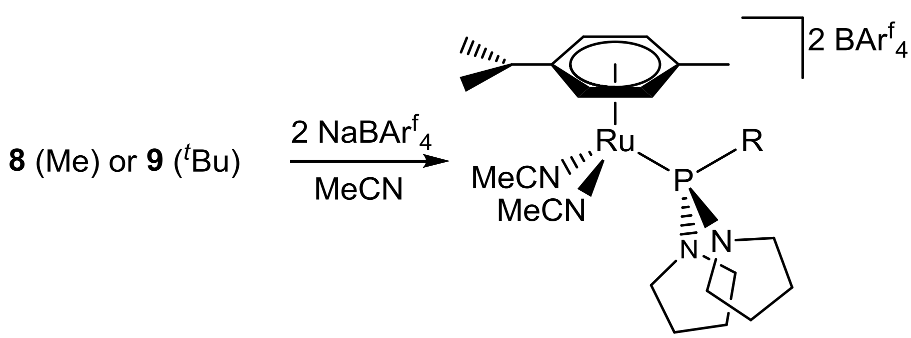

R = Me (**10**), ^{t}Bu (**11**)

The ^{31}P{^{1}H} NMR spectra reveal sharp signals at δ = 86.4 ppm and δ = 110.3 ppm for **10** and **11**, respectively. Interestingly, in the coordinated arene region of the ^{1}H NMR spectra of **10** and **11**, four signals, two of which are overlapped for **11**, integrating to four protons are observed for the coordinated *p*-cymene ligands (**Figure 4.8** and **Figure 4.9**), and contrasts what is observed for complexes **8** and **9**, which display only two aromatic signals.

Figure 4.8: ^{1}H NMR spectrum of complex 10 (arene region expanded)

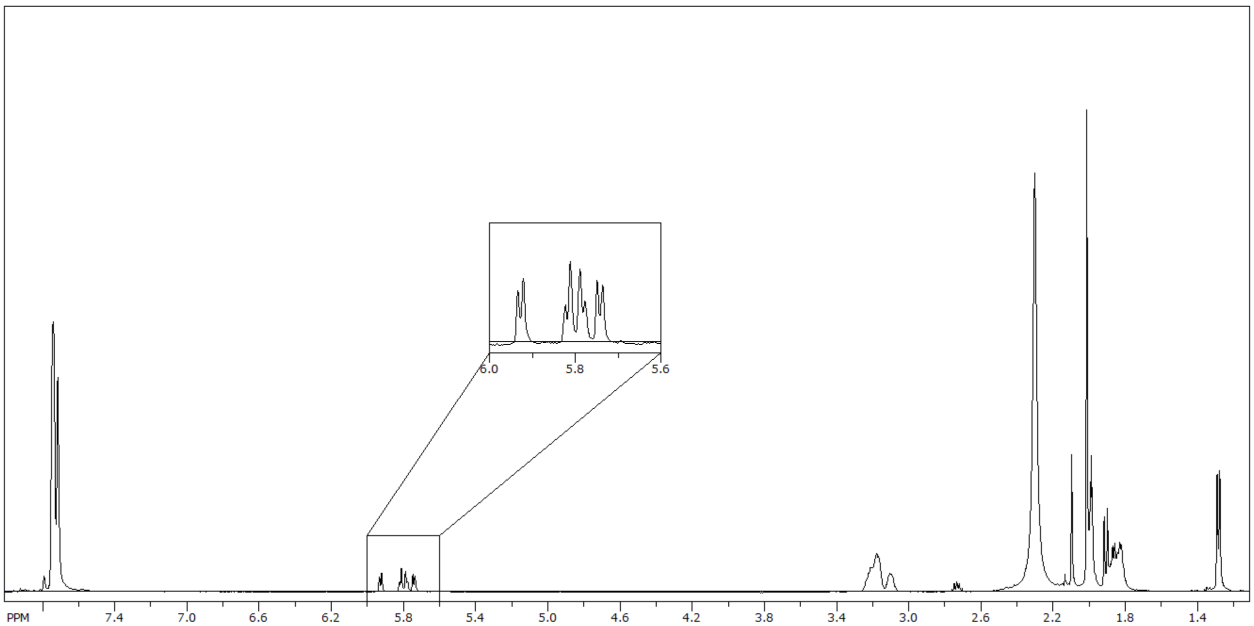

Figure 4.9: ^{1}H NMR spectrum of complex 11 (arene region expanded)

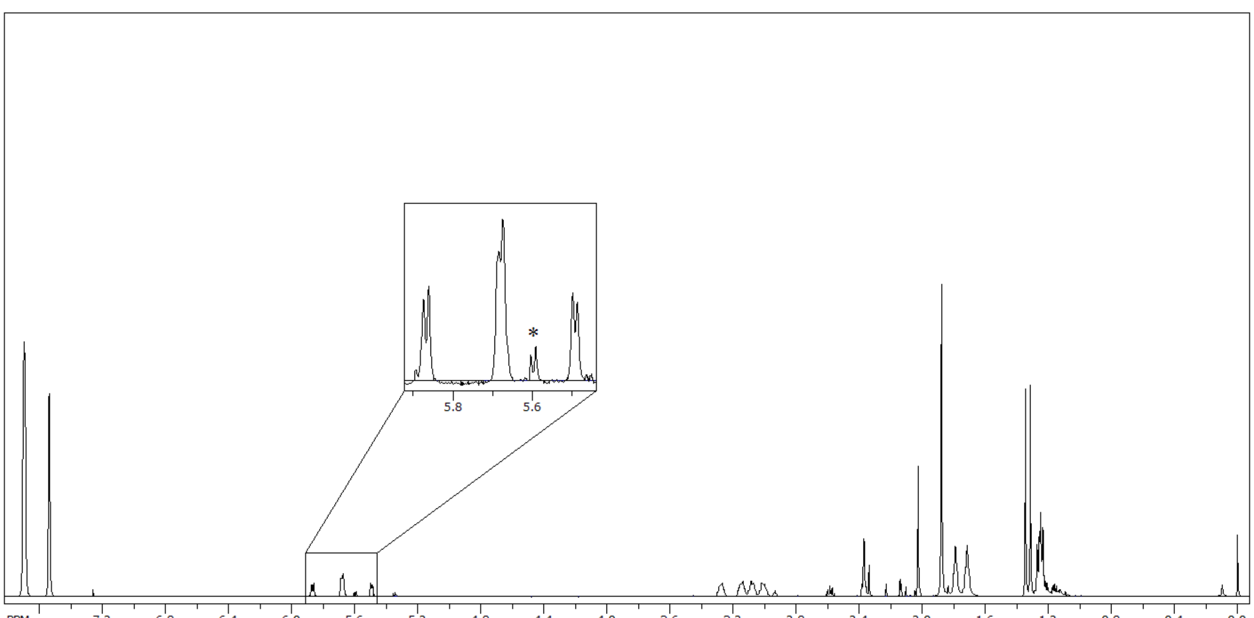

*Signal at δ = 5.6 ppm is a residual impurity.

This apparent decrease in symmetry in solution is likely linked to a larger barrier of rotation about the Ru-P bonds in **10** and **11**. The $^{31}P\{^1H\}$ NMR spectra of each complex display sharp singlets, which can be explained by the presence of rotamers in each case. These rotamers are be chemically equivalent meaning the environment about the phosphorus are equivalent, thus exchange between them would not result in the broadening of the signals in the $^{31}P\{^1H\}$ NMR spectra. However, the chemical environment of the arene ring are non-equivalent so restricted rotation will lead to splitting into four arene resonances. Interestingly, at elevated temperatures the arene hydrogen signals of complex **11** simplify considerably, and by 60 °C only two aromatic signals, at δ = 6.09 ppm and 5.87 ppm are observed in the ^1H NMR spectrum (**Figure 4.10**).

Figure 4.10: ^{1}H NMR spectrum of complex 11 at 60 °C (arene region expanded)

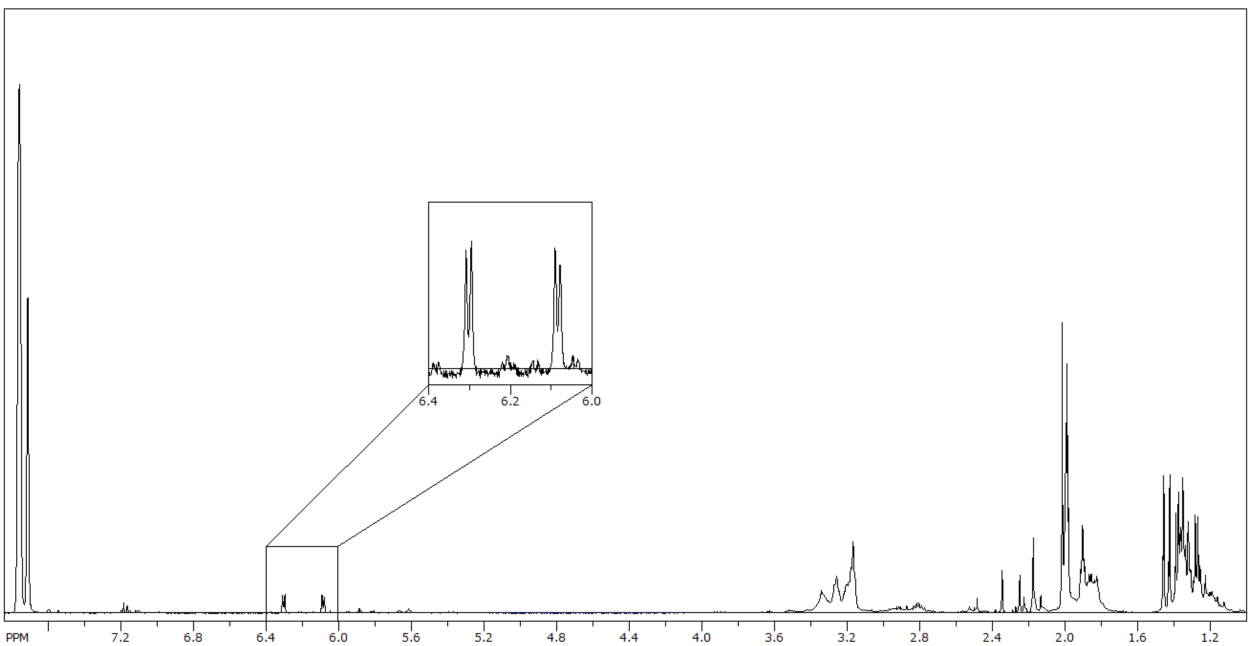

However, when complex **10** – which contains the smaller of the two phosphines – was examined under similar conditions, no changes were observed in the arene region of its ^1H NMR spectrum. Currently, the complexity of the room temperature ^1H NMR spectra of **10** and **11** is not fully understood.

Since the bis(acetonitrile)complexes **10** and **11** were synthesized in good yields and high spectroscopic purity the synthesis of the mono-acetonitrile species, [(*p*-cymene)Ru(Me(pyr)$_2$P)(MeCN)Cl][BAr$^f_4$], and [(*p*-cymene)Ru(^{t}Bu(pyr)$_2$P)(MeCN)Cl][BAr$^f_4$], were also attempted. Utilizing a similar synthetic route to that used to synthesize **10** and **11**, diethyl ether solutions of **8** or **9** were treated with only 1 equivalent of $NaBAr^f_4$ in the presence of an excess of acetonitrile. The $^{31}P\{^1H\}$ NMR spectra, however, suggested the bis(acetonitrile) complexes had formed as the main products (**10**, *ca.* 83%; **11**, *ca.* 85%). Although the ^1H NMR spectra for both complexes were complicated by the presence small amounts of other products, signals pertaining to complexes **10** and **11** could be identified. These results suggest chloride dissociation in **9** and **10** is facile in a polar solvent such as MeCN, which is also present in a large excess in these reactions, and this ultimately leads to the production of the bis(acetonitrile) products, despite the deficiency in halide abstracting agent used.

4.6.1 X-ray Crystal Structure Analysis of 11

Crystals of **11** were grown through slow diffusion of hexanes into a concentrated diethyl ether solution over several days at room temperature. Similar efforts to grow single crystals of complex **10** for further X-ray crystallographic analysis proved unsuccessful. The X-ray crystallographic data for **11** were acquired, and the structure solved by Dr. Ruiyao Wang in the Department of Chemistry at Queen's University. The X-ray crystal structure is illustrated in **Figure 4.11**, and selected bond lengths and angles are listed in **Table 4.4**.

Figure 4.11: Solid state X-ray structure of 11 (hydrogens omitted for clarity)

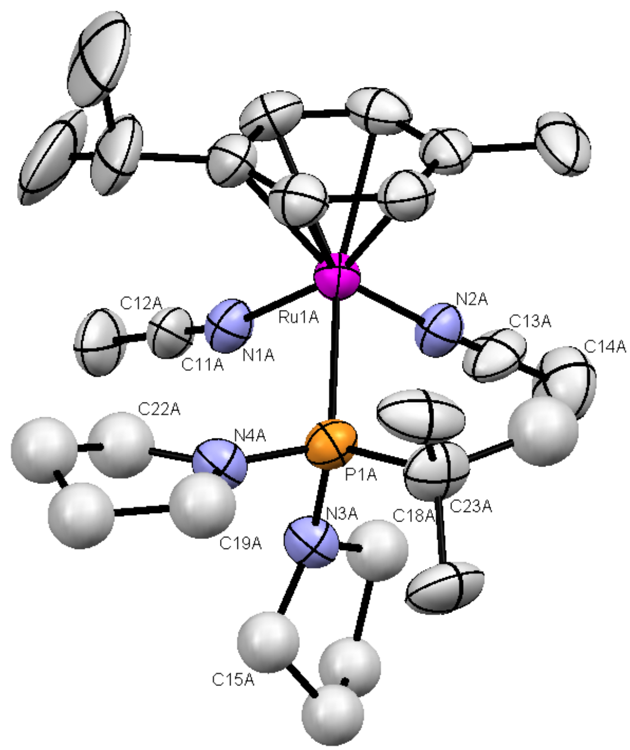

Table 4.4: Selected bond lengths and angles for 11

Selected Bond Lengths (Å)	
Ru(1A)-P(1A)	2.407(3)
Ru(1A)-N(1A)	2.075(11)
Ru(1A)-N(2A)	2.028(14)
P(1A)-N(3A)	1.73(2)
P(1A)-N(4A)	1.597(18)
P(2A)-C(23A)	1.858(15)
Ru(1)-centroid	1.736*

Selected Bond Angles (°)	
N(1A)-Ru(1A)-N(2A)	83.5(5)
N(1A)-C(11A)-C(12A)	176.5(18)
N(2A)-C(13A)-C(14A)	178.7(17)
P(1A)-N(3A)-C(15A)	123.3(18)
P(1A)-N(3A)-C(18A)	120.3(18)
C(15A)-N(3A)-C(18A)	111(2)
P(1A)-N(4A)-C(19A)	122.6(15)
P(1A)-N(4A)-C(22A)	127.8(16)
C(19A)-N(4A)-C(22A)	109.5(15)
N(3A)-P(1A)-N(4A)	90.1(11)

*Calculated

As expected, the structure is reminiscent of a piano-stool figure. The orientation of the arene ring in the solid state structure reveals that the symmetrical differences seen in the ^{1}H NMR spectra (see **Section 4.6.1** above) could also arise from restricted rotation of the arene ring, since this too would result in non-equivalent proton environments. The ^{t}Bu substituent of the phosphine ligand rests parallel to the plane of the capping ligand, while one pyrrolidine ring substituent faces down, directed away from the *p*-cymene ring. The remaining pyrrolidinyl substituent is adjacent to the ^{t}Bu substituent. Not unlike the solid state structures of **1**, **3** and **6a** (see **Sections 4.1.2** and **4.3.1.1** above) the pyrrolidinyl ring substituents of **11** possess a nearly planar geometry about the nitrogen atoms, with the sum of the angles being 359.9° (N(3A)) and 354.6° (N(4A)). The P-N bond distances are 1.597(3) Å (P-N(3A)) and 1.73(2) Å (P-N(4A)), showing a correlation between the degree of planarity about the nitrogen and the length of the P-N bond (see **Figure 4.5** above). This increased planarity and subsequent shortening of the P-N bonds are, once again, likely due to greater extent of additional π-donation from the nitrogen lone pair into a vacant phosphorus-based orbital. The structure shows some disordered with most of the carbon atoms of the phosphine ligand being isotropically refined. The acetonitrile ligands display nearly linear geometries at (176.5(18)° and 178.7(17)°). Finally, the Ru-P bond distance was found at 2.407(3) Å. Unfortunately, crystal structures of analogous ruthenium-arene-acetonitrile complexes containing conventional phosphines where not found in the literature, thus, a ruthenium-phosphine bond length comparison cannot be made at this time.

4.7 Synthesis and Chemistry of [(*p*-cymene)Ru(R(pyr)$_2$P)(CO)Cl][BAr$^f_4$] (R = Me, 12; ^{t}Bu, 13)

Considering the lability of the chloride ligands in **8** and **9**, attempts were also made to produce the corresponding CO complexes. Thus, by treating diethyl ether solutions of **8** or **9** with 1 equivalent of NaBAr$^f_4$ under a CO atmosphere, the subsequent species [(*p*-cymene)Ru(Me(pyr)$_2$P)(CO)Cl][BAr$^f_4$], **12**, and [(*p*-cymene)Ru(^{t}Bu(pyr)$_2$P)(CO)Cl][BAr$^f_4$], **13**, were obtained, respectively (**Scheme 4.7**).

Scheme 4.7: Synthetic strategy utilized in forming 12 and 13

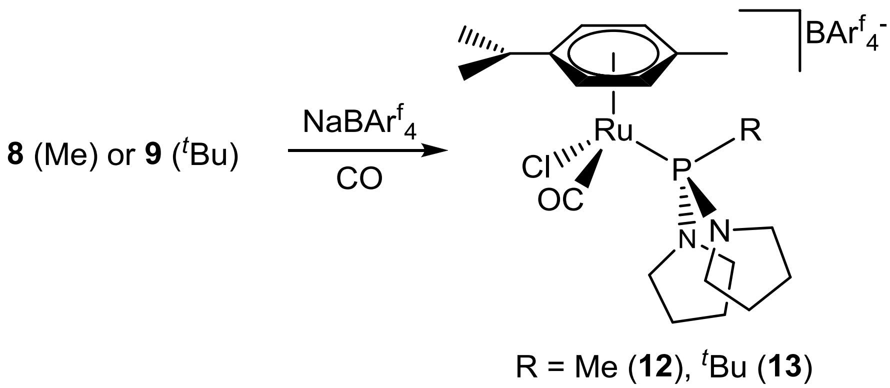

The $^{31}P\{^{1}H\}$ NMR spectra of **12** and **13** reveal sharp signals at δ = 86.16 ppm and 115.64 ppm, respectively. The ^{1}H NMR spectra of **12** and **13** revealed the chiral nature of the ruthenium centres in each complex, with four separate aromatic hydrogen signals appearing for each of the protons of the *p*-cymene ring (**Figure 4.12** and **Figure 4.13**, respectively). In addition to NMR spectroscopic analysis of complexes **12** and **13**, infrared spectroscopic analysis was attempted, however, both species showed the presence of a broad stretch crowding the typical CO stretch region, as a result of the phenyl stretches, so confirmation of the CO ligand was not obtained using this method. Through $^{13}C\{^{1}H\}$ NMR spectroscopic analysis, however, the presence of the CO ligands in **12** and **13** was confirmed.[48] Thus, the $^{13}C\{^{1}H\}$ NMR spectrum of complex **12** revealed a doublet at δ = 193.4 ppm with a coupling constant of $^{2}J_{PC}$ = 27.8 Hz, while complex **13** revealed a doublet at δ = 195.5 ppm with $^{2}J_{PC}$ = 24.8 Hz.

Figure 4.12: ^{1}H NMR spectrum of complex 12 (arene region expanded)

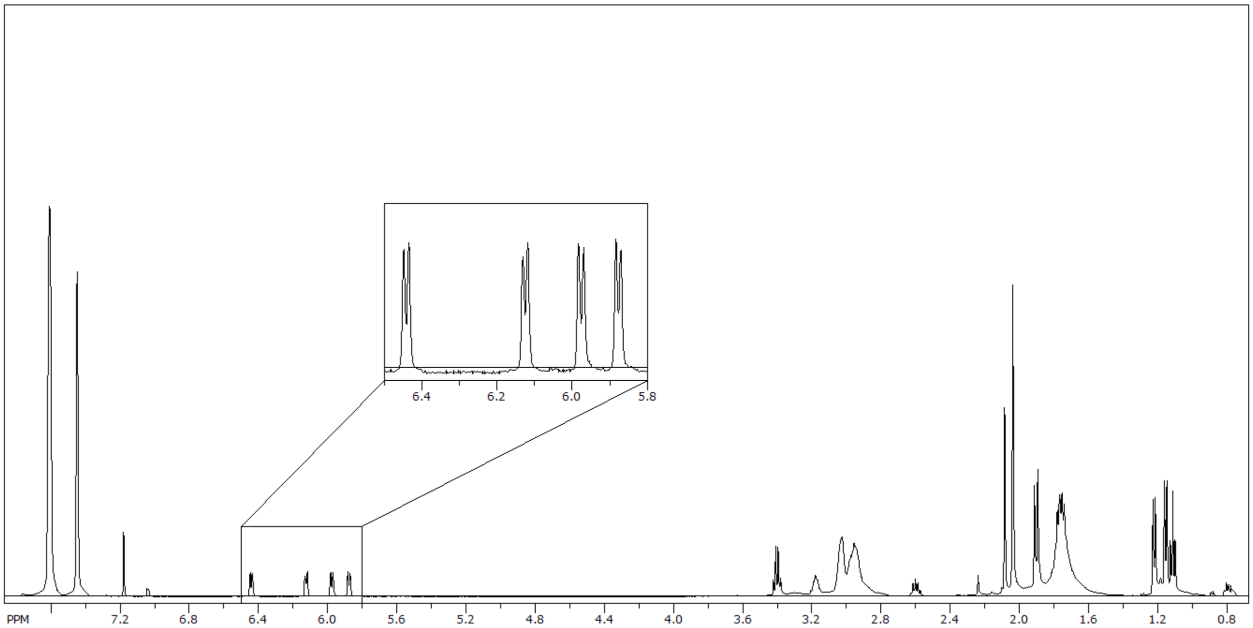

Figure 4.13: ^{1}H NMR spectrum of complex 13 (arene region expanded)

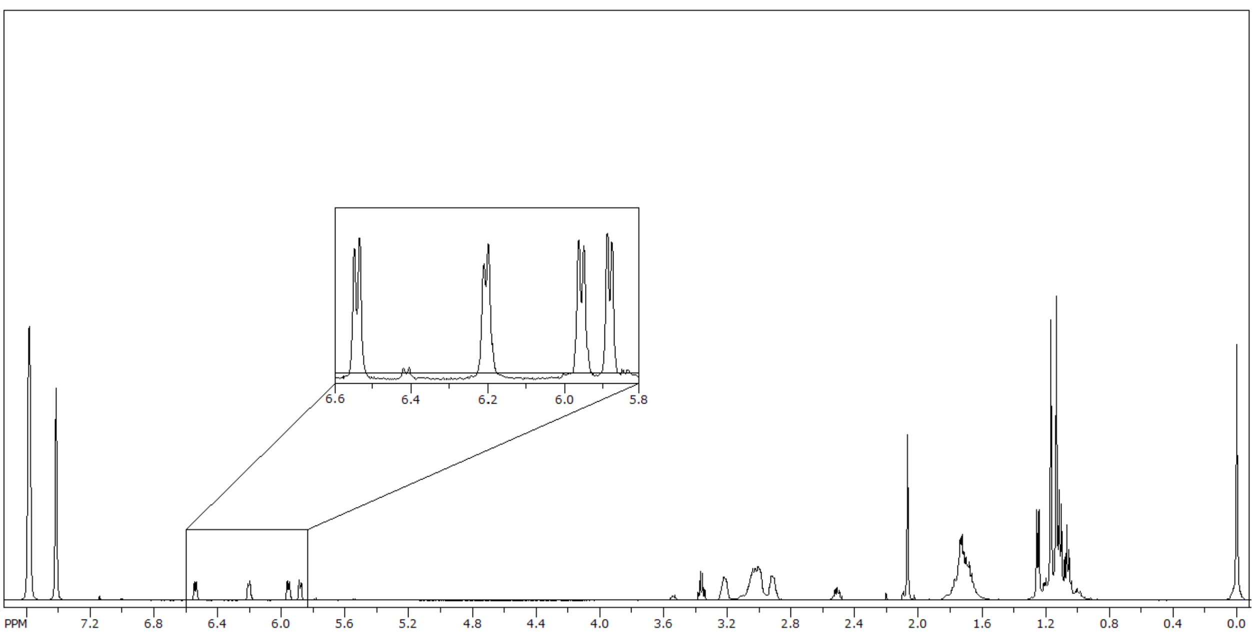

All attempts to synthesize the bis(CO) complexes by reacting complexes **8** or **9** with excess $NaBAr^{f}_{4}$ under CO, or starting from complexes **10** or **11** were unsuccessful.

4.8 Catalytic Transfer Hydrogenation Reactions Involving Complexes 10 and 11

Ruthenium-arene complexes represent some of the fastest, most efficient catalysts in catalytic transfer hydrogenation reactions.[49] As part of these studies, a wide variety of ancillary ligands have been screened. In some cases, the ancillary ligands are thought to participate in reversible transformations during the catalytic cycle,[49b,d,50] while in other instances they appear to play a direct role in transferring hydrogen to the substrate. This latter mechanistic feature prompted us to consider the role of pyrrolidinylalkylphosphine ligands in transfer hydrogenation reactions. The presence of the pyrrolidinyl substituents as part of the general ligand framework, especially the close proximity of the pyrrolidine nitrogen atoms to the metal, suggested these ligands might be good candidates for promoting the transfer hydrogenation reaction. To this end, complexes **10** and **11** were examined as transfer hydrogenation catalysts. These complexes were chosen since ruthenium-acetonitrile complexes often serve as convenient catalyst precursors.[47] For example, our laboratory recently showed the tris(acetonitrile) catalyst $[(PhB(CH_2PPh_2)_3)Ru(NCMe)_3]PF_6$ displayed excellent catalytic activity as a transfer hydrogenation catalyst for a variety of aliphatic and aromatic substrates.[47a]

In order to establish the catalytic potential of **10** and **11** as transfer hydrogenation catalysts, the conversion of the model substrate acetophenone to 1-phenylethanol was examined using standard transfer hydrogenation conditions (**Scheme 4.8**).[47a]

Scheme 4.8: Catalytic transfer hydrogenation of acetophenone to 1-phenyl ethanol

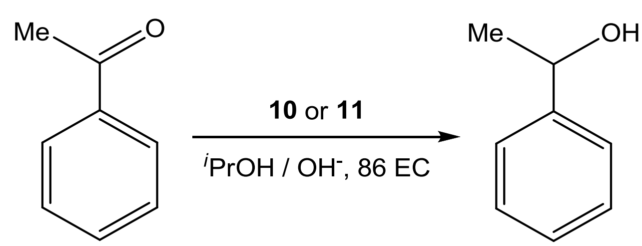

Unfortunately, both complexes proved to be poorly active under the conditions examined. For example, complex **10** was very slow, yielding only about 13% of product after 60 minutes, as determined by GC analysis, with little improvement being observed over longer periods (16% after 4 hours) (**Figure 4.14**). Complex **11** fared only slightly better, yielding about 23% product after 60 minutes, and 29% after 4 hours (**Figure 4.15**).

Figure 4.14: Transfer hydrogenation of acetophenone using 10

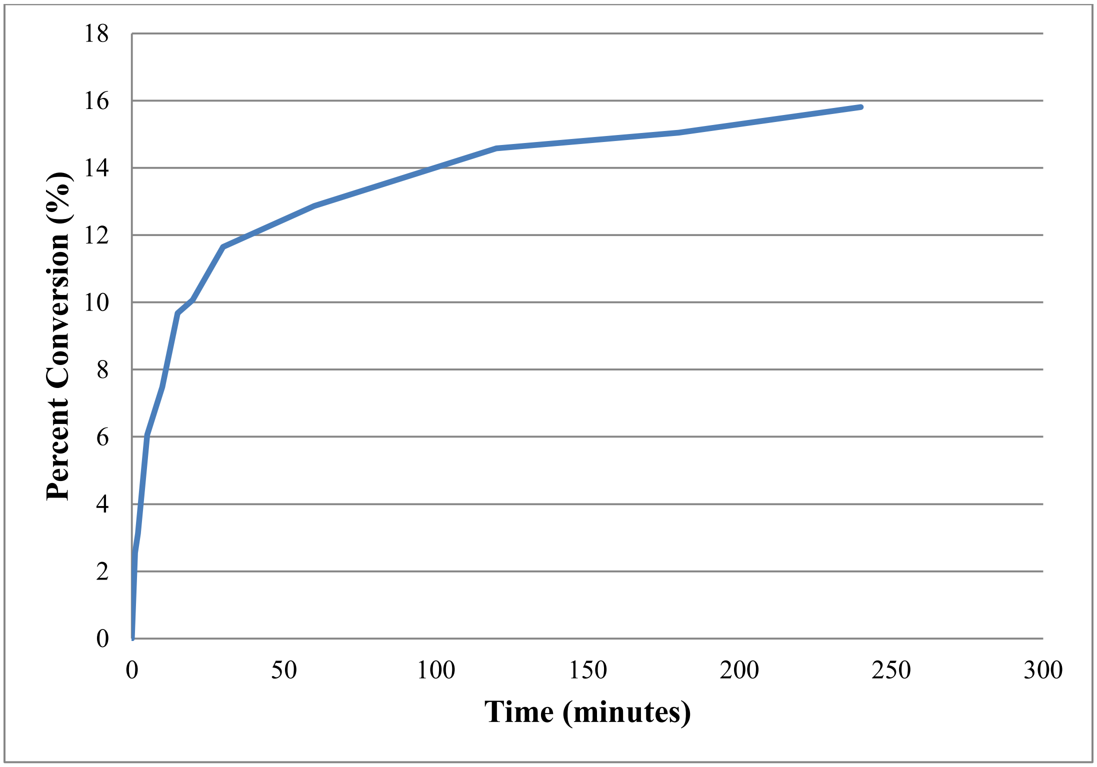

Figure 4.15: Transfer hydrogenation of acetophenone using 11

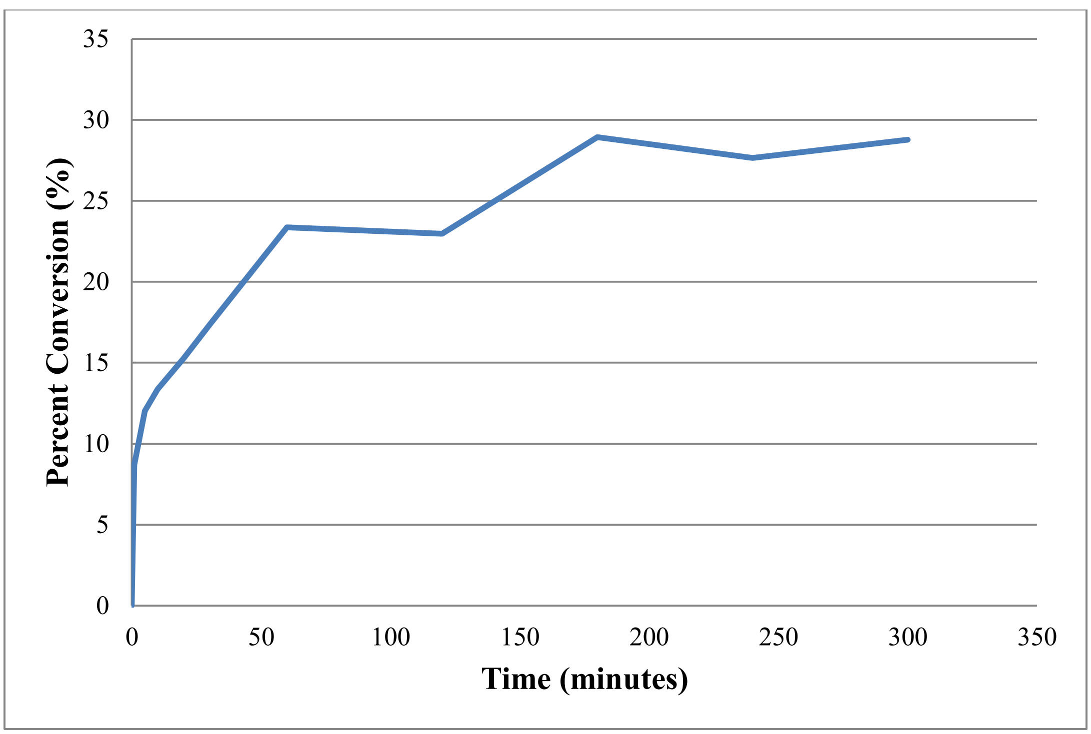

The decrease in activity over longer periods suggested the catalyst was likely decomposing under the conditions employed. It was speculated that the catalysts might be sensitive towards alcohol solvents. In order to test this, both complexes were individually dissolved in neat isopropanol under N_2 gas, and their stability was monitored via NMR spectroscopy. After 1 hour at room temperature, both showed complete degradation, with no **10** or **11** present in solution. Thus, the poor activity of each complex likely can be traced to their incompatibility with the solvent used.

5. Conclusions

Two series of ruthenium piano-stool complexes incorporating bis(*N*-pyrrolidinyl)alkylphosphines, **I**, and the newly synthesized bidentate analogue, 1,2-bis(dipyrrolidin-1ylphosphino)ethane, **II**, were prepared and characterized mainly through variable temperature NMR spectroscopic analysis and, in some cases, X-ray crystallography. These complexes include [Cp*Ru(PP)Cl], (PP = $[Me(pyr)_2P]_2$, **1**; dpyrpe, **2**), [CpRuCl(dpyrpe)], **3**, and [(*p*-cymene)Ru(R$(pyr)_2$P)Cl_2] (R = Me, **8**; ^{t}Bu, **9**), along with their substitution complexes [Cp*RuL(PP)][BAr^f_4], (PP = $[Me(pyr)_2P]_2$; L = MeCN, **5a**; CO, **5b**; N_2, **5c**; PP = dpyrpe; L = MeCN, **6a**; CO, **6b**; N_2, **6c**; $(H)_2$, **6d**), [(*p*-cymene)Ru(R$(pyr)_2$P)$(MeCN)_2$][BAr^f_4]$_2$ (R = Me, **10**; R= ^{t}Bu, **11**), and [(*p*-cymene)Ru(R$(pyr)_2$P)(CO)Cl][BAr^f_4] (R = Me, **12**; R= ^{t}Bu, **13**). The X-ray crystallographic studies of complexes **1**, **3**, **6a**, and **11** revealed a number of interesting features. Sterically, the pyrrolidinyl substituent appears to resemble that of a phenyl group, which agrees with previous reports.[15] Interestingly, the solid state studies also revealed a planar geometry about most or all of the pyrrolidinyl nitrogen atoms of the respective pyrrolidinylalkylphosphine ligand, suggesting additional (*i.e.*, π) bonding is occurring between the nitrogen lone pair and the phosphorus atom to which it is attached. It has been claimed that this additional interaction enhances the overall donor power of the phosphine. However, the results from the IR studies of the CO derivatives were not as definitive in this context, and unexpectedly indicate the donor strengths of ligands **Ia** and **II** closely resemble their conventional analogues, $MePh_2P$ and dppe, respectively, in contradiction to the findings of a previous study.[1b,c] Complexes **10** and **11** were screened for their catalytic potential as transfer hydrogenation catalysts using acetophenone as a model substrate. Unfortunately, both catalysts showed fair conversions likely degraded under the conditions employed in the reactions.

6. References

1. (a) M. Rodriguez i Zubiri, J.D. Woollins, *Comments Inorg. Chem.*, **2003**, *24*, 189; (b) M.L. Clarke, D.J. Cole-Hamilton, A.M.Z. Slawin, J.D. Woollins, *Chem. Commun.*, **2000**, 2065; (c) M.L. Clarke, G.L. Holliday, A.M. Z. Slawin, J.D. Woollins, *J. Chem. Soc., Dalton Trans.*, **2002**, 1093; (d) M.L. Clarke, D.J. Cole-Hamilton, J.D. Woollins, *J. Chem. Soc., Dalton Trans.*, **2001**, 2721; (e) M. Rodriguez i Zubiri, M.L. Clarke, D.F. Foster, D.J. Cole-Hamilton, A.M.Z. Slawin, J.D. Woollins, *J. Chem. Soc., Dalton Trans.*, **2001**, 969.
2. For recent examples, see: (a) M.H. Garcia, P.J. Mendes, M.P. Robuls, M.T. Duarte, N. Lopes, *J. Organomet. Chem.*, **2009**, *694*, 2888; (b) W. Buchowicz, A. Makal, K. Wozniak, *J. Organomet. Chem.*, **2009**, *694*, 3179; (c) M. Daniels, R.U. Kirss, *J. Organomet. Chem.*, **2007**, *692*, 1716.
3. For a review, see: (d) P.D. Dias, M.E.M. de Piedade, J.A.M. Simoes, *Coord. Chem. Rev.*, **1994**, *135*, 737.
4. R.H. Grubbs, T.M. Trnka, *Acc. Chem. Res.*, **2001**, *34*, 18.
5. C.A. Tolman, *Chem. Rev.*, **1977**, *77*, 313.
6. M. Rahman, H. Liu, A. Prock, W.P. Giering, *Organometallics*, **1987**, *6*, 650.
7. D. Imberly, H. Friebolin, *Z. Naturforsch*, **1968**, *23b*, 759.
8. R. Mathis, L. Lafaille, *Spectrochim. Acta.*, **1974**, *30A*, 357.
9. G.W. Buchanan, S.H. Preusser, *Org. Mag. Reson.*, **1984**, *22*, 1984.
10. L.K. Atkinson, D.C. Smith, *J. Organomet. Chem.*, **1971**, *33*, 189.
11. D.E.C. Corbridge, *Phosphorus: An Outline of its Chemistry, Biochemistry, and Technology*, 5th Edition Elsevier: Amsterdam.
12. M. Rodriguez i Zubiri, A.M.Z. Slawin, M. Wainwright, J.D. Woollins, *Polyhedron*, **2002**, *21*, 1729.
13. For examples, see: (a) T.J. Colacot, H. Qian, R. Cea-Olivares, S. Hernandez-Ortega, *J. Organomet. Chem.*, **2001**, 691; (b) W. Oberhauser, C. Bachmann, P. Brüggeller, *Inorg. Chim. Acta*, **1995**, *238*, 35; (c) J.M. Bevilacqua, J.A. Zuleta, R. Eisenberg, *Inorg. Chem.*, **1994**, *33*, 258; (d) Y. You, J. Chen, M. Cheng, and Y. Wang, *Inorg. Chem.*, **1991**, *30*,

3621; (e) L.M. Engelhardt, J.M. Patrick, C.L. Raston, P. Twiss, A.H. White, *Aust. J. Chem.*, **1984**, *37*, 2193.

14. M.T. Beach, R. Wang, G.J. Spivak, *Unpublished results*, **2010**.
15. K.G. Moloy, J.L. Petersen, *J. Am. Chem. Soc.*, **1995**, *117*, 7696.
16. A.W. Verstuyft, D.A. Redfield, L.W. Cary, J.H. Nelson, *Inorg. Chem.*, **1977**, *16*, 2776.
17. L.T. Stangeland, T. Austad, J. Sonstad, *Acta Chem. Scand.*, **1973**, *27*, 3919.
18. T. Thorstenson, J. Sonstad, *Acta Chem. Scand.*, **1976**, *A30*, 3919.
19. K.P. Balashev, T. Engebretsen, P. Kvam, K. Maartmann-Moe, M.V. Puzyk, J. Sonstad, *Acta Chem. Scand.*, **1996**, *50*, 1108.
20. T.A. Luiz, A. Doddi, B. Varghese, M.N.S. Rao, *Trans. Met. Chem.*, **2008**, *33*, 745.
21. M.S. Davies, M.J. Aroney, I.E. Buys, T.W. Hambley, J.L. Calvert, *Inorg. Chem.*, **1995**, *34*, 330.
22. F.A. Cotton, D.L. Darensbourg, W.H. Isley, *Inorg. Chem.*, **1981**, *20*, 578.
23. For examples, see: (a) L. Ackermann, R. Vicente, *Top. Curr. Chem.*, **2010**, 292, 211; (b) F. Nicks, R. Aznar, D. Sainz, G. Muller, A. Demonceau, *Eu. J. Org. Chem.*, **2009**, *29*, 5020; (c) R. Martinez, M. Simon, R. Chevalier, C. Pautigny, J.P. Genet, S. Darses, *J. Am. Chem. Soc.*, **2009**, *131*, 7887; (d) M. Pagliaro, S. Campestrini, R. Ciriminna, *Chem. Soc. Rev.*, **2005**, *34*, 837; (e) Y. Wakatsuki, H. Yamazaki, *J. Organomet. Chem.*, **1995**, *500*, 349.
24. (a) S. Dérien, P.H. Dixneuf, *J. Organomet. Chem.*, **2004**, *689*, 1382; (b) M. Jiménez-Tenorio, M.C. Puerta, P. Valerga, *Eur. J. Inorg. Chem.*, **2004**, 17; (c) D.M. Tellers, S.J. Skoog, R.G. Bergman, T.B. Gunnoe, W.D. Harman, *Organometallics*, **2000**, *19*, 2429; (d) U. Koelle, *Chem. Rev.*, **1998**, *98,* 1313.
25. For examples, see: (a) K.D. Hesp, M.A. Rankin, R. McDonald, M. Stradiotto, *Inorg. Chem.*, **2008**, *47*, 7471; (b) T.J. Johnson, P.S. Coan, K.C. Caulton, *Inorg. Chem.*, **1993**, *32*, 4594.
26. For a review, see: (a) B. Therrein, *Coord. Chem. Rev.*, **2009**, 493; (b) B.M. Trost, F.D. Toste, A.B. Pinkerton, *Chem. Rev.*, **2001**, *101*, 2067; (c) T. Noata, H. Takaya, S.I. Murahshi, *Chem. Rev.*, **1998**, *98*, 2549; For examples, see (d) L. Zhang, L. Wang, X.-Y. Ma, R.-X. Li, X.-J. Li, *Cat. Commun.*, **2007**, *8*, 2238; (e) A.B. Chaplin, P.J. Dyson, *Organometallics*, **2007**, *26*, 2447; (f) A.B. Chaplin, P.J. Dyson, *Organometallics*, **2007**,

26, 4357; (g) L. Qiu, F.Y. Kwong, J. Wu, W.H. Lam, S. Chan, W.-Y. Yu, Y.-M. Li, R. Guo, Z. Zhou, A.S.C. Chan, *J. Am. Chem. Soc.*, **2006**, *128*, 5955.

27. P.J. Fagan, M.D. Ward, J.C. Calabrese, *J. Am. Chem. Soc.*, **1989**, *111*, 1698.

28. U. Koelle, J. Kossakowski, *Inorg. Synth.*, **1992**, *29*, 225.

29. M.I. Bruce, C. Hameister, A.G. Swincer, R.C. Wallis, *Inorg. Synth.*, **1982**, *21*, 79.

30. (a) M.A. Bennett, T.N. Huang, T.W. Matheson, A.K. Smith, *Inorg. Synth.*, **1982**, *21*, 74; (b) M.A. Bennett, A.K. Smith, *J. Chem. Soc., Dalton Trans.*, **1974**, 233.

31. Bruker AXS Crystal Structure Analysis Package:
Bruker (2000). SHELXTL. Version 6.14. Bruker AXS Inc., Madison, Wisconsin, USA.
Bruker (2005). XPREP. Version 2005/2. Bruker AXS Inc., Madison, Wisconsin, USA.
Bruker (2005). SAINT. Version 7.23A. Bruker AXS Inc., Madison, Wisconsin, USA.
Bruker (2006). APEX2. Version 2.0-2. Bruker AXS Inc., Madison, Wisconsin, USA.

32. D.T. Cromer, J.T. Waber, International Tables for X-ray Crystallography, vol. 4, Kynoch Press, Birmingham, UK, 1974 (Table 2.2 A).

33. $R_1 = \sum | |Fo| - |Fc| | / \sum |Fo|$
$wR_2 = \{\sum [w (Fo^2 – Fc^2)^2] / \sum [w(Fo^2)^2]\}^{1/2}$
($w = 1 / [\sigma^2(Fo^2) + (0.0267P)^2 + 9.016P]$, where $P = [Max (Fo^2, 0) + 2Fc^2] / 3$)

34. $R_1 = \sum | |Fo| - |Fc| | / \sum |Fo|$
$wR_2 = \{\sum [w (Fo^2 – Fc^2)^2] / \sum [w(Fo^2)^2]\}^{1/2}$
($w = 1 / [\sigma^2(Fo^2) + (0.0657P)^2 + 3.23P]$, where $P = [Max (Fo^2, 0) + 2Fc^2] / 3$)

35. P.V.D Sluis, A.L. Spek, *Acta Cryst.*, **1990**, *A64*, 194.

36. $R_1 = \sum | |Fo| - |Fc| | / \sum |Fo|$
$wR_2 = \{\sum [w (Fo^2 – Fc^2)^2] / \sum [w(Fo^2)^2]\}^{1/2}$
($w = 1 / [\sigma^2(Fo^2) + (0.200P)^2]$, where $P = [Max (Fo^2, 0) + 2Fc^2] / 3$)

37. (a) S. Grim, W. McFarlane, E.F. Davidoff, *J. Org. Chem.*, **1967**, *32*, 781; (b) $^{31}P\{^1H\}$ NMR (202.3 MHz, $CDCl_3$, 22°C): -12.56 (s, -PCH_2CH_2P-).

38. (a) T. Arliguie, C. Border, B. Chaudret, J. Devillers, R. Poilblanc, *Organometallics*, **1989**, *8*, 1308; (b) A. Coto, M.J. Tenorio, M.C. Puerta, P. Valerga, *Organometallics*, **1989**, *17*, 4392; (c) G. Jia, A.J. Lough, R.H. Morris, *Organometallics*, **1992**, *11*, 161.

39. (a) R.P. Hughes, R.B. Laritchev, A. Williamson, C.D. Incarvito, L.N. Zakharov, A.L. Rheingold, *Organometallics*, **2003**, *22*, 2134; (b) T. Daniel, H. Werner, *J. Chem. Soc.,*

Dalton Trans., **1994**, 221; (c) J.A. Chudek, G. Hunter, R.L. MacKay, P. Kremminger, K. Schlogl, W. Weissensteiner, *J. Chem. Soc., Dalton Trans.*, **1990**, 2001; (d) L.J. Lyons, L. Anderson, R.A. Crane, P.M. Treichel, *Organometallics*, **1991**, *10*, 587; (e) L. Li, A. Decken, B.G. Sayer, M.J. McGlinchey, P. Bregaint, J.Y. Thepot, L. Toupet, J.R. Hamon, C. Lapinte, *Organometallics*, **1994**, *13*, 682; (f) J.A. Chudek, G. Hunter, R.L. MacKay, G. Farber, W. Weissensteiner, *J. Organomet. Chem.*, **1989**, *377*, C69-C72.

40. (a) A. Bondi, *J. Phys. Chem.*, **1964**, *68*, 441; (b) R.S. Rowland, R. Taylor, *J. Phys. Chem.*, **1996**, *100*, 7384.
41. R.T. Lubián, M.A. Paz-Sandoval, *J. Organomet. Chem*., **1997**, *532*, 17.
42. S. Suravajjala, L. C. Porter, *Acta Cryst*., **1993**, *C49*, 1456.
43. For examples, see: (a) H. Aneetha, M. Jiménez-Tenorio, M.C. Puerta, P. Valerga, V.N. Sapunov, R. Schmid, K. Kirchner, K. Mereiter, *Organometallics*, **2002**, *21*, 5334; (b) M. Jiménez-Tenorio, K. Mereiter, M.C. Puerta, P. Valerga, *J. Am. Chem. Soc.*, **2000**, *122*, 11230; (c) M. Jiménez-Tenorio, M.C. Puerta, P. Valerga, *J. Organomet. Chem.*, **2000**, 161; (d) I. de los Rios, M. Jiménez-Tenorio, J. Padilla, M.C. Puerta, P. Valerga, *Organometallics*, **1996**, *15*, 4565; (e) I. de los Rios, M. Jiménez-Tenorio, J. Padilla, M.C. Puerta, P. Valerga, *J. Chem. Soc., Dalton Trans.*, **1996**, 377; (f) T. Arliguie, C. Border, B. Chaudret, J. Devillers, R. Poilblanc, *Organometallics*, **1989**, *8*, 1308; (g) B.K. Campion, R.H. Heyn, T.D. Tilley, *J. Chem. Soc., Chem. Comm.*, **1988**, 278.
44. T.D. Tilley, R.H. Grubbs, J.E. Bercaw, *Organometallics*, **1984**, *3*, 274.
45. K. Kirchner, K. Mauthner, K. Mereiter, R. Schmid, *J. Chem. Soc., Chem. Commun.*, **1993**, 892.
46. (a) M. Jiménez-Tenorio, M. Puerta, P. Valerga, *Organometallics*, **1994**, *13*, 3330; (b) F.R. Lemke, L. Brummer, *Organometallics*, **1995**, *14*, 3980.
47. (a) J.M. Walker, A.M. Cox, R. Wang, G.J. Spivak, *Organometallics*, **2010**, *29*, 6121; (b) V.Y. Kukushkin, N.A. Bokach, *Russ. J. Gen. Chem.*, **2007**, *77*, 194; (c) S.I. Murahashi, *Ruthenium in Organic Synthesis*, WILEY-VCH: Weinheim, **2004**; (d) A. Doppiu, U. Englert, A. Salzer, *Inorg. Chim. Acta*, **2003**, *350*, 435; (e) E. Rüba, W. Simanko, K. Mauthner, K.M. Soldouzi, C. Slugovc, K. Mereiter, R. Schmid, K. Kirchner, *Organometallics*, **1999,** *18*, 3843.
48. (a) N.J. Beach, A.E. Williamson, G.J. Spivak, *J. Organomet. Chem.*, **2005**, *690*, 4640;

(b) N.J. Beach, H.A. Jenkins, G.J. Spivak, *Organometallics*, **2003**, *22,* 5179.

49. (a) T. Glöge, D. Petrovic, C. Hrib, P.G. Jones, M. Tamm, *Eur. J. Inorg. Chem.*, **2009**, 4538; (b) R.J. Lundgren, M.A. Rankin, R. McDonald, G. Schatte, M. Stradiotto, *Angew. Chem. Int. Ed.*, **2007**, *46*, 4732; (c) A.C. Marr, M. Nieuwenhuyzen, C.L. Pollock, G.C. Saunders, *Organometallics*, **2007**, *26*, 2659; (d) R.K. Rath, M. Nethaji, A.R. Chakravarty, *Polyhedron*, **2001**, *20*, 2735; (e) P. Braunstein, M.D. Fryzuk, F. Naud, S.J. Rettig, *J. Chem. Soc*., *Dalton Trans*., **1999**, 589.

50. (a) A. Del Zotto, W. Baratta, M. Ballico, E. Herdtweck, P. Rigo, *Organometallics*, *26*, **2007**, 5636; (b) W. Baratta, G. Chelucci, S. Gladiali, K. Siega, M. Toniutti, M. Zanette, E. Zangrando, P. Rigo, *Angew. Chem. Int. Ed.*, *44*, **2005**, 6214; (c) S.E. Clapham, A. Hadzovic, R.H. Morris, *Coord. Chem. Rev.*, **2004**, *248*, 2201; (d) W. Baratta, P. Da Ros, A. Del Zotto, A. Sechi, E. Zangrando, P. Rigo, *Angew. Chem. Int. Ed.*, *43*, **2004**, 3584.